University of California - Davis
University of Wisconsin - Madison

arXiv:hep-ph/9602415v1 27 Feb 1996

Higgs Boson Physics in the s-channel at $\mu^+\mu^-$ Colliders

V. Barger[a], M.S. Berger[b], J.F. Gunion[c], T. Han[c],

[a]*Physics Department, University of Wisconsin, Madison, WI 53706, USA*
[b]*Physics Department, Indiana University, Bloomington, IN 47405, USA*
[c]*Physics Department, University of California, Davis, CA 95616, USA*

Abstract

Techniques and strategies for discovering and measuring the properties of Higgs bosons via s-channel production at a $\mu^+\mu^-$ collider, and the associated requirements for the machine and detector, are discussed in detail. The unique feature of s-channel production is that, with good energy resolution, the mass, total width and partial widths of a Higgs boson can be directly measured with remarkable accuracy in most cases. For the expected machine parameters and luminosity the Standard Model (SM) Higgs boson h_{SM}, with mass $\lesssim 2m_W$, the light h^0 of the minimal supersymmetric Standard Model (MSSM), and the heavier MSSM Higgs bosons (the CP-odd A^0 and the CP-even H^0) can all be studied in the s-channel, with the heavier states accessible up to the maximal $\sqrt{s}$ over a large fraction of the MSSM parameter space. In addition, it may be possible to discover the A^0 and H^0 by running the collider at full energy and observing excess events in the bremsstrahlung tail at lower energy. The integrated luminosity, beam resolution and machine/detector features required to distinguish between the h_{SM} and h^0 are delineated.

Contents

Appendices   **72**

A Effects of bremsstrahlung   **72**

B The $\mu^+\mu^- \to h \to WW^{(\star)}, ZZ^{(\star)}$ modes   **78**

C Three-point determination of $m_{h_{SM}}$ and $\Gamma^{\mathrm{tot}}_{h_{SM}}$ **80**

1 Introduction

Despite the extraordinary success of the Standard Model (SM) in describing particle physics up to the highest energy available today, the mechanism responsible for electroweak symmetry-breaking (EWSB) has yet to be determined. In particular, the Higgs bosons predicted in the minimal Standard Model and the theoretically attractive Supersymmetric (SUSY) Grand Unified Theory (GUT) extensions thereof have yet to be observed. If EWSB does indeed derive from non-zero vacuum expectation values for elementary scalar Higgs fields, then one of the primary goals of constructing future colliders must be to *completely* delineate the associated Higgs boson sector. In particular, it will be crucial to discover all of the physical Higgs bosons and determine their masses, widths and couplings.

The remainder of the introduction is divided into two subsections. In the first, we briefly review crucial properties of the Standard Model and MSSM Higgs bosons. In the second, we outline basic features and parameters of the proposed $\mu^+\mu^-$ colliders, and give a first description of how they relate to our ability to discover and study the SM and MSSM Higgs bosons in s-channel $\mu^+\mu^-$ collisions.

1.1 Higgs bosons in the SM and the MSSM

The EWSB mechanism in the Standard Model is phenomenologically characterized by a single Higgs boson (h_{SM}) in the physical particle spectrum. The mass of the h_{SM} is undetermined by the theory, but its couplings to fermions and vector bosons are completely determined, being given by $gm_f/(2m_W)$, gm_W and $gm_Z/\cos\theta_W$ for a fermion f, the W and the Z, respectively. Although the SM Higgs sector is very simple, it leads to problems associated with naturalness and mass hierarchies which suggest that the SM is simply an effective low-energy theory. Recent summaries of the phenomenology of the SM Higgs sector can be found in Refs. [1,2].

The most attractive extensions of the SM that solve the naturalness and hierarchy problems are those based on supersymmetry. The Higgs sector of a supersymmetric model must contain at least two Higgs doublet fields in order to give masses to both up and down quarks and to be free of anomalies. If it contains two, and only two, Higgs doublet fields, then the strong and electroweak coupling constants all unify reasonably well at a GUT scale of order 10^{16} GeV. Thus, the minimal supersymmetric Standard Model, defined as having exactly two Higgs doublets, is especially attractive. The

resulting spectrum of physical Higgs fields includes three neutral Higgs bosons, the CP-even h^0 and H^0 and the CP-odd A^0. At tree-level the entire Higgs sector is completely determined by choosing values for the parameters $\tan\beta = v_2/v_1$ (where v_2 and v_1 are the vacuum expectation values of the neutral members of the Higgs doublets responsible for up-type and down-type fermion masses, respectively) and m_{A^0} (the mass of the CP-odd A^0). For a summary, see Refs. [1,2].

In the MSSM there is a theoretical upper bound on the mass of the lightest state h^0 [3,4] which is approached at large m_{A^0} and large $\tan\beta$. After including two-loop/RGE-improved radiative corrections [5,6] the bound depends upon the top quark (t) and top squark $(\tilde{t})$ masses and upon parameters associated with squark mixing. Assuming $m_t = 175$ GeV and $m_{\tilde{t}} \lesssim 1$ TeV, the maximal mass is

$$m_{h^0}^{\max} \sim 113 \text{ to } 130 \text{ GeV}, \tag{1}$$

depending upon the amount of squark mixing. The 113 GeV value is obtained in the absence of squark mixing. Figure 1 illustrates the mass of the h^0 versus the parameter $\tan\beta$ for $m_{A^0} = 100$, 200 and 1000 GeV. Mass contours for the MSSM Higgs bosons are illustrated in Fig. 2 in the conventional $m_{A^0}, \tan\beta$ parameter plane. Both these figures include two-loop/RGE-improved radiative corrections to the Higgs masses computed for $m_t = 175$ GeV, $m_{\tilde{t}} = 1$ TeV and neglecting squark mixing.

The Higgs sector of the MSSM can be extended to include extra singlet fields without affecting any of its attractive features. A general supersymmetric model bound of

$$m_{h^0} \lesssim 130 \sim 150 \text{ GeV} \tag{2}$$

applies for such non-minimal extensions of the MSSM, assuming a perturbative renormalization group (RGE) evolved grand unified theory (GUT) framework.

The couplings of the MSSM Higgs bosons to fermions and vector bosons are generally proportional to the couplings of the SM Higgs boson, with the constant of proportionality being determined by the angle β (from $\tan\beta$) and the mixing angle α between the neutral Higgs states (α is determined by m_{A^0}, $\tan\beta$, m_t, $m_{\tilde{t}}$, and the amount of stop mixing). Those couplings of interest in this report are [7]

$$
\begin{array}{ccccc}
 & \mu^+\mu^-, b\bar{b} & t\bar{t} & ZZ, W^+W^- & ZA^0 \\
h^0 & -\sin\alpha/\cos\beta & \cos\alpha/\sin\beta & \sin(\beta-\alpha) & \cos(\beta-\alpha) \\
H^0 & \cos\alpha/\cos\beta & \sin\alpha/\sin\beta & \cos(\beta-\alpha) & -\sin(\beta-\alpha) \\
A^0 & -i\gamma_5\tan\beta & -i\gamma_5/\tan\beta & 0 & 0
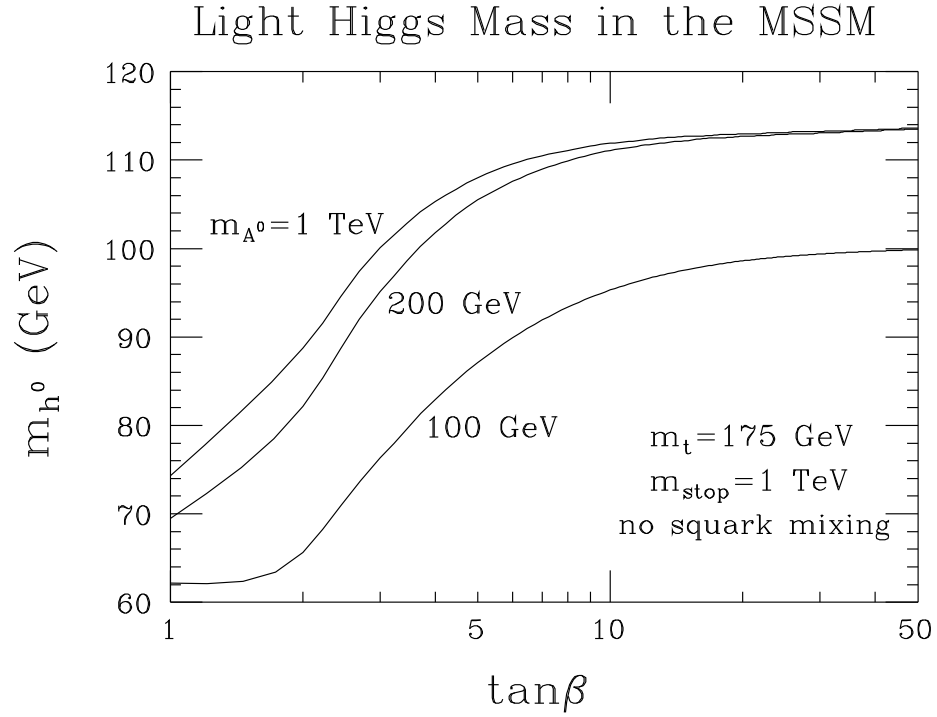\end{array} \tag{3}
$$

2

Figure 1: m_{h^0} versus $\tan\beta$ for m_{A^0} = 100, 200 and 1000 GeV. Two-loop/RGE-improved radiative corrections are included, see Refs. [5,6], taking m_t = 175 GeV, $m_{\tilde{t}}$ = 1 TeV and neglecting squark mixing.

times the Standard-Model factor of $gm_f/(2m_W)$ in the case of fermions (where m_f is the relevant fermion mass), or $gm_W, gm_Z/\cos\theta_W$ in the case of the W, Z, and $g(p_A - p_h)^\mu/2\cos\theta_W$ in the case of ZA^0, where $p_A(p_h)$ is the outgoing momentum of $A^0(h^0, H^0)$.

Higgs Mass Contours

$m_{TOP} = 175$ GeV, $m_{STOP} = 1$ TeV / 500 GeV
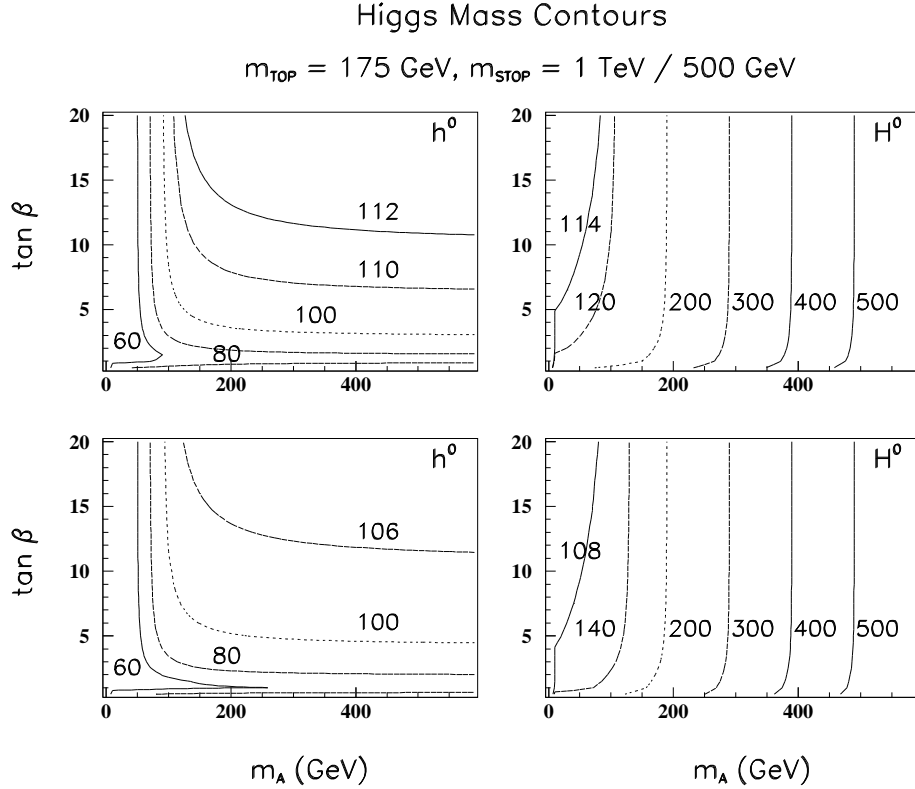
Figure 2: Contours for the h^0 and H^0 masses in $(m_{A^0}, \tan\beta)$ parameter space. Results include two-loop/RGE-improved radiative corrections computed for $m_t = 175$ GeV, with $m_{\tilde{t}} = 1$ TeV (upper plots) and $m_{\tilde{t}} = 500$ GeV (lower plots), neglecting squark mixing.

An important illustrative limit is $m_{A^0} \gtrsim 2m_Z$, since this is typical of SUSY GUT models [8]. In this limit, $\alpha \approx \beta - \pi/2$, $m_{A^0} \sim m_{H^0}$, m_{h^0} approaches its upper limit for the given value of $\tan\beta$, and the coupling factors of the Higgs bosons are

4

approximately

$$
\begin{array}{ccccc}
 & \mu^+\mu^-, b\bar{b} & t\bar{t} & ZZ, W^+W^- & ZA^0 \\
h^0 & 1 & 1 & 1 & 0 \\
H^0 & \tan\beta & -1/\tan\beta & 0 & -1 \\
A^0 & -i\gamma_5\tan\beta & -i\gamma_5/\tan\beta & 0 & 0
\end{array}
\tag{4}
$$

times the Standard-Model factors as given below Eq. (3). Thus at large m_{A^0} it is the h^0 which is SM-like, while the H^0, A^0 have similar fermion couplings and small, zero (respectively) tree-level WW, ZZ couplings. Note that the H^0 and A^0 couplings to $\mu^+\mu^-$ and $b\bar{b}$ are enhanced in the (preferred) $\tan\beta > 1$ portion of parameter space.

For $m_{A^0} \lesssim m_Z$, the roles of the h^0 and H^0 are reversed: in this mass range the H^0 becomes roughly SM-like, while the h^0 has couplings (up to a possible overall sign) roughly like those given for H^0 in Eq. (4). (See Refs. [2,9,1] for details; Ref. [1] gives the corrections that imply that the simple rules are only roughly correct after including radiative corrections.) It is also useful to recall [7,9] that the ZA^0H^0 (ZA^0h^0) coupling is maximal (~ 0) at large m_{A^0}, while at small m_{A^0} the reverse is true. The following discussions emphasize the case of large m_{A^0}.

The Higgs boson widths are crucial parameters for the searches and studies. In particular, we shall see that the width compared to the resolution in $\sqrt{s}$ of the machine is a crucial issue. Widths for the Standard Model Higgs h_{SM} and the three neutral Higgs bosons h^0, H^0, A^0 of the MSSM are illustrated in Fig. 3; for the MSSM Higgs bosons, results at $\tan\beta = 2$ and 20 are shown. As a function of $\tan\beta$, the total width of h^0 is plotted in Fig. 4 for $m_{h^0} = 100$, 110 and 120 GeV. We note that for masses below ~ 130 GeV, both the h_{SM} and a SM-like h^0 have very small widths (in the few MeV range); we will discover that these widths are often smaller than the expected resolution in $\sqrt{s}$. At high $\tan\beta$ and large $m_{A^0} \sim m_{H^0}$, the $\mu^+\mu^-$, $\tau^+\tau^-$ and $b\bar{b}$ couplings of the H^0 and A^0 are greatly enhanced (being proportional to $\tan\beta$). Consequently, $\Gamma^{\rm tot}_{H^0}$ and $\Gamma^{\rm tot}_{A^0}$ are generally large compared to the expected $\sqrt{s}$ resolution.

Figure 5 illustrates the h_{SM} branching fractions for the $\mu^+\mu^-$, $b\bar{b}$, $WW^{(\star)}$ and $ZZ^{(\star)}$ decay modes. For an h_{SM} with $m_{h_{SM}} \lesssim 130$ GeV, the $b\bar{b}$ branching fraction is of order 0.8–0.9, implying that this will be the most useful discovery channel. Once the $WW^{(\star)}$ and $ZZ^{(\star)}$ modes turn on ($m_{h_{SM}} \gtrsim 2m_W$), the h_{SM} becomes broad and the branching fraction $BF(h_{SM} \to \mu^+\mu^-)$, which governs s-channel production, declines

5

Higgs Total Widths
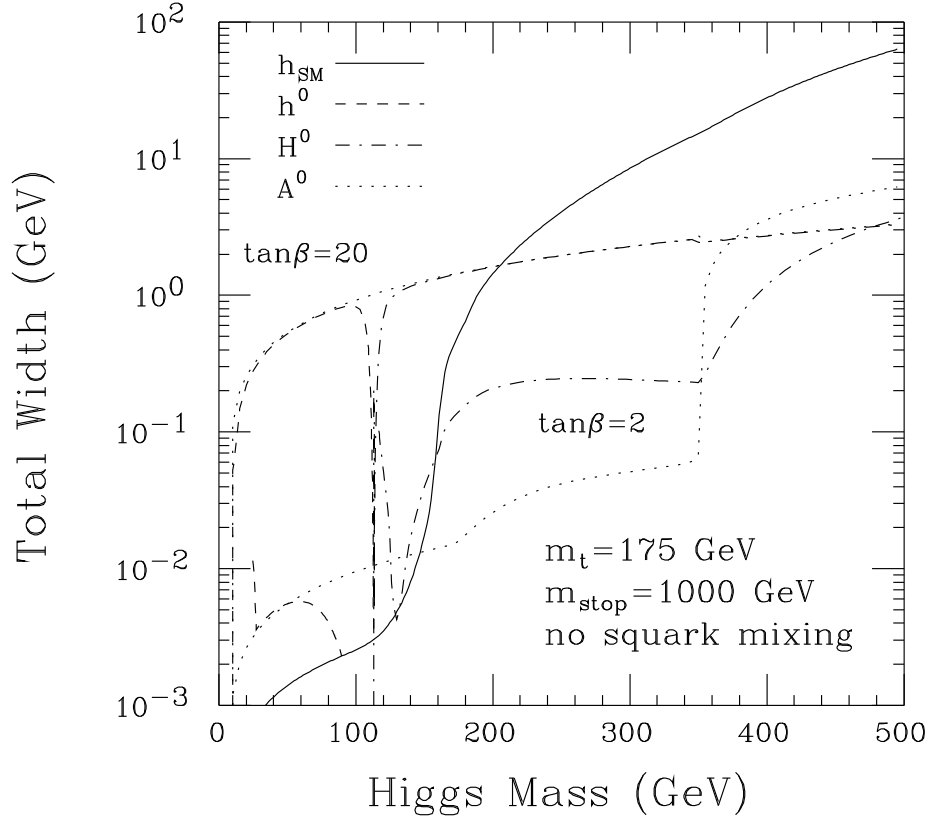
Figure 3: Total width versus mass of the SM and MSSM Higgs bosons for $m_t = 175$ GeV. In the case of the MSSM, we have plotted results for $\tan\beta = 2$ and 20, taking $m_{\tilde{t}} = 1$ TeV and including two-loop radiative corrections following Refs. [5,6] neglecting squark mixing; SUSY decay channels are assumed to be absent.

Figure 4: $\Gamma_{h^0}^{\mathrm{tot}}$ versus $\tan\beta$ for $m_{h^0} = 80$, 100, 110 and 113 GeV, assuming $m_t = 175$ GeV. Two-loop/RGE-improved radiative corrections to Higgs masses, mixing angles and self-couplings have been included, taking $m_{\widetilde{t}} = 1$ TeV and neglecting squark mixing. SUSY decay channels are assumed to be absent.

precipitously. Branching fractions for the h^0 of the MSSM are similar to those of h_{SM} for $m_{h_{SM}} = m_{h^0}$ when m_{A^0} is large. At high $\t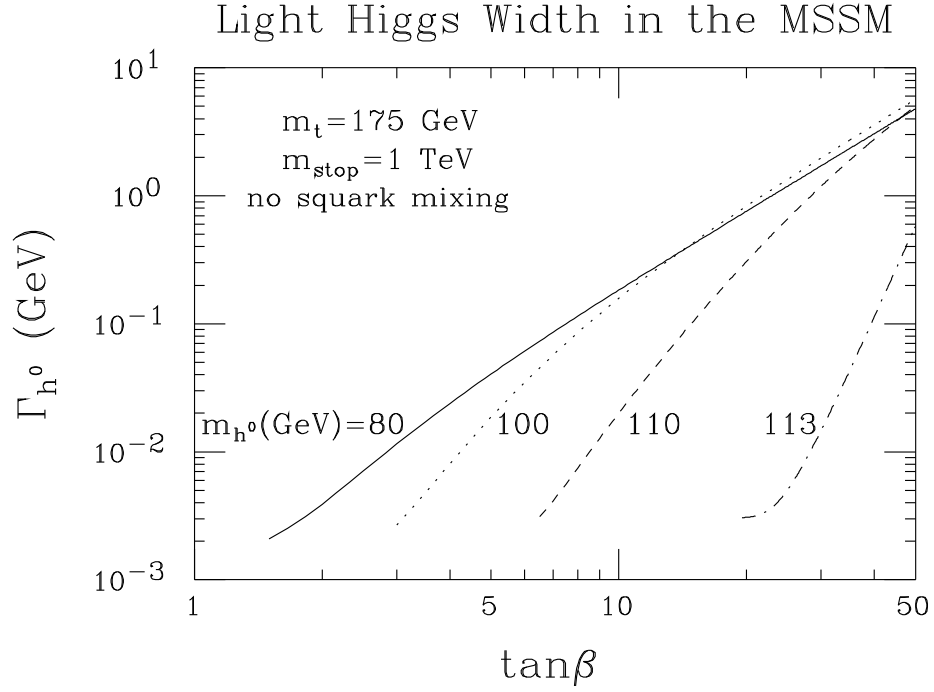an\beta$ and large $m_{A^0} \sim m_{H^0}$, the enhancement of the $\mu^+\mu^-$, $\tau^+\tau^-$ and $b\bar{b}$ couplings implies that the $b\bar{b}$, $\tau^+\tau^-$ and $\mu^+\mu^-$ branching fractions of the H^0 and A^0 are the only important ones, and are not unlike those of a light h_{SM}, with relative magnitudes determined by $m_b^2 : m_\tau^2 : m_\mu^2$.
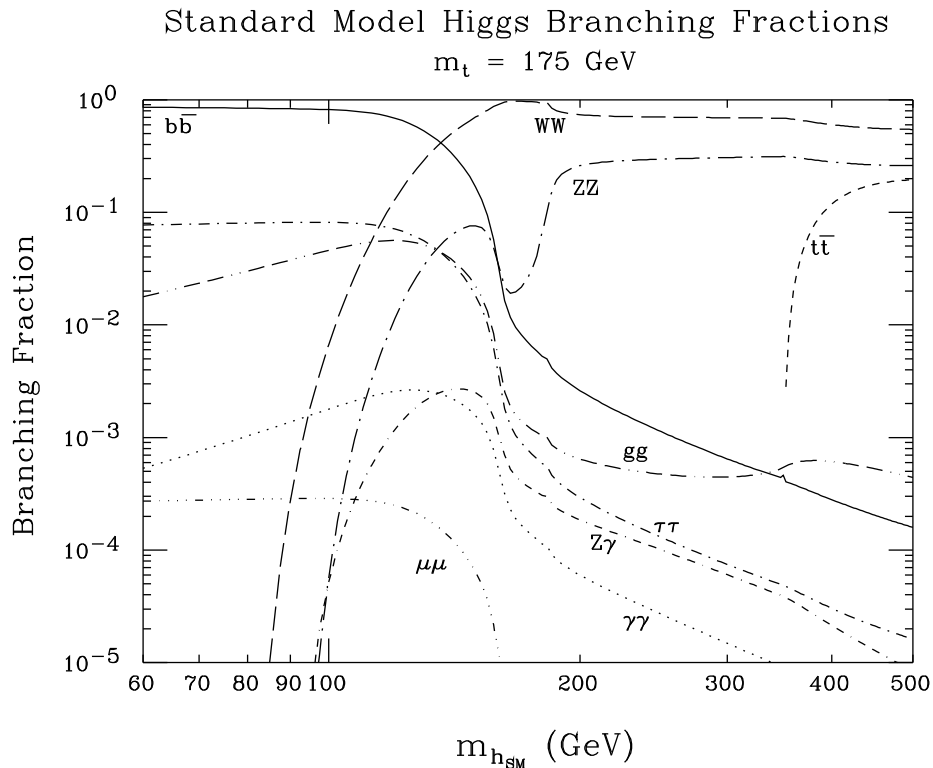
Figure 5: Branching fractions for the Standard Model h_{SM}.

Finally, it is relevant to note that in non-minimal extensions of the MSSM, parameter choices are possible such that the lightest Higgs boson to which the bound of Eq. (2) applies has very weak coupling to ZZ. This has been demonstrated [10] in the case of the minimal non-minimal supersymmetric model (MNMSSM), which contains one extra singlet Higgs representation, yielding three neutral Higgs bosons in all. However, for parameter choices such that the lightest Higgs decouples from ZZ, there is a strong upper bound on the mass of the least massive Higgs boson *with significant ZZ coupling*. The proof of this fact in the MNMSSM case relies on the observation that as the lighter Higgs bosons decouple from ZZ, the upper bound on

8

the next heaviest Higgs boson moves down. This result may generalize to the case of more singlets.

1.2 s-channel Higgs boson physics at $\mu^+\mu^-$ colliders

The ability of a new accelerator to fully explore EWSB physics weighs heavily in its justification. Recently, there has been much interest in the possibility of constructing a $\mu^+\mu^-$ collider [11,12,13,14], and a survey of the physics opportunities at such a collider has been made [15]. It is currently anticipated that a $\mu^+\mu^-$ collider can, at a minimum, achieve the same integrated luminosities and energies as an e^+e^- collider [16,17,18]. Further, with adequate detector segmentation the extra backgrounds resulting from muon decays can be tamed [19]. It then follows that a $\mu^+\mu^-$ collider can essentially explore all the same physics that is accessible at an e^+e^- collider of the same energy. In particular, all the established techniques for probing EWSB at e^+e^- colliders are applicable at a $\mu^+\mu^-$ collider. In addition, should one or more Higgs boson(s) (generically denoted by h) with substantial $\mu^+\mu^-$ coupling(s) exist, a $\mu^+\mu^-$ collider opens up the particularly interesting possibility of direct s-channel $\mu^+\mu^- \to h$ production. The SM Higgs boson, h_{SM}, is a prototypic example. Direct s-channel h_{SM} production is greatly enhanced at a $\mu^+\mu^-$ collider compared to an e^+e^- collider because its coupling to the incoming $\mu^+\mu^-$ is proportional to the lepton mass. Quantitative studies of s-channel Higgs production have been presented in Refs. [15,20]. With the machine energy set to the Higgs mass ($\sqrt{s} = m_h$) the $\mu^+\mu^- \to h_{SM}$ rate is sufficiently large to allow detection of the h_{SM}, provided that $m_{h_{SM}} \lesssim 2m_W$ (the so-called intermediate Higgs mass region). In addition, *all* the Higgs bosons of the minimal supersymmetric model (MSSM) are produced in sufficient abundance in s-channel $\mu^+\mu^-$ collisions to allow their detection for most of the model parameter space.

In the present report, we expand on these results and provide the documentation underlying the discussion of Ref. [20] on precision studies of both the SM h_{SM} and the MSSM Higgs bosons. We find that the basic properties of the h_{SM} can be determined with remarkable accuracy in $\mu^+\mu^-$ s-channel production, and that the properties of MSSM Higgs bosons can be detailed over a larger fraction of model parameter space than at any other proposed accelerator. One particularly important conclusion is that s-channel Higgs production at a $\mu^+\mu^-$ collider of appropriate design has greater

9

potential for distinguishing between a light SM h_{SM} and the SM-like h^0 of the MSSM than other processes/machines. The techniques and strategies for attaining the above results, and the associated requirements for the machine and detector, are discussed at length.

Two possible $\mu^+\mu^-$ machines are being actively studied [12,13,14]:

- A first muon collider (FMC, for short) with low c. m. energy ($\sqrt{s}$) between 100 and 500 GeV and $\mathcal{L} \sim 2 \times 10^{33}\,\mathrm{cm}^{-2}\,\mathrm{s}^{-1}$ delivering an annual integrated integrated luminosity $L \sim 20\ \mathrm{fb}^{-1}$.

- A next muon collider (NMC) with high $\sqrt{s} \gtrsim 4$ TeV and $\mathcal{L} \sim 10^{35}\,\mathrm{cm}^{-2}\,\mathrm{s}^{-1}$ giving $L \sim 1000\ \mathrm{fb}^{-1}$ yearly; the extent to which such a machine could be run at high luminosity for $\sqrt{s}$ values starting at 500 GeV remains to be determined.

One of our goals will be to quantify the amount of integrated luminosity that is required to detect and study the various Higgs bosons via s-channel production as the Higgs mass is varied. For s-channel study of a SM-like Higgs boson, only the lower energy machine is relevant because a SM-like Higgs can only be detected in s-channel collisions if it has mass $\lesssim 2m_W$, given the anticipated luminosity. However, higher $\sqrt{s}$ will be important if the MSSM is the correct theory. The expected luminosity will allow detection and study of the heavier MSSM Higgs bosons (the CP-odd A^0 and the CP-even H^0) via s-channel production at the FMC for m_{A^0}, m_{H^0} up to the maximal $\sqrt{s}$. If the NMC can be run with high luminosity at $\sqrt{s}$ values starting at the maximal FMC energy (~ 500 GeV) and above, then the ability to discover the A^0 and H^0 via s-channel production would extend to correspondingly higher masses.

For s-channel Higgs studies, it will be important to deliver the maximum possible luminosity at c.m. energies where Higgs bosons are either expected or observed. Fortunately, this should be possible for the proposed FMC designs due to the fact that the final muon storage ring(s) would comprise a modest fraction of the overall cost [21]. (The most costly component of a muon collider is the muon source — decays of pions produced by proton collisions.) It is thus envisioned that multiple storage rings could eventually be tailor-made for c.m. energies spanning the desired range. This approach could presumably also be used to allow the high energy NMC to run with high luminosity at $\sqrt{s}$ values starting at ~ 500 GeV, where the FMC leaves off.

A crucial machine parameter for s-channel studies of Higgs bosons is the energy resolution of the colliding beams. A Gaussian shape for the energy spectrum of

10

each beam is expected to be a good approximation, with an rms deviation, R, most naturally in the range [22]

$$R = 0.04\% \text{ to } 0.08\%$$

which could be decreased to as low as

$$R = 0.01\%$$

via additional cooling. Excellent energy resolution is mandatory to detect and study a Higgs boson with a very narrow width, which is the case for the h_{SM} with $m_{h_{SM}} \lesssim 2m_W$ and the lightest MSSM Higgs boson. The large value of the muon mass compared to the electron mass makes possible the required energy resolution in three ways:

i) it is possible (albeit, probably expensive) to achieve $R = 0.01\%$;

ii) bremsstrahlung smearing, while non-negligible, leaves a large portion of the narrow central Gaussian beam energy peak intact.

iii) designs with small beamstrahlung are naturally achieved;

Henceforth, we neglect beamstrahlung since quantitative calculations of this are unavailable.

The rms spread in $\sqrt{s}$ (denoted by $\sigma_{\sqrt{s}}$) prior to including bremsstrahlung is given by

$$\sigma_{\sqrt{s}} = R\sqrt{s}/\sqrt{2} \,, \tag{5}$$

where R is the resolution in the energy of each beam. A convenient formula for $\sigma_{\sqrt{s}}$ is

$$\sigma_{\sqrt{s}} = (7 \text{ MeV}) \left(\frac{R}{0.01\%} \right) \left(\frac{\sqrt{s}}{100 \text{ GeV}} \right) \,. \tag{6}$$

The critical issue is how this resolution compares to the calculated total widths of Higgs bosons when $\sqrt{s} = m_h$. For $R \lesssim 0.01\%$, the energy resolution in Eq. (6) is smaller than the Higgs widths in Fig. 3 for all but a light SM-like Higgs. We shall demonstrate that the smallest possible R allows the best measurement of a narrow Higgs width, and that the total luminosity required for discovery by energy scanning when $\Gamma_h^{\text{tot}} \lesssim \sigma_{\sqrt{s}}$ is minimized by employing the smallest possible R. For a Higgs boson with width larger than $\sigma_{\sqrt{s}}$, results from a fine scan with small R can be
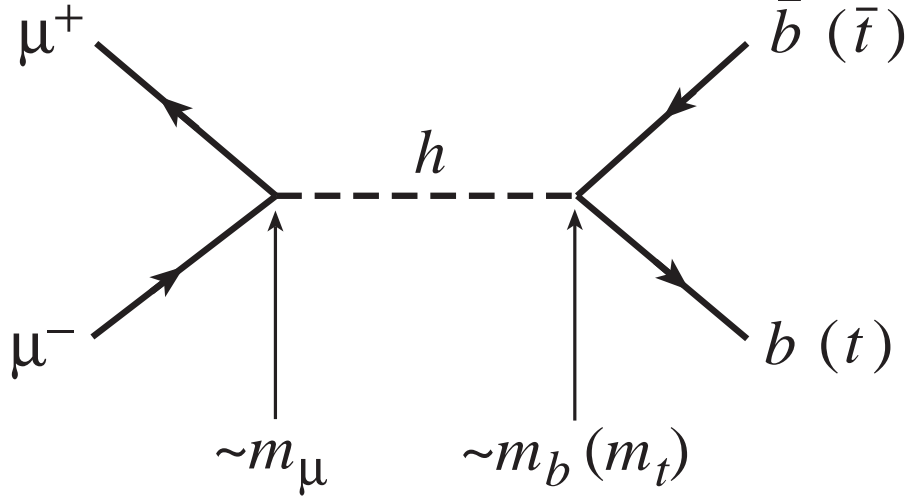
11

Figure 6: s-channel diagram for production of a Higgs boson.

combined without any increase in the luminosity required for discovery and width measurement.

The Feynman diagram for s-channel Higgs production is illustrated in Fig. 6. The s-channel Higgs resonance cross section is

$$\sigma_h(\sqrt{\hat{s}}) = \frac{4\pi\Gamma(h \to \mu\mu)\,\Gamma(h \to X)}{\left(\hat{s} - m_h^2\right)^2 + m_h^2[\Gamma_h^{\text{tot}}]^2} \ , \tag{7}$$

where $\hat{s} = (p_{\mu^+} + p_{\mu^-})^2$ is the c. m. energy squared of a given $\mu^+\mu^-$ annihilation, X denotes a final state and Γ_h^{tot} is the total width.* The sharpness of the resonance peak is determined by Γ_h^{tot}. Neglecting bremsstrahlung for the moment, the effective signal cross section is obtained by convoluting $\sigma_h(\hat{s})$ with the Gaussian distribution in $\sqrt{\hat{s}}$ centered at $\sqrt{\hat{s}} = \sqrt{s}$:

$$\overline{\sigma}_h(\sqrt{s}) = \int \sigma_h(\sqrt{\hat{s}})\, \frac{\exp\left[-(\sqrt{\hat{s}} - \sqrt{s})^2\big/(2\sigma_{\sqrt{s}}^2)\right]}{\sqrt{2\pi}\sigma_{\sqrt{s}}}\, d\sqrt{\hat{s}} \ . \tag{8}$$

Figure 7 illustrates the effective cross section, $\overline{\sigma}_h(\sqrt{s})$, as a function of $\sqrt{s}$ for $m_h = 110$ GeV and beam energy resolutions of $R = 0.01\%$, $R = 0.06\%$, and $R = 0.1\%$.

---

*Effects arising from implementing an energy-dependent generalization of the $m_h\Gamma_h^{\text{tot}}$ denominator component of this simple resonance form are of negligible importance for our studies, especially for a Higgs boson with $\Gamma_h^{\text{tot}} \ll m_h$.

Results are given for the cases: h_{SM}, h^0 with $\tan\beta = 10$, and h^0 with $\tan\beta = 20$. All channels X are summed over.
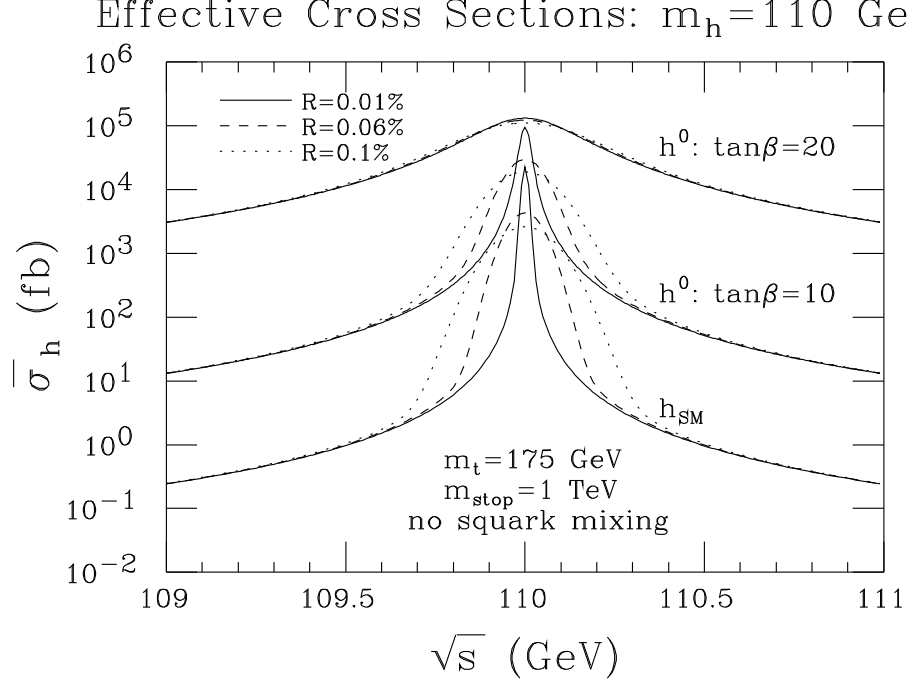

Figure 7: The effective cross section, $\overline{\sigma}_h$, obtained after convoluting σ_h with the Gaussian distributions for $R = 0.01\%$, $R = 0.06\%$, and $R = 0.1\%$, is plotted as a function of $\sqrt{s}$ taking $m_h = 110$ GeV. Results are displayed in the cases: h_{SM}, h^0 with $\tan\beta = 10$, and h^0 with $\tan\beta = 20$. In the MSSM h^0 cases, two-loop/RGE-improved radiative corrections have been included for Higgs masses, mixing angles, and self-couplings assuming $m_{\widetilde{t}} = 1$ TeV and neglecting squark mixing. The effects of bremsstrahlung are not included in this figure.

In the case where the Higgs width is much smaller than the Gaussian width $\sigma_{\sqrt{s}}$, the effective signal cross section result for $\sqrt{s} = m_h$, denoted by $\overline{\sigma}_h$, is

$$\overline{\sigma}_h = \frac{2\pi^2 \Gamma(h \to \mu\mu)\, BF(h \to X)}{m_h^2} \times \frac{1}{\sigma_{\sqrt{s}}\sqrt{2\pi}} \qquad (\Gamma_h^{\text{tot}} \ll \sigma_{\sqrt{s}}) \, . \tag{9}$$

Henceforth, we adopt the shorthand notation

$$G(X) = \Gamma(H \to \mu\mu)\, BF(h \to X) \tag{10}$$

13

for the numerator of Eq. (9). The increase of $\overline{\sigma}_h(\sqrt{s} = m_h)$ with decreasing $\sigma_{\sqrt{s}}$ when $\Gamma_h^{\rm tot} \ll \sigma_{\sqrt{s}}$ is apparent from the h_{SM} curves of Fig. 7. In the other extreme where the Higgs width is much broader than $\sigma_{\sqrt{s}}$, then at $\sqrt{s} = m_h$ we obtain

$$\overline{\sigma}_h = \frac{4\pi BF(h \to \mu\mu)BF(h \to X)}{m_h^2} \qquad (\Gamma_h^{\rm tot} \gg \sigma_{\sqrt{s}}) . \qquad (11)$$

Note that this equation implies that if there is a large contribution to the Higgs width from some channel other than $\mu\mu$, we will get a correspondingly smaller total event rate due to the small size of $BF(h \to \mu\mu)$. That $\overline{\sigma}_h(\sqrt{s} = m_h)$ is independent of the value of $\sigma_{\sqrt{s}}$ when $\Gamma_h^{\rm tot} \gg \sigma_{\sqrt{s}}$ is illustrated by the $\tan\beta = 20$ curves for the h^0 in Fig. 7. Raw signal rates (*i.e.* before applying cuts and including other efficiency factors) are computed by multiplying $\overline{\sigma}_h$ by the total integrated luminosity L.

The basic results of Eqs. (9) and (11) are modified by the effects of photon bremsstrahlung from the colliding muon beams. In the case of a narrow Higgs boson, the primary modification for $\sqrt{s} = m_h$ is due to the fact that not all of the integrated luminosity remains in the central Gaussian peak. These modifications are discussed in Appendix A; to a good approximation, the resulting signal rate is obtained by multiplying $\overline{\sigma}_h$ of Eq. (9) by the total luminosity L times the fraction f of the peak luminosity in the Gaussian after including bremsstrahlung relative to that before (typically $f \approx 0.6$). For a broad Higgs resonance, the lower energy tail in the luminosity distribution due to bremsstrahlung makes some contribution as well. In the results to follow, we avoid any approximation and numerically convolute the full effective luminosity distribution (including bremsstrahlung) with the Higgs cross section of Eq. (7). In performing this convolution, we require that the effective $\mu^+\mu^-$ c.m. energy be within 10 GeV of the nominal value. Such a requirement can be implemented by reconstructing the mass of the final state as seen in the detector; planned detectors would have the necessary resolution to impose the above fairly loose limit. This invariant mass selection is imposed in order to reduce continuum (non-resonant) backgrounds that would otherwise accumulate from the entire low-energy bremsstrahlung tail of the luminosity distribution.

As is apparent from Fig. 7, discovery and study of a Higgs boson with a very narrow width at the $\mu^+\mu^-$ collider will require that the machine energy $\sqrt{s}$ be within $\sigma_{\sqrt{s}}$ of m_h. The amount of scanning required to find the correct $\sqrt{s}$ depends upon R. From Fig. 7 it is apparent that the larger R is, the less the accuracy with which the machine energy needs to be set at each scan point and the fewer the number of

14

scan points needed. But, small R results in much greater event rate for $\sqrt{s} \simeq m_h$. *If $\sqrt{s}$ can be rapidly changed with an accuracy that is a small fraction of R*, then we shall find that smaller R implies that less total time (and, hence, luminosity) will be required for the scan. Further, we find that $R \sim 0.01\%$ and the ability to set $\sqrt{s}$ with an accuracy of order 1 part in 10^6 are both required if we are to be able to measure the Higgs width with sufficient precision to distinguish between the SM h_{SM} and the MSSM h^0 when the latter is SM-like. Thus, for a $\mu^+\mu^-$ collider to reach its full potential, it should be designed so that $R \sim 0.01\%$ and so that it is possible to vary $\sqrt{s}$ rapidly and with great precision. These are not insurmountable tasks [21], but careful planning is certainly required. For Higgs bosons with a large width, the design demands upon the $\mu^+\mu^-$ collider are clearly less.

Due to the bremsstrahlung tail, it is also possible to search for a Higgs boson by running the $\mu^+\mu^-$ collider at an energy well above the mass of the Higgs boson itself. In some collisions, one (or both) of the muons will have radiated enough of its initial energy that the effective $\sqrt{\hat{s}}$ of the collision is much lower than $\sqrt{s}$. In this circumstance, detection of the Higgs boson requires reconstruction with good resolution of the effective $\sqrt{\hat{s}}$ of each collision from the final state momenta. For a final state mass bin centered at $\sqrt{\hat{s}} = m_h$, if $d\mathcal{L}/d\sqrt{\hat{s}}$ is slowly varying in the vicinity of $\sqrt{\hat{s}} = m_h$ over an interval several times the Higgs total width Γ_h^{tot}, the effective cross section is

$$\overline{\sigma}_h = \frac{2\pi^2 \Gamma(h \to \mu\mu) BF(h \to X)}{m_h^2} \times \left. \frac{d\mathcal{L}}{d\sqrt{\hat{s}}} \right|_{\sqrt{\hat{s}}=m_h} . \tag{12}$$

In exploring the possible utility of this bremsstrahlung tail for Higgs detection, we have performed our explicit calculations using the spectrum obtained for $R = 0.1\%$. However, we note that the bremsstrahlung tail well away from the central Gaussian peak is essentially independent of the beam energy resolution R. If a mass resolution in the final state of ± 5 GeV is possible in the $b\bar{b}$ final state, then even when running the FMC at full nominal energy of $\sqrt{s} = 500$ GeV we find that it will be possible to detect a Higgs boson with m_h in a broad range below $\sqrt{s}$ (but not near m_Z) provided that the $h \to \mu^+\mu^-$ coupling is significantly enhanced with respect to the SM $h_{SM} \to \mu^+\mu^-$ coupling. The total integrated luminosity required for Higgs discovery using the bremsstrahlung tail will be compared to that needed for discovery by scanning using a large number of $\sqrt{s}$ machine energy settings.

Highly polarized beams may be possible since the muons are naturally polarized

from $\pi^\pm$ ($K^\pm$) decays in the parent rest-frame. However, the luminosity for polarized beams may be significantly reduced during the cooling and acceleration process. If a degree of polarization P is possible for *both* beams, then, relative to the unpolarized case, the s-channel Higgs signal is enhanced by the factor $(1 + P^2)$ while the background is suppressed by $(1 - P^2)$. High polarization P of both beams would be useful if the luminosity reduction is less than a factor of $(1 + P^2)^2 / (1 - P^2)$, *i.e.* the factor which would leave the significance of the signal unchanged. For example, $P = 0.84$ would compensate a factor of 10 reduction in luminosity [23]. We mainly present our results without assuming high polarization beams, but we comment on improvements with beam polarization.

With this introduction, we now proceed with a detailed description of the capability of a $\mu^+\mu^-$ collider to detect and study different types of Higgs bosons. In the next section, we begin with SM-like Higgs bosons. The following section explores the non-SM-like Higgs bosons of the MSSM. The final section gives our conclusions.

2 A SM-like Higgs boson

We first review the prospects for discovering and studying a SM-like Higgs boson without s-channel production at a $\mu^+\mu^-$ collider. We then turn to the role of s-channel $\mu^+\mu^- \to h$ production, emphasizing the prospects for precision studies of the Higgs mass and width.

2.1 Discovery and study without s-channel production

Neutral Higgs bosons that are coupled to ZZ with roughly SM-like strength can be discovered via $Z^\star \to Zh$ production for $m_h \lesssim 0.7\sqrt{s}$ at either an e^+e^- collider or a $\mu^+\mu^-$ collider [24]. This discovery reach applies to both the h_{SM} and to the h^0 of the MSSM in the large-m_{A^0} portion of parameter space where it is SM-like in its couplings. The stringent upper bound on m_{h^0}, Eq. (1), in the MSSM implies that even a $\sqrt{s} = 300$ GeV machine is guaranteed to find the h^0 if it exists.

As described in the Introduction, we can also consider adding extra singlets to the MSSM two-doublet Higgs sector. In the MNMSSM model, containing one singlet Higgs field, we noted that even if the lightest Higgs boson has small ZZ coupling, there is always a CP-even Higgs boson with substantial ZZ coupling and modest

16

mass. Refs. [10] demonstrate that at least one of the CP-even Higgs bosons of the MNMSSM model will be detected in the Zh mode at a machine with c.m. energy $\sqrt{s} = 500$ GeV. Since it appears that this result may generalize to the case of more than one additional singlet, we regard it as relatively certain that any supersymmetric theory in the SUSY GUT context will contain at least one CP-even Higgs boson that will be discovered in the Zh mode at a machine with $\sqrt{s} = 500$ GeV, and its mass will be in the intermediate mass range ($\lesssim 2m_W$).

Assuming that a SM-like h is discovered in the Zh mode, an important question for s-channel production and study of the h in $\mu^+\mu^-$ collisions is the accuracy with which its mass can be measured á priori via Zh production. The better this accuracy, the easier it will be to set $\sqrt{s}$ of the $\mu^+\mu^-$ collider to a value centered on m_h within the rms spread $\sigma_{\sqrt{s}}$. Another critical question bearing on the importance of the s-channel $\mu^+\mu^- \to h$ production mode is whether the Zh mode is useful for measurement of the h width. We find that it is not.

Generally speaking, the accuracy of the Higgs boson mass measurements depends on the detector performance and the signal statistics. As a general guide, we consider two examples for the uncertainty on m_h in the mass range $m_h < 2m_W$ (*i.e.* below where W-pair decays become important)

$$\Delta m_h \simeq 4.0 \text{ GeV}/\sqrt{N} \quad (\text{SLD}), \tag{13}$$

$$\simeq 0.3 \text{ GeV}/\sqrt{N} \quad (\text{super} - \text{LC}). \tag{14}$$

where our notation will always be that ΔX represents the absolute magnitude of the 1σ error on the quantity X; that is the 1σ limits on X are $X \pm \Delta X$. Equation (13) results for performance typified by the SLD detector [25], where 4 GeV is the single event resolution and N is the number of events in the $Z(\to q\bar{q})h(\to b\bar{b})$, $Z(\to q\bar{q})h(\to \tau\bar{\tau})$, plus $Z(\to \ell^+\ell^-)h(\to$ any$)$ modes. For a SM-like Higgs, these modes have an effective final state branching fraction that varies between about 70% and 50% as m_h varies from low masses up to 140 GeV. We plot Δm_h in Fig. 8 according to Eqs. (13) and (14), with $N = \epsilon L \sigma(Zh) BF(\text{effective})$, assuming detection efficiencies of $\epsilon = 0.9$ [$\epsilon = 0.5$] for the $Z(\to \ell^+\ell^-)h(\to$ any$)$ [$Z(\to q\bar{q})h(\to b\bar{b})$, $Z(\to q\bar{q})h(\to \tau\bar{\tau})$] modes and assuming a fixed $\sqrt{s} = 500$ GeV. For SLD detector performance, results for luminosities of $L = 1, 10$, and 50 fb^{-1} are shown; with these integrated luminosities, m_h (for $m_h \lesssim 150$ GeV) will be determined to an accuracy of at least 1.4, 0.5, 0.21 GeV (respectively).
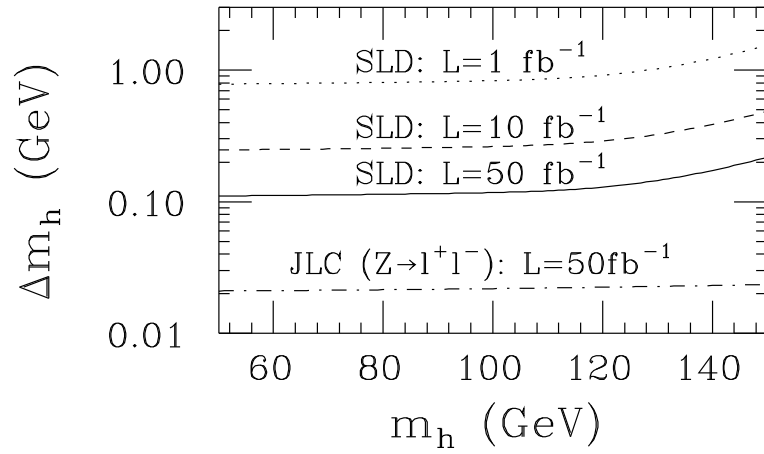
Figure 8: The uncertainty Δm_h in the determination of m_h for a SM-like Higgs boson using Zh production and a ± 4 GeV single event mass resolution, as for an SLD-type detector, and for a ± 0.3 GeV single event mass resolution in the $Z(\to \ell^+\ell^-)h(\to$ any) mode, as for the super-LC detector.

Equation (14) is applicable for a "super" performance Linear Collider detector (hereafter referred to as the super-LC detector) [26,27], the special features of which include excellent momentum resolutions and high b-tagging efficiency. For this detector, the best determination of $m_{h_{SM}}$ is obtained by examining the recoil mass peak in Zh_{SM} production. For $Z \to \ell^+\ell^-$ events, the resolution for the recoil mass is expected to be of order 0.3 GeV per event. A measurement of $m_{h_{SM}}$ to ± 0.3 GeV$/\sqrt{N} \sim \pm 20$ MeV would be possible for $m_{h_{SM}} \lesssim 140$ GeV and $L = 50$ fb^{-1}, as illustrated in Fig. 8, assuming detection efficiency of $\epsilon = 0.9$ for the $Z(\to \ell^+\ell^-)h(\to$ any) mode. The total width $\Gamma_{h_{SM}}^{\rm tot}$ could also be measured down to ~ 200 MeV using the Zh_{SM} recoil mass distribution. However, this latter sensitivity is not likely to be useful since $\Gamma_{h_{SM}} \lesssim 10$ MeV for $m_{h_{SM}} \lesssim 140$ GeV (see Fig. 3).

It could happen that there is no e^+e^- collider at the time the $\mu^+\mu^-$ collider is built but that the LHC has been operational for several years. One of the primary modes for discovery of a SM-like Higgs boson at the LHC is the $\gamma\gamma$ mode. Simulations by the LHC collaborations indicate that this mode is detectable for $50 \lesssim m_h \lesssim 150$ GeV. For $m_h \gtrsim 130$ GeV, discovery will be possible in the 4ℓ mode. Both modes, but especially the $\gamma\gamma$ mode, offer the possibility of a very accurate determination of the Higgs mass. Resolution will be 1% or better in the $\gamma\gamma$ mode, and probably not much worse than 1% in the 4ℓ mode. Thus, even in the absence of an e^+e^- collider, the LHC can reasonably be expected to provide us with a $\lesssim 1\%$ determination of m_h in the mass region where the Higgs total width is small.

2.2 s-channel production of a SM-like h

Once a SM-like Higgs boson is found in the Zh mode at either an e^+e^- collider or the $\mu^+\mu^-$ collider itself,[†] or at the LHC, it will generally be easy to also produce and detect it via direct s-channel production at a $\mu^+\mu^-$ collider [20] if $m_h \lesssim 2m_W$. Should there be no e^+e^- collider in operation, an important question at a $\mu^+\mu^-$ collider will then be whether to concentrate subsequent running on s-channel production or on Zh production, as the best means for studying the properties of the h in detail. Generally speaking, these two different processes provide complementary information and it would be very valuable to accumulate substantial integrated luminosity in both

---

[†] While discovery at a $\mu^+\mu^-$ collider is also possible by scanning in s, the Zh mode is more luminosity efficient for discovery.

modes.

The potential importance of s-channel production of a SM-like h is illustrated by two facts pertaining to distinguishing between the MSSM h^0 and the SM h_{SM}.

(1) Expected experimental errors imply that the ability to discriminate between the SM h_{SM} and the MSSM h^0 on the basis of the branching fractions and production rates that can be measured in the Zh channel is limited to m_{A^0} values below about 300 GeV [1].

(2) Both the total width and the production rate (proportional to $\Gamma(h \to \mu^+\mu^-)$) of a SM-like h could be measured at a muon collider with sufficient accuracy so as to distinguish the h^0 from the h_{SM} in the large-m_{A^0} region 300 GeV $\lesssim m_A \lesssim$ 600 GeV where the h^0 is approximately SM-like.

A quantitative discussion of the MSSM parameter space region for which deviations of the total width and production rate from SM expectations are measurable will be given later. For now we emphasize that (2) requires the excellent $R = 0.01\%$ beam energy resolution.

2.2.1 Choosing the right $\sqrt{s}$

Our proposed strategy is to first discover the SM-like h via $\ell^+\ell^- \to Zh$ or in hadron collisions in order to determine the $\sqrt{s}$ region in which $\mu^+\mu^- \to h$ s-channel production should be explored. If Γ_h^{tot} is smaller than the rms spread $\sigma_{\sqrt{s}}$ in $\sqrt{s}$ (as is the case for the SM when $m_{h_{SM}} \lesssim 140$ GeV), then to obtain the maximum $\mu^+\mu^- \to h$ production rate it is necessary to set $\sqrt{s}$ equal to m_h within $\lesssim \sigma_{\sqrt{s}}$. The ability to do this is assessed by comparing the errors on m_h from Zh production to both the $\sqrt{s}$ spread $\sigma_{\sqrt{s}}$ at a $\mu^+\mu^-$ collider and to Γ_h^{tot}. As an illustration, consider $h = h_{SM}$. With the super-LC $L = 50$ fb^{-1} determination of $m_{h_{SM}}$ to ± 20 MeV, $\sigma_{\sqrt{s}}$ for $R = 0.01\%$ will be at worst a factor of 2 or 3 smaller than the uncertainty in $m_{h_{SM}}$ and only two or three tries will be needed to set the $\mu^+\mu^-$ collider energy to a value equal to $m_{h_{SM}}$ within the rms spread in $\sqrt{s}$. If the SLD $L = 50$ fb^{-1} determination of $m_{h_{SM}}$ to 210 MeV is all that is available, then for $m_{h_{SM}} \lesssim 2m_W$ two or three tries would be adequate to set $\sqrt{s} \simeq m_{h_{SM}}$ within $\sigma_{\sqrt{s}}$ only if $R = 0.06\%$. The number of settings required in the case of $R = 0.01\%$ would be a factor of 6 larger. If only SLD performance and $L = 1$ fb^{-1} is available in the Zh_{SM} mode, or if

20

only a $\sim 1\%$ determination of $m_{h_{SM}}$ from the LHC is provided, both of which imply errors on $m_{h_{SM}}$ that are $\gtrsim 1$ GeV, then even with $R = 0.06\%$ one must scan over 10 to 20 $\sqrt{s}$ values to determine the central $\sqrt{s} \simeq m_{h_{SM}}$ value within the rms $\sqrt{s}$ error, $\sigma_{\sqrt{s}}$. Later, we will compute the amount of luminosity that must be invested at each $\sqrt{s} = m_h$ choice in order to detect a SM-like Higgs signal.

In contrast to the above narrow width situation, for $m_{h_{SM}} \gtrsim 200$ GeV one finds $\Gamma_{h_{SM}}^{\text{tot}} \gtrsim \sigma_{\sqrt{s}}$ for $R \leq 0.06\%$. Then, even if $m_{h_{SM}}$ is only known to within $\Gamma_{h_{SM}}^{\text{tot}}$, we can immediately set $\sqrt{s}$ for the $\mu^+\mu^-$ collider to be within the Higgs peak. Unfortunately, we find that the event rate in s-channel collisions is too low to allow detection of the h_{SM} in this case. This situation does not arise in the case of the h^0 of the MSSM, which is guaranteed to have $m_{h^0} \lesssim 130$ GeV.

2.2.2 Detecting a SM-like h in the s-channel

The effective cross section, $\overline{\sigma}_{h_{SM}}(\sqrt{s} = m_{h_{SM}})$ for inclusive SM Higgs production is given in Fig. 9 versus $\sqrt{s} = m_{h_{SM}}$ for resolutions of $R = 0.01\%$, 0.06%, 0.1% and 0.6%. These results include Gaussian and bremsstrahlung smearing effects. For comparison, the $\mu^+\mu^- \to Z^\star \to Zh_{SM}$ cross section is also shown, evaluated at the energy $\sqrt{s} = m_Z + \sqrt{2}m_{h_{SM}}$ for which it is a maximum. The s-channel $\mu^+\mu^- \to h_{SM}$ cross sections for small R and $m_{h_{SM}} \lesssim 2m_W$ are much larger than the corresponding Zh_{SM} cross section. The increase in the $\mu^+\mu^- \to h_{SM}$ cross section that results if bremsstrahlung smearing is removed is illustrated in the most sensitive case ($R = 0.01\%$).

For a SM-like Higgs boson, the only potentially useful final state modes X are $b\overline{b}$, $WW^{(\star)}$ and $ZZ^{(\star)}$, where the $^{(\star)}$ indicates the possibility that the weak boson is virtual. The $t\overline{t}$ channel does not give a viable signal for the range of luminosity that we consider. All these channels have irreducible backgrounds from $\mu^+\mu^-$ continuum production processes. We note that

(a) The light-quark backgrounds to the $b\overline{b}$ channel can be rejected using b-tagging. We assume a 50% efficiency for isolating the $2b$ final state (via tagging one of the b's); this efficiency is to include cuts and detector efficiencies.

(b) For the $b\overline{b}$ final state, we have checked that interference between the s-channel signal and the backgrounds is never of importance. This is because the Higgs signal contributes to RR and LL helicity amplitudes for the incoming muons,
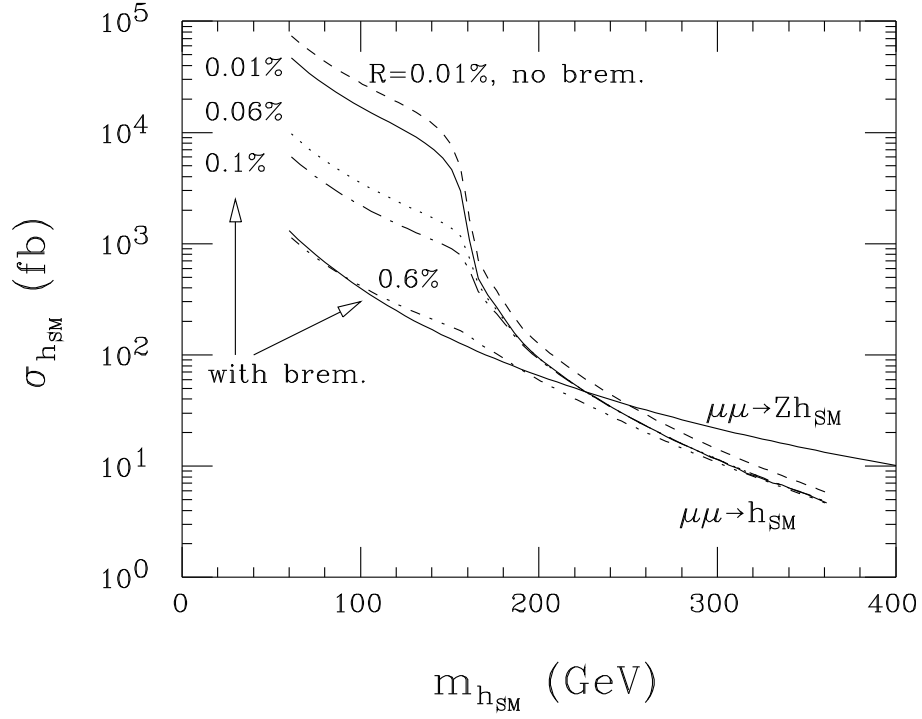
Figure 9: Cross sections versus $m_{h_{SM}}$ for inclusive SM Higgs production: (i) the s-channel $\overline{\sigma}_h$ for $\mu^+\mu^- \to h_{SM}$ with $R = 0.01\%$, 0.06%, 0.1% and 0.6%, and (ii) $\sigma(\mu^+\mu^- \to Zh_{SM})$ at $\sqrt{s} = m_Z + \sqrt{2}m_{h_{SM}}$. Also shown is the result for $R = 0.01\%$ if bremsstrahlung effects are not included.

22

whereas the backgrounds come almost entirely from RL and LR helicity combinations (the RR and LL background contributions are suppressed by a factor of m_μ/E at the amplitude level).

(c) For the $WW^{(\star)}$ and $ZZ^{(\star)}$ final states the useful channels depend upon whether or not the $W^{(\star)}$ or $Z^{(\star)}$ is virtual. We shall find that discovery in these channels is only possible for $m_h \lesssim 2m_W$, in which case the final states of interest are $WW^\star \to \ell\nu 2j$ with $BF_{WW}^{\text{eff}} \sim 0.3$ and $ZZ^\star \to 2\ell 2j, 2\nu 2j, 4\ell, 2\ell 2\nu$ with $BF_{ZZ}^{\text{eff}} \sim 0.42$, $4j$ final states having too large a QCD background and mass reconstruction of the real W or Z being impossible in the $2\ell 2\nu$ or 4ν final states, respectively. (Here, we consider only $\ell = e$ or μ.) In our analysis, we assume an overall efficiency of 50% for isolating these channels. For the $ZZ^\star$, a cut requiring that $M^\star$ (the invariant mass of the virtual $Z^\star$) be greater than a given value $M^{\star\,\text{min}}$ is imposed. Full details regarding our procedures in the $WW^{(\star)}$ and $ZZ^{(\star)}$ channels are presented in Appendix B.

The h_{SM} signal and background cross sections, $\epsilon\overline{\sigma}BF(X)$, for $X = b\overline{b}$, and the above $WW^{(\star)}$ and $ZZ^{(\star)}$ final states are presented in Fig. 10 (including a channel-isolation efficiency of $\epsilon = 0.5$) as a function of $m_{h_{SM}}$ for SM Higgs s-channel production with resolution $R = 0.01\%$ and $R = 0.06\%$. For both resolutions, we also plot the luminosity required for a $S/\sqrt{B} = 5\sigma$ signal in the $b\overline{b}$, $WW^{(\star)}$ and $ZZ^{(\star)}$ channels. In the case of the $WW^{(\star)}$ final state, we give event rates only for the mixed leptonic/hadronic final state modes; in the case of the $ZZ^{(\star)}$ final state we include the mixed hadronic/leptonic and (visible) purely leptonic final state modes listed earlier. From Fig. 10 we see that:

- $R = 0.01\%$, $L = 0.1$ fb^{-1} would yield a detectable s-channel Higgs signal for all $m_{h_{SM}}$ values between the current LEP I limit of 63 GeV and $2m_W$ except in the region of the Z peak; a luminosity $L \sim 1$ fb^{-1} at $\sqrt{s} = m_{h_{SM}}$ is needed for $m_{h_{SM}} \sim m_Z$.

- For $R = 0.06\%$, 5σ signals typically require about 20–30 times the luminosity needed for $R = 0.01\%$; $L = 30$ fb^{-1} would be required for a 5σ signal if $m_{h_{SM}} \sim m_Z$.

This argues for a $\mu^+\mu^-$ collider design with R near the 0.01% level. A search for the h_{SM} (or any Higgs with width smaller than the achievable resolution) by scanning
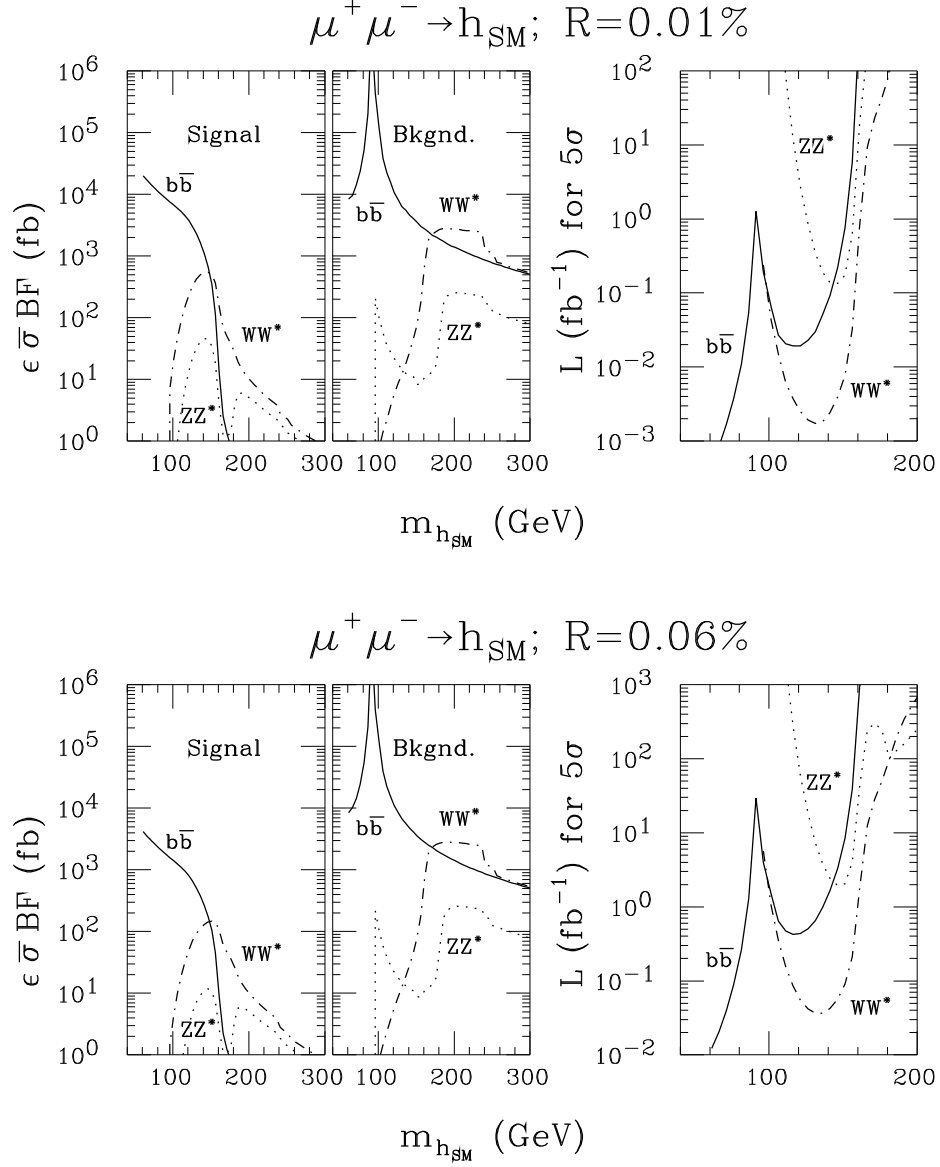
23

Figure 10: The (a) h_{SM} signal and (b) background cross sections, $\epsilon\overline{\sigma}BF(X)$, for $X = b\overline{b}$, and useful (reconstructable, non-4j) $WW^{(\star)}$ and $ZZ^{(\star)}$ final states (including a channel-isolation efficiency of $\epsilon = 0.5$) versus $m_{h_{SM}}$ for SM Higgs s-channel production. Also shown: (c) the corresponding luminosity required for a $S/\sqrt{B} = 5$ standard deviations signal in each of the three channels. Results for $R = 0.01\%$ and $R = 0.06\%$ are given.

would be most efficient for the smallest possible R. For a specific illustration, let us consider $m_{h_{SM}} \sim 110$ GeV and assume that just $L = 1$ fb^{-1} has been accumulated in the Zh_{SM} mode (at either an e^+e^- collider or at the $\mu^+\mu^-$ collider itself). Fig. 8 shows that the error in the determination of $m_{h_{SM}}$ will be of order ± 0.8 GeV (assuming an SLD-type detector). How much luminosity will be required to observe the h_{SM} in the s-channel by zeroing in on $m_{h_{SM}}$ within the rms resolution $\sigma_{\sqrt{s}}$? The number of scan points required to cover the 1.6 GeV mass zone at intervals of $\sigma_{\sqrt{s}}$, the luminosity required to observe (or exclude) the Higgs at each point, and the total luminosity required to zero-in on the Higgs using the scan is given in Eq. (15), for resolutions of $R = 0.01\%$ and 0.06%.

$$
\begin{array}{ccccc}
R & \sigma_{\sqrt{s}} & \#\text{points} & L/\text{point} & L_{\text{tot}} \\
0.01\% & 7 \text{ MeV} & 230 & 0.01 \text{ fb}^{-1} & 2.3 \text{ fb}^{-1} \\
0.06\% & 45 \text{ MeV} & 34 & 0.3 \text{ fb}^{-1} & 10.2 \text{ fb}^{-1}
\end{array}
\tag{15}
$$

More generally, the L required at each scan point decreases as (roughly) $R^{1.7}$, whereas the number of scan points only grows like $1/R$, implying that the total L required for the scan decreases as $\sim R^{0.7}$. Thus, the $\mu^+\mu^-$ collider should be constructed with the smallest possible R value. (Note that if the Higgs resonance is broad, using small R, although not necessary, is not harmful since the data from a fine scan can be rebinned to test for its presence.) In the case of a narrow Higgs, a by-product of the above zeroing-in scan will be to ascertain if the Higgs width is in the $\lesssim \sigma_{\sqrt{s}}$ range. However, the large number of $\sqrt{s}$ settings required when conducting a scan with small R implies that it must be possible to quickly and precisely adjust the energy of the $\mu^+\mu^-$ collider. For example, if the machine can deliver 50 fb^{-1} per year and $R = 0.01\%$, so that only $L \sim 0.01$ fb^{-1} should be devoted to each point, we must be able to step the machine energy in units of ~ 7 MeV once every hour or so.

Let us compare the above procedure, where the Zh mode at low luminosity is used to find the SM-like h and then s-channel collisions are used to zero-in on m_h, to the possibility of searching directly for the h by s-channel scanning without the benefit of Zh data. The latter would be a possible alternative if the $\mu^+\mu^-$ collider were to be built before the light Higgs boson is observed at either the LHC or an e^+e^- collider. The question is whether it is most useful to employ the Zh mode or direct s-channel production for initial discovery. We shall suppose that precision radiative corrections pin down the mass of the SM-like Higgs boson to a 20 GeV interval, although this may

be way too optimistic. Let us again focus on $m_h = 110$ GeV. The number of scan points required to cover the 20 GeV mass zone at intervals of $\sigma_{\sqrt{s}}$, the luminosity required to observe (or exclude) the Higgs at each point, and the total luminosity required to zero-in on the Higgs using the scan is given in Eq. (16), for resolutions of $R = 0.01\%$ and 0.06%.

$$
\begin{array}{ccccc}
R & \sigma_{\sqrt{s}} & \#\text{points} & L/\text{point} & L_{\text{tot}} \\
0.01\% & 7 \text{ MeV} & 2857 & 0.01 \text{ fb}^{-1} & 29 \text{ fb}^{-1} \\
0.06\% & 45 \text{ MeV} & 426 & 0.3 \text{ fb}^{-1} & 128 \text{ fb}^{-1}
\end{array} \tag{16}
$$

Thus, much greater luminosity would be required (not to mention the much greater demands upon the machine for performing efficiently such a broad scan) than if the Zh mode is employed for the initial h discovery. Note that it is not useful to expend more than $L \sim 1$ fb^{-1} in the Zh mode simply to pin down the mass; however, precision studies with $L = 50$ fb^{-1} in this mode would be useful for determining $\sigma(Zh) \times BF(h \to X)$ for various different final states, X [1].

For $m_{h_{SM}}$ above $2m_W$, $\Gamma^{\text{tot}}_{h_{SM}}$ rises dramatically, $BF(h_{SM} \to \mu^+\mu^-)$ falls rapidly and, thus [see Eq. (11) and Fig. 9], $\overline{\sigma}_h$ declines precipitously. Even after combining all channels, the luminosity requirements in the double-on-shell WW and ZZ final states are such that Higgs detection in s-channel production will be difficult. How severe a drawback is this? One of the unique and most important features of s-channel Higgs production is the ability to scan with sufficient statistics to determine the width of a narrow Higgs boson. In the case of the h_{SM}, only below WW threshold is the Higgs so narrow that this is the only possible measurement technique. The h_{SM} can be detected straightforwardly in the standard Zh_{SM} mode and, at the super-LC detector, its width can be measured down to 0.2 GeV via the recoil mass spectrum in Zh_{SM} events with $Z \to \ell^+\ell^-$. Since $\Gamma^{\text{tot}}_{h_{SM}} \gtrsim 0.2$ GeV for $m_{h_{SM}} \gtrsim 2m_W$, this Zh_{SM} technique becomes viable just as s-channel detection becomes difficult. Without the super-LC detector there could, however, be a gap between the $m_{h_{SM}} \lesssim 2m_W$ region where s-channel measurement of $\Gamma^{\text{tot}}_{h_{SM}}$ will be possible at a muon collider and the region $m_{h_{SM}} \gtrsim 200$ GeV where $\Gamma^{\text{tot}}_{h_{SM}}$ becomes comparable to the event by event mass resolution of ~ 4 GeV (see earlier discussion and Fig. 3) and would become measurable at a linear e^+e^- collider. The high resolution for lepton momenta of the super-LC detector could thus prove critical in avoiding a gap in the region between about 150 GeV and 200 GeV where $\Gamma^{\text{tot}}_{h_{SM}}$ measurement might not be possible using either s-channel scanning or the Zh_{SM} mode.

The most important conclusions of this subsection are two:

(1) Excellent beam energy resolution is absolutely critical to guaranteeing success in detecting a SM-like h in $\mu^+\mu^- \to h$ s-channel collisions and to our ability to perform detailed studies once the Higgs boson mass is known. Every effort should therefore be made to achieve excellent resolution. (It is only if $m_h > 2m_W$ where the SM-like Higgs boson begins to become broad that the advantage of having small R declines. But, for such masses s-channel discovery of the SM Higgs will be very difficult in any case, as we have discussed.)

(2) The scanning required when R is small implies that the machine design must be such that $\sqrt{s}$ can be *quickly* reset with a precision that is a small fraction of $\sigma_{\sqrt{s}}$.

2.3   Precision measurements: m_h and Γ_h^{tot}

Once the machine is set to the central value of $\sqrt{s} = m_h$, one can proceed to precisely measure the mass m_h and the total width Γ_h^{tot}. A precision determination of the total width Γ_h^{tot} is of particular interest to differentiate between the h_{SM} and the h^0 of the MSSM. Knowledge of the total width will also allow extraction of the partial width (and associated Higgs couplings) for any channel in which the Higgs can be observed.

A precise measurement of the Higgs mass is possible via s-channel collisions. We initially focus our discussion on $m_{h_{SM}} \lesssim 2m_W$, for which $\Gamma_{h_{SM}}^{\text{tot}}$ is quite likely to be smaller, perhaps much smaller, than the rms $\sqrt{s}$ resolution, $\sigma_{\sqrt{s}}$. Despite this, a highly accurate determination of $m_{h_{SM}}$ is still possible via a straightforward scan in the vicinity of $\sqrt{s} = m_{h_{SM}}$. In Fig. 11 we illustrate sample data points (statistically fluctuated) in the case of $m_{h_{SM}} = 110$ GeV, assuming $L = 0.5$ fb^{-1} is accumulated at each $\sqrt{s}$ setting. A resolution of $R = 0.01\%$ is assumed. The solid curve is the theoretical prediction. A visual inspection reveals that $m_{h_{SM}}$ can be pinned down to within about 4 MeV using seven scan points centered around $\sqrt{s} = m_{h_{SM}}$ (involving a combined luminosity of 3.5 fb^{-1}). Using somewhat more sophisticated techniques, to be described shortly, we will find that with this same total luminosity we can do better. These latter techniques are those needed for a direct measurement of the total Higgs width $\Gamma_{h_{SM}}^{\text{tot}}$.
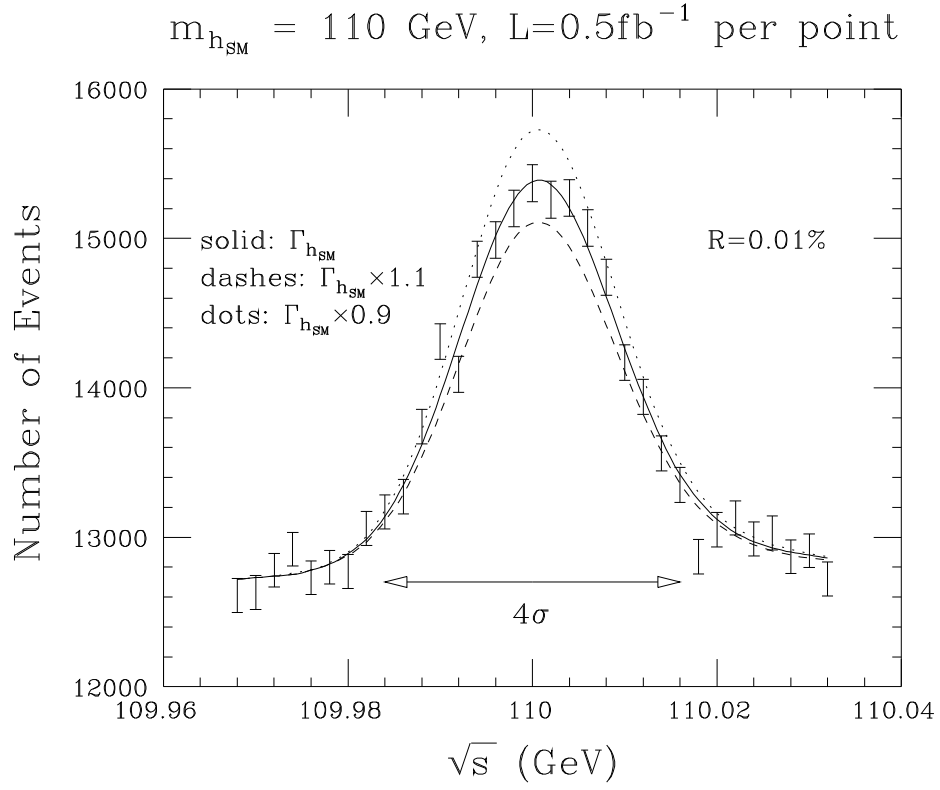
Figure 11: Number of events and statistical errors in the $b\overline{b}$ final state as a function of $\sqrt{s}$ in the vicinity of $m_{h_{SM}} = 110$ GeV, assuming $R = 0.01\%$, and $L = 0.5$ fb^{-1} at each data point. The precise theoretical prediction is given by the solid line. The dotted (dashed) curve is the theoretical prediction if $\Gamma_{h_{SM}}^{tot}$ is decreased (increased) by 10%, *keeping the* $\Gamma(h_{SM} \to \mu^+\mu^-)$ *and* $\Gamma(h_{SM} \to b\overline{b})$ *partial widths fixed at the predicted SM value.*

If the partial widths for $h_{SM} \to \mu^+\mu^-$ and $h_{SM} \to b\bar{b}$ are regarded as theoretically computable with no systematic uncertainties (not a valid assumption in the case of the MSSM h^0), then determination of $\Gamma^{\text{tot}}_{h_{SM}}$ is straightforward based on Eq. (9). We have plotted the theoretical predictions for $m_{h_{SM}} = 110$ GeV in Fig. 11 corresponding to keeping the above partial widths constant while varying only $\Gamma^{\text{tot}}_{h_{SM}}$ by $\pm 10\%$. Assuming that the background can be absolutely normalized by a combination of theory and experiment, the height of the peak is a measure of $\Gamma^{\text{tot}}_{h_{SM}}$. The seven central points would determine $\Gamma^{\text{tot}}_{h_{SM}}$ to better than 10%.

Since in practice we are not able to accurately pre-determine the partial widths, a *model-independent* technique for discriminating between the total width of the SM h_{SM} and that of some other SM-like h must be devised that does not involve a theoretical computation of the partial widths. Such a determination of the total width requires measurements sensitive to the breadth of the spectrum illustrated in Fig. 11. We outline below a procedure by which roughly $L \sim 3$ fb^{-1} of total luminosity will allow a $\pm 33\%$ determination of $\Gamma^{\text{tot}}_{h_{SM}}$ (for $m_{h_{SM}} = 110$ GeV) without any assumption regarding the partial widths.

The key observation is that if one adjusts the partial widths so that the normalization of the theoretical curve at $\sqrt{s} = m_{h_{SM}}$ agrees with experiment, then the normalization of the wings of the theoretical curve will be correspondingly increased or decreased in the case that Γ^{tot}_h is larger or smaller, respectively. Experimental measurements of sufficient precision both at a central $\sqrt{s}$ value and on the wings would thus allow a direct measurement of $\Gamma^{\text{tot}}_{h_{SM}}$ via the ratio of the central peak cross section to the cross sections on the wings (the partial widths cancel out in the ratio). With this in mind, we define the quantity

$$d \equiv |\sqrt{s} - m_{h_{SM}}|/\sigma_{\sqrt{s}} \tag{17}$$

and propose the following procedure:

(1) Perform a rough scan to determine $m_{h_{SM}}$ to a precision $\sigma_{\sqrt{s}}d$, with $d \lesssim 0.3$; d will not be known ahead of time, but the value of d, and hence of $m_{h_{SM}}$ will be determined by the procedure.

(2) Then perform three measurements. At $\sqrt{s}_1 = m_{h_{SM}} + \sigma_{\sqrt{s}}d$ we employ a luminosity of L_1 and measure the total rate $N_1 = S_1 + B_1$. Then perform two

additional measurements at

$$\sqrt{s_2} = \sqrt{s_1} - n_{\sigma_{\sqrt{s}}} \sigma_{\sqrt{s}} \tag{18}$$

and one at

$$\sqrt{s_3} = \sqrt{s_1} + n_{\sigma_{\sqrt{s}}} \sigma_{\sqrt{s}} \tag{19}$$

yielding $N_2 = S_2 + B_2$ and $N_3 = S_3 + B_3$ events, respectively, employing luminosities of $L_2 = \rho_2 L_1$ and $L_3 = \rho_3 L_1$. We find that $n_{\sigma_{\sqrt{s}}} \sim 2$ and $\rho_2 = \rho_3 \sim 2.5$ are optimal for maximizing sensitivity and minimizing the error in determining d (*i.e.* $m_{h_{SM}}$) and $\Gamma^{\text{tot}}_{h_{SM}}$.

(3) To determine $m_{h_{SM}}$ and $\Gamma^{\text{tot}}_{h_{SM}}$ consider the ratios

$$r_2 \equiv (S_2/\rho_2)/S_1 = (S_2/L_2)/(S_1/L_1) \qquad r_3 \equiv (S_3/\rho_3)/S_1 = (S_3/L_3)/(S_1/L_1) \,. \tag{20}$$

The ratios r_2 and r_3 are governed by d and $\Gamma^{\text{tot}}_{h_{SM}}$. Conversely, we have implicitly $d = d(r_2, r_3)$ and $\Gamma^{\text{tot}}_{h_{SM}} = \Gamma^{\text{tot}}_{h_{SM}}(r_2, r_3)$. Determining the statistical errors $\Delta m_{h_{SM}}$ and $\Delta\Gamma^{\text{tot}}_{h_{SM}}$ is then simply a matter of computing the partial derivatives of d and $\Gamma^{\text{tot}}_{h_{SM}}$ with respect to the $r_{2,3}$ (we do this numerically) and using errors on the ratios $r_{2,3}$ implied by statistics. The procedure is detailed in Appendix C, as is the cross check on its accuracy that we have used.

The utility of the ratios r_2 and r_3 is basically governed by how rapidly they vary as d and Γ^{tot}_h are varied in the ranges of interest. Since we are most interested in Γ^{tot}_h here, we illustrate the sensitivity of $r_{2,3}$ to Γ^{tot}_h in Fig. 12 taking $\sqrt{s} = m_h = 120$ GeV. For this figure we employ $n_{\sigma_{\sqrt{s}}} = 2$ for computing r_2 and r_3, respectively. Results are shown for resolutions $R = 0.01\%$ and $R = 0.06\%$. Because of the bremsstrahlung tail, r_2 is substantially larger than r_3. Nonetheless, both r_2 and r_3 show rapid variation as Γ^{tot}_h varies in the vicinity of $\Gamma^{\text{tot}}_{h_{SM}}$ in the case of $R = 0.01\%$, but much less variation if $R = 0.06\%$. The error in the determination of Γ^{tot}_h is basically determined by $d\Gamma^{\text{tot}}_h/dr_{2,3}$. Figure 12 shows that these derivatives are almost the same and quite small for $R = 0.01\%$. The much larger values of these derivatives for $R = 0.06\%$ imply that determining Γ^{tot}_h accurately would be very difficult in this case.

In Fig. 13, we plot the total luminosity $L = L_1 + L_2 + L_3 = 6L_1$ required to achieve $\Delta\Gamma^{\text{tot}}_{h_{SM}}/\Gamma^{\text{tot}}_{h_{SM}} = 1/3$ in the $b\bar{b}$ final state as a function of $m_{h_{SM}}$ for several beam resolutions. (The error scales statistically; *e.g.* to achieve a 10% measurement
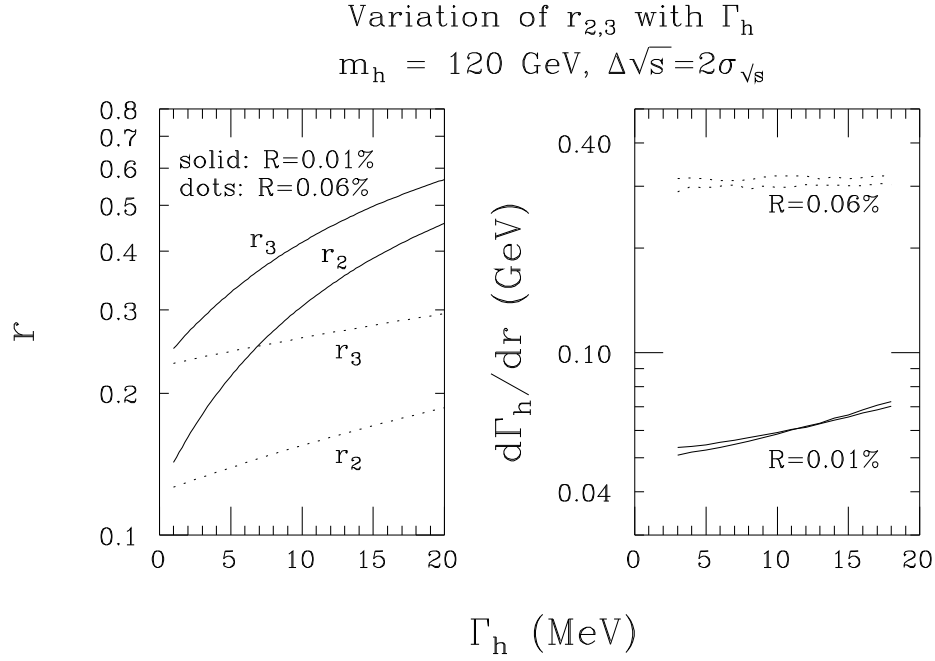
Figure 12: We plot r_2 and r_3 as a function of Higgs width, Γ_h^{tot}, for resolutions of $R = 0.01\%$ and $R = 0.06\%$, assuming that $\sqrt{s} = m_h = 120$ GeV. Also shown are the derivatives $d\Gamma_h^{\text{tot}}/dr$ as a function of Γ_h^{tot}. We have taken $n_{\sigma_{\sqrt{s}}} = 2$ corresponding to a shift in $\sqrt{s}$ of $\mp 2\sigma_{\sqrt{s}}$ in computing r_2 and r_3, respectively.
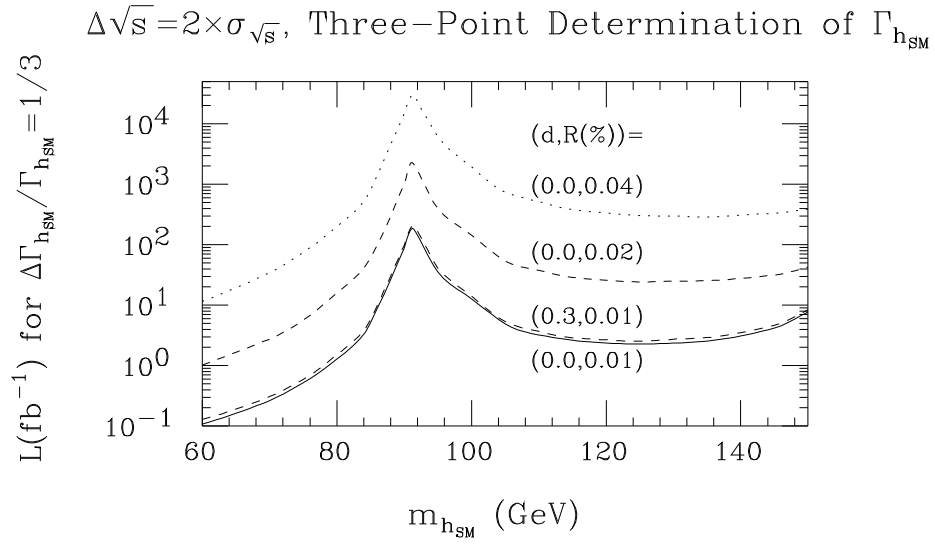
$\Delta\sqrt{s} = 2 \times \sigma_{\sqrt{s}}$, Three$-$Point Determination of $\Gamma_{h_{SM}}$

Figure 13: Luminosity required for a $\Delta\Gamma^{\rm tot}_{h_{SM}}/\Gamma^{\rm tot}_{h_{SM}} = 1/3$ measurement in the $b\bar{b}$ final state using the three point technique described in the text. Results for resolutions of $R = 0.01\%$, 0.02% and 0.04% are shown for $d = 0$, where $d = |\sqrt{s} - m_{h_{SM}}|/\sigma_{\sqrt{s}}$. The result for $d = 0.3$ and $R = 0.01\%$ is also shown.

would require $(10/3)^2$ as much luminosity.) We also illustrate the fact that the total luminosity required is rather insensitive to the initial choice of d for $d \lesssim 0.3$; $d = 0.3$ results in no more than a 20% increase in the luminosity needed relative to $d = 0$.
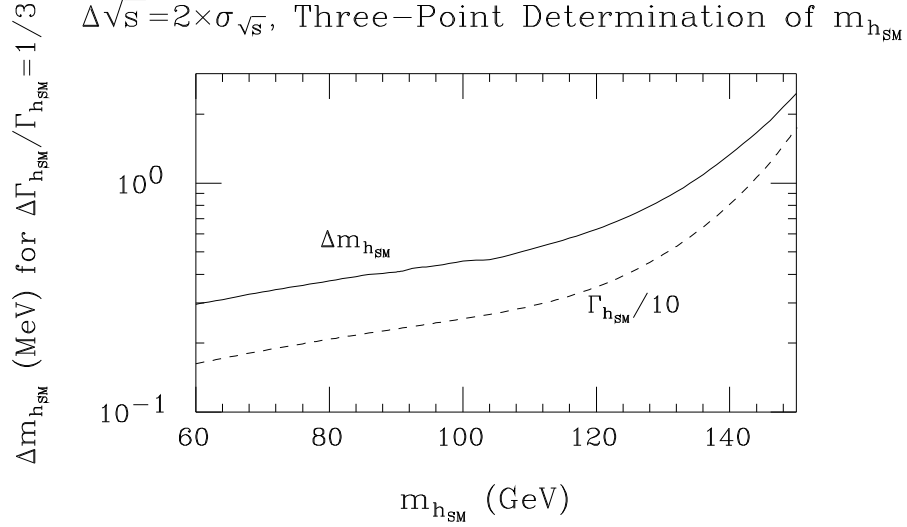

Figure 14: We plot the 1σ error, $\Delta m_{h_{SM}}$, in the determination of $m_{h_{SM}}$ using the three point technique described in the text with $R = 0.01\%$ and $d = 0$. The error given is that achieved for the luminosity that allows a $\Delta\Gamma_{h_{SM}}^{\text{tot}}/\Gamma_{h_{SM}}^{\text{tot}} = 1/3$ measurement in the $b\bar{b}$ final state. For such luminosity, $\Delta m_{h_{SM}}$ is essentially independent of R and d. Also shown, for comparison, is $\Gamma_{h_{SM}}^{\text{tot}}/10$.

In Fig. 14, we plot the 1σ error $\Delta m_{h_{SM}}$ that results using our three-point technique after accumulating the luminosity required for a $\Delta\Gamma_{h_{SM}}^{\text{tot}}/\Gamma_{h_{SM}}^{\text{tot}} = 1/3$ measurement in the $b\bar{b}$ final state. The specific result plotted is for $R = 0.01\%$ and $d = 0$, but is essentially independent of R and d given the stated luminosity. Also shown, for comparison, is $\Gamma_{h_{SM}}^{\text{tot}}$ itself. We see that $\Delta m_{h_{SM}}$ is of order 1.5–2 times $\Gamma_{h_{SM}}^{\text{tot}}/10$, $i.e.$ a fraction of an MeV for $m_{h_{SM}} \lesssim 130$ GeV. (Again, $\Delta m_{h_{SM}}$ scales as $1/\sqrt{L}$.)

It should be stressed that the ability to precisely set the energy of the machine when the three measurements are taken is crucial for the success of the three-point technique. A misdetermination of the spacing of the measurements in Eqs. (18) and (19) by just 3% ($i.e.$ $\sqrt{s}$ uncertainty of order 0.25 MeV for any one setting near $m_{h_{SM}} \sim 120$ GeV) would result in an error in $\Gamma_{h_{SM}}^{\text{tot}}$ of 30%. For a measurement of

$\Gamma^{\text{tot}}_{h_{SM}}$ at the 10% level the $\sqrt{s}$ settings must be precise at a level of better than one part in 10^6. This is possible [21] provided the beam can be partially polarized so that the precession of the spin of the muon as it circulates in the final storage ring can be measured. From the precession and the rotation rate the energy can be determined. The ability to perform this critical measurement needed for the determination of the total width of a narrow Higgs must be incorporated in the machine design.

2.4 Precision measurements: $\Gamma(h \to \mu^+\mu^-) \times BF(h \to X)$

Assuming that the Higgs width is much narrower than the rms uncertainty in $\sqrt{s}$, Eq. (9) shows that the event rate in a given channel measures $G(X) = \Gamma(h \to \mu^+\mu^-) \times BF(h \to X)$. If the background can be determined precisely (either by off-resonance measurements or theory plus Monte Carlo calculation), the error in the determination of this product is $\sqrt{N}/S$, where $N = S + B$ and S, B are the number of signal, background events, respectively. The results for $\sqrt{N}/S$ in the case of $P = 0$ and $L = 50$ fb^{-1} in the $b\bar{b}$, $WW^{(\star)}$ and $ZZ^{(\star)}$ modes are shown in Fig. 15 for $h = h_{SM}$. For each final state, the efficiencies and procedures employed are precisely those discussed with regard to Fig. 10. Good accuracy in this measurement is possible for $m_{h_{SM}} \lesssim 2m_W$ even if $m_{h_{SM}}$ is near m_Z.

2.5 h^0 or h_{SM}?

We now discuss the possibility of distinguishing the MSSM h^0 from the SM h_{SM} using precision measurements of Γ^{tot}_h and $G(b\bar{b}) \equiv \Gamma(h \to \mu\mu) \times BF(h \to b\bar{b})$. The accuracy to which Γ^{tot}_h and $G(b\bar{b})$ need to be determined can be gauged by the ratio of the h^0 predictions to the h_{SM} predictions for these quantities at $m_{h^0} = m_{h_{SM}}$. Contours for various fixed values of these ratios are plotted in Fig. 16 in the standard $(m_{A^0}, \tan\beta)$ parameter space [28]. In computing results for Γ^{tot}_h and $G(b\bar{b})$ for h^0 we have taken $m_{\tilde{t}} = 1$ TeV, $m_t = 175$ GeV, and included two-loop/RGE-improved radiative corrections to the Higgs masses, mixing angles and self-couplings, neglecting squark mixing. The ratios for both Γ^{tot}_h and $G(b\bar{b})$ are substantially bigger than 1, even out to fairly large m_{A^0} values. This is because the h^0 retains somewhat enhanced $b\bar{b}$, $\tau^+\tau^-$ and $\mu^+\mu^-$ couplings until quite large m_{A^0} values. Two facts are of particular importance:
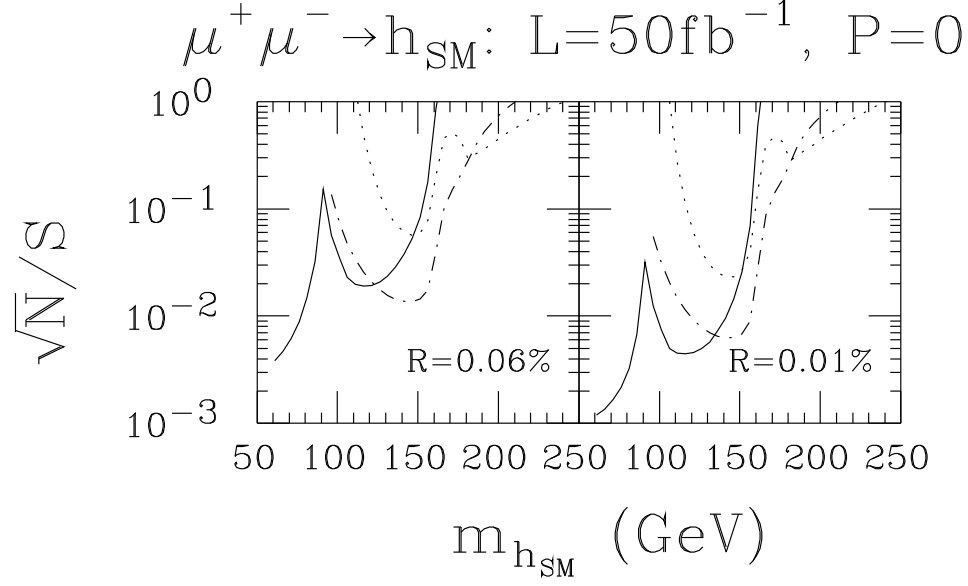
$$\mu^+\mu^- \to h_{SM}:\ L=50fb^{-1},\ P=0$$

Figure 15: Fractional error in determining $\Gamma(h_{SM} \to \mu\mu) \times BF(h_{SM} \to X)$ for $X = b\bar{b}$ (solid), $WW^{(\star)}$ (dotdash) and $ZZ^{(\star)}$ (dots), assuming $L = 50$ fb^{-1}. (See text for $WW^\star$ and $ZZ^\star$ final states employed.)

- $\Gamma_{h^0}^{\rm tot}$ is enhanced relative to $\Gamma_{h_{SM}}^{\rm tot}$ by virtue of the enhanced partial widths into its dominant decay channels, $b\bar{b}$ and $\tau^+\tau^-$.

- The enhancement in $G(b\bar{b})$ derives mainly from $\Gamma(h \to \mu\mu)$, as can be deduced by comparing Fig. 16(b) and 16(c).

This latter point is also apparent in Fig. hltohsmratios(d), where we observe that the MSSM to SM ratio of $BF(h \to b\bar{b})$'s is very close to 1 along the 1.1 contour of the MSSM/SM $G(b\bar{b})$. This is because the enhanced $b\bar{b}$ partial width in the numerator of $BF(h \to b\bar{b})$ is largely compensated by the extra contribution to the total width from this same channel. Thus, in comparing the MSSM to the SM, a measurement of $G(b\bar{b})$ is most sensitive to deviations of $\Gamma(h \to \mu\mu)$ from SM expectations. As seen numerically in Fig. 16(e), $\Gamma(h \to \mu\mu)$ grows rapidly at lower m_{A^0} or higher $\tan\beta$. For small squark mixing, a deviation in $G(b\bar{b})$ from the SM value implies almost the same percentage deviation of $\Gamma(h \to \mu\mu)$ from its SM value. However, when squark mixing is large, this equality breaks down. In general, one must separately determine $\Gamma(h \to \mu\mu)$ in order to probe MSSM vs. SM differences. The procedure for this will

be discussed shortly.

The measured value of m_h provides a further constraint. For example, suppose that a Higgs boson is observed with $m_h = 110$ GeV. A fixed value for m_h implies that the parameters which determine the radiative corrections to m_{h^0} must change as m_{A^0} and $\tan \beta$ are varied. For example, if squark mixing is neglected, then the appropriate value of $m_{\widetilde{t}}$ is a function of m_{A^0} and $\tan \beta$. Given the assumption of no squark mixing and the fixed value of $m_h = 110$ GeV, results for the same ratios as plotted in Fig. 16 are given in Fig. 17. Also shown are contours of fixed $\Gamma(h^0 \to \mu\mu)$ and contours of fixed $m_{\widetilde{t}}$ (as required to achieve $m_{h^0} = 110$ GeV). The vertical nature of the $\mu\mu$ ratio and partial width contours implies that a measurement of any of these quantities could provide a determination of m_{A^0} (but would yield little information about $\tan \beta$).

Contours for other mixing assumptions, can also be plotted. The only contours that remain essentially unaltered as the amount of squark mixing is varied (keeping $m_h = 110$ GeV) are those for the ratio $\Gamma(h^0 \to \mu\mu)/\Gamma(h_{SM} \to \mu\mu)$ and for the $\Gamma(h^0 \to \mu\mu)$ partial width itself. Once $m_{h^0} \lesssim 100$ GeV, even these contours show substantial variation as a function of the squark mixing parameters. However, it remains true that a determination of the $\mu\mu$ partial width or partial width ratio provides at least a rough determination of m_{A^0}.

In order to assess the observability of the differences between predictions for Γ_h^{tot}, $G(b\overline{b})$, and $\Gamma(\mu\mu)$ for the h^0 compared to the h_{SM}, we must examine more closely the error in the experimental determination of these quantities, and consider the theoretical uncertainties in our predictions for them.

2.5.1 Interpreting a measurement of Γ_h^{tot}

Consider first the total width measurement. Here, the experimental error is the key issue. The h^0 may have a mass of order 110 GeV in the large-m_{A^0} region where it is SM-like, provided $\tan \beta$ is not near 1 (see Fig. 2). According to Fig. 13, $L \sim 3$ fb^{-1} is required to measure Γ_h^{tot} to $\pm 33\%$, provided $R = 0.01\%$. A $\pm 10\%$ measurement would require $L \sim 33$ fb^{-1} (using $\Delta \Gamma_{h_{SM}}^{\text{tot}} \propto 1/\sqrt{L}$). As seen most clearly from Fig. 17, this accuracy would probe MSSM/SM differences at the 3σ level for $m_{A^0} \lesssim 400$ GeV if squark mixing is small.

Detecting a difference between the h^0 and h_{SM} using Γ_h^{tot} could prove either some-

FMC: MSSM/SM Light Higgs Ratio and $\Gamma(h \to \mu\mu)$ Contours

$m_{TOP} = 175$ GeV, $m_{STOP} = 1$ TeV

Figure 16: Contours of constant MSSM/SM ratios for Γ_h^{tot}, $\Gamma(h \to \mu\mu) \times BF(h \to b\bar{b})$, $\Gamma(h \to \mu\mu)$ and $BF(h \to b\bar{b}, \tau\tau)$ in $(m_{A^0}, \tan\beta)$ parameter space. We have taken $m_t = 175$ GeV, $m_{\tilde{t}} = 1$ TeV, and included two-loop/RGE-improved radiative corrections, neglecting squark mixing, for Higgs masses, mixing angles and self-couplings. Also shown are contours for fixed values of $\Gamma(h^0 \to \mu\mu)$ using units of keV, and contours of fixed m_{h^0}. This graph was obtained using the programs developed for the work of Ref. [28].
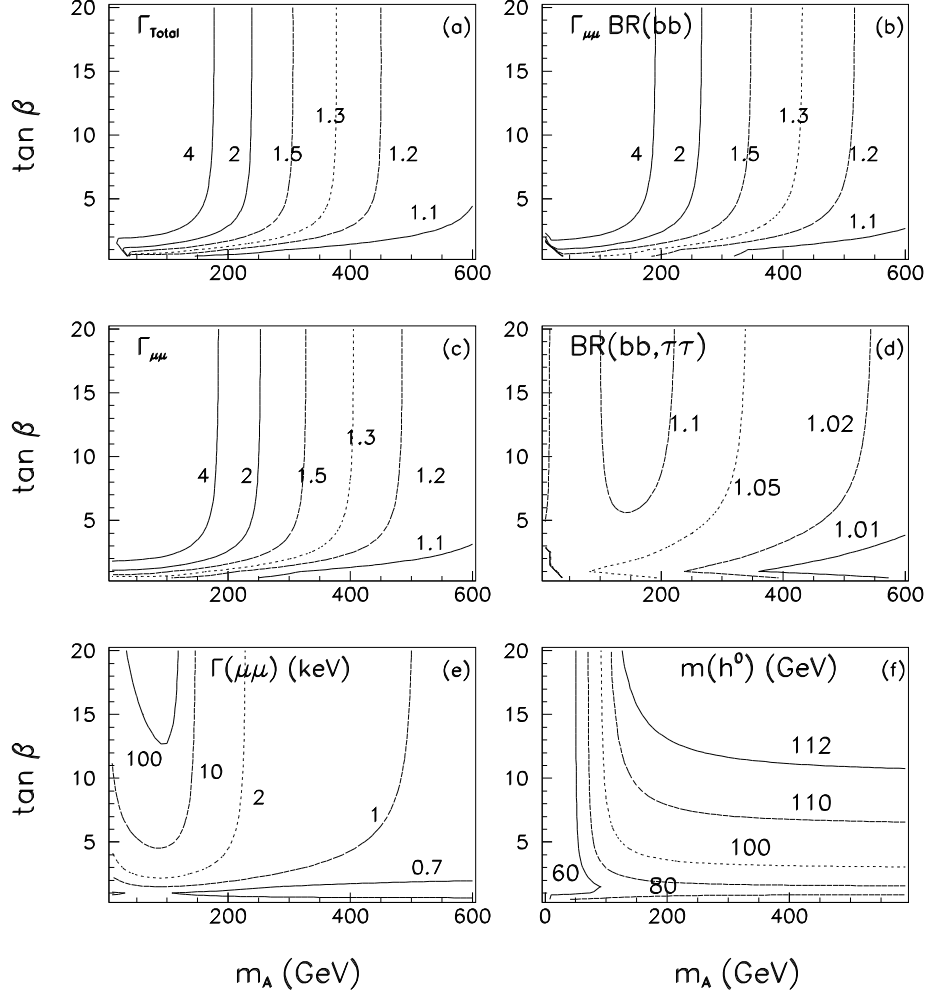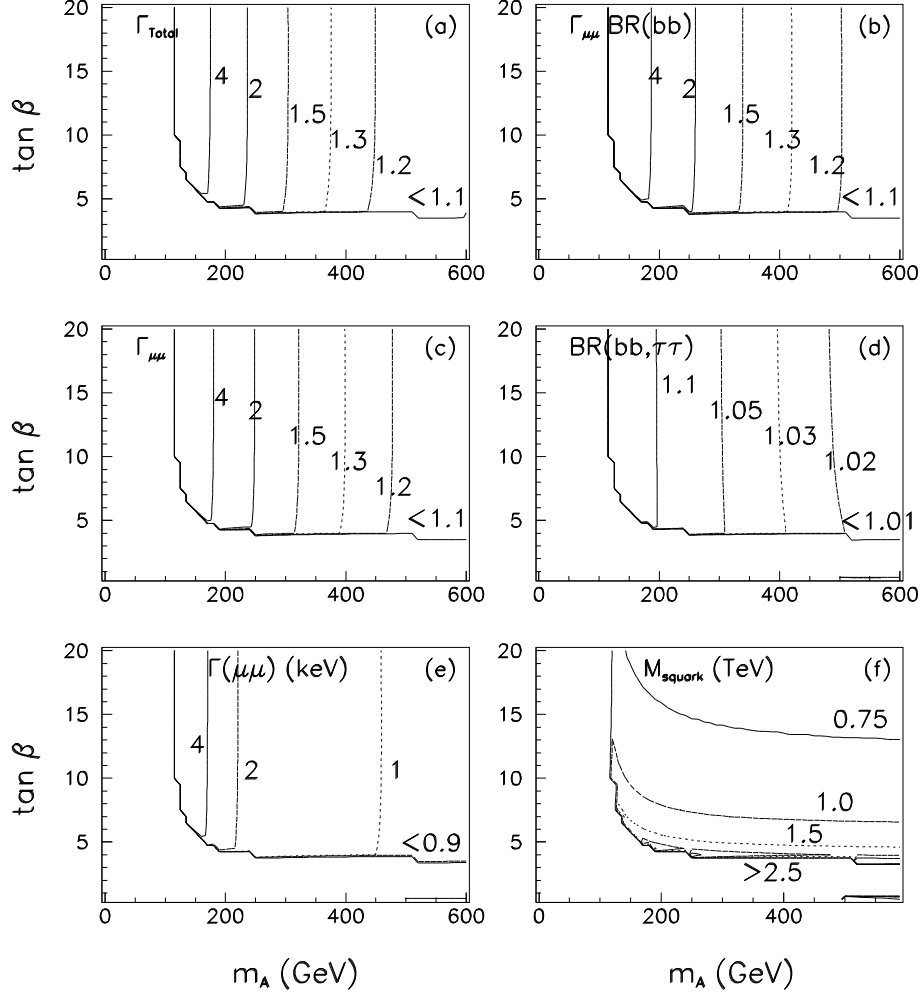
Figure 17: Contours of constant MSSM/SM ratios for Γ_h^{tot}, $\Gamma(h \rightarrow \mu\mu) \times BF(h \rightarrow b\bar{b})$, $\Gamma(h \rightarrow \mu\mu)$ and $BF(h \rightarrow b\bar{b}, \tau\tau)$ in $(m_{A^0}, \tan\beta)$ parameter space. We have taken $m_t = 175$ GeV, and we adjust $m_{\tilde{t}}$ so as to keep a fixed value of $m_{h^0} = 110$ GeV after including two-loop/RGE-improved radiative corrections for Higgs masses, mixing angles and self-couplings, neglecting squark mixing. Also shown are contours for fixed values of $\Gamma(h^0 \rightarrow \mu\mu)$ in keV units, and contours for fixed values of $m_{\tilde{t}}$ in TeV units. This graph was obtained using the programs developed for the work of Ref. [28].

what easier or much more difficult than outlined above, because the $\tan\beta$, $m_{\tilde{t}}$ values and the degree of squark mixing could very well be different from those assumed above. For example, if $m_{h^0} = 110$ GeV, $\tan\beta \gtrsim 5$ and squark mixing is large, m_{A^0} values above 400 GeV would be probed at the 3σ level by a 10% measurement of Γ_h^{tot}. On the other hand, the radiative corrections could yield a smaller m_{h^0} value, *e.g.* $m_{h^0} \lesssim 100$ GeV is quite likely if $\tan\beta$ is near 1 or $m_{\tilde{t}}$ is small. In this range, predicted deviations from predictions for the h_{SM} with $m_{h_{SM}} = m_{h^0}$ are not dissimilar to those obtained discussed above. However, a luminosity $L \gtrsim 100$ fb^{-1} would be required for a $\pm 10\%$ measurement of Γ_h^{tot} for 80 GeV $\lesssim m_{h^0} \lesssim 100$ GeV.

Other theoretical uncertainties include: i) extra contributions to $\Gamma_{h^0}^{\text{tot}}$ in the MSSM model from SUSY decay modes; ii) the gg decay width of the h^0 could be altered by the presence of light colored sparticles; iii) the h_{SM} could have enhanced gg decay width due to heavy colored fermions (*e.g.* from a fourth family).

Nonetheless, a $\mu^+\mu^-$ collider determination of Γ_h^{tot} will be a crucial component in a model-independent determination of all the properties of a SM-like h, and could provide the first circumstantial evidence for a MSSM Higgs sector prior to direct discovery of the non-SM-like MSSM Higgs bosons.

2.5.2 Interpreting a measurement of $\Gamma(h \to \mu\mu) \times BF(h \to b\overline{b})$

How does the h^0–h_{SM} discrimination power of the total width measurement compare to that associated with a measurement of $G(b\overline{b}) \equiv \Gamma(h \to \mu\mu) \times BF(h \to b\overline{b})$? Figure 15 shows that $\pm 0.4\%$ accuracy in the determination of $G(b\overline{b})$ is possible for $L = 50$ fb^{-1} and $R = 0.01\%$ in the $m_{h^0} \sim 110$–115 GeV mass range predicted for $m_{A^0} \gtrsim 2m_Z$ and larger $\tan\beta$ values, assuming $m_{\tilde{t}} \gtrsim 0.75$ TeV and no squark mixing.

An uncertainty in $BF(h \to b\overline{b})$ arises from $\Gamma(h \to b\overline{b}) \propto m_b^2$ due to the uncertainty in m_b. Writing $BF(h \to b\overline{b}) = \Gamma_b/(\Gamma_b + \Gamma_{\text{non}-b})$, the error in $BF(h \to b\overline{b})$ is given by

$$\Delta BF(h \to b\overline{b}) = \frac{2\Delta m_b}{m_b} BF(h \to b\overline{b}) BF(h \to \text{non} - b) . \tag{21}$$

Since $BF(h \to \text{non-}b)$ is not very large (0.1 to 0.2 in the mass range in question for either the h_{SM} or h^0), even a 10% uncertainty in m_b only leads to $\Delta BF(h \to b\overline{b}) \lesssim 0.05$. Eventually m_b may be known to the 5% level, leading to $\lesssim 2.5\%$ uncertainty in the branching fraction. Comparison to Fig. 17 shows that a 2.5% uncertainty from m_b, in combination with a still smaller statistical error, has the potential for

h^0–h_{SM} discrimination at the 3σ statistical level out to large m_{A^0} for $m_h = 110$ GeV, if squark mixing is small. However, as squark mixing is increased, it turns out that the maximum m_{A^0} that can potentially be probed decreases if $\tan\beta$ is large.

$BF(h \to b\overline{b})$ is also subject to an uncertainty from the total width. For example, in the MSSM $BF(h^0 \to b\overline{b})$ could be smaller than the SM prediction if $\Gamma_{h^0}^{tot}$ is enhanced due to channels other than the $b\overline{b}$ channel itself (*e.g.* by supersymmetric decay modes, or a larger than expected gg decay width due to loops containing supersymmetric colored sparticle or heavy colored fermions). Thus, a measurement of $G(b\overline{b})$ alone is not subject to unambiguous interpretation.

We note that the $L = 50$ fb^{-1} $\mu^+\mu^-$ collider measurement of $G(b\overline{b})$ is substantially more powerful than a $L = 50$ fb^{-1} precision measurement of $\sigma(e^+e^- \to Zh) \times BF(h \to b\overline{b})$ at an e^+e^- collider [1]. The ratio of the h^0 prediction to the h_{SM} prediction is essentially equal to the h^0 to h_{SM} $BF(h \to b\overline{b})$ ratio and is predicted to be within 1% (2%) of unity along a contour very close to the 1.1 (1.2) contour of $\Gamma(h \to \mu^+\mu^-)BF(h \to b\overline{b})$; see panels (b) and (d) in Figs. 16 and 17. Since at best 5% deviations in $G(b\overline{b})$ and $BF(h \to b\overline{b})$ can be detected at the 1σ level (after combining a possibly small statistical error with a large theoretical error), we see from the 1.05 ratio contour for $BF(h \to b\overline{b})$ in Figs. 16 and 17 that the $\sigma(Zh)BF(h \to b\overline{b})$ and $BF(h \to b\overline{b})$ ratios, that can be determined experimentally at an e^+e^- collider, only probe as far as $m_{A^0} \lesssim 250$–300 GeV at the 1σ significance level, with even less reach at the 3σ level.

We must again caution that if m_h is close to m_Z, there could be substantially worse experimental uncertainty in the $G(b\overline{b})$ measurement than taken above. Pre-knowledge of m_h is necessary to determine the level of precision that could be expected for this measurement.

2.5.3 Combining measurements

We now discuss how the independent measurements of Γ_h^{tot} and $G(b\overline{b})$ can be combined with one another and other experimental inputs to provide a model-independent determination of the properties of the h. We consider three complementary approaches.

(1) A model-independent determination of $\Gamma(h \to \mu\mu)$ can be made by combining the s-channel $\mu^+\mu^-$ collider measurement of $G(b\overline{b})$ with the value of $BF(h \to b\overline{b})$

measured in the Zh mode at an e^+e^- collider or the $\mu^+\mu^-$ collider. With $L = 50$ fb^{-1} of luminosity, $BF(h \to b\overline{b})$ can potentially be measured to $\pm 7\%$ [1]. From our earlier discussion, the error on $G(b\overline{b})$ will be much smaller than this if $m_h \gtrsim 100$ GeV, and $\Gamma(h \to \mu\mu)$ would be determined to roughly ± 8–10%. Figures 16 and 17 show that this procedure would probe the h^0 versus h_{SM} differences at the 3σ level out to $m_{A^0} \sim 400$ GeV if $\tan\beta$ is not close to 1 (see the 1.3 ratio contour in the figures). This is a far superior reach to that possible at the 3σ level at either the LHC, NLC and/or $\gamma\gamma$ collider. Further, we note that the $\mu\mu$ partial width at fixed $m_h \gtrsim 100$ GeV is relatively independent of the squark mixing scenario and provides a rather precise determination of m_{A^0} [1].

(2) A model-independent determination of $\Gamma(h \to b\overline{b})$ is possible by computing $\Gamma_h^{\mathrm{tot}} BF(h \to b\overline{b})$ using the value of Γ_h^{tot} measured at the $\mu^+\mu^-$ collider and the value of $BF(h \to b\overline{b})$ measured in the Zh mode. Taking 10% accuracy for the former and 7% accuracy for the latter, we see that the error on $\Gamma(h \to b\overline{b})$ would be of order 12%. The ratio contours for $\Gamma(h \to b\overline{b})$ are the same as the ratio contours for $\Gamma(h \to \mu\mu)$. Thus, ignoring systematics, this measurement could also probe out to $m_{A^0} \gtrsim 400$ GeV at the 3σ level if $m_h \sim 110$ GeV, see Fig. 17. However, the $2\Delta m_b/m_b$ systematic uncertainty in the partial width is also of order 10% for 5% uncertainty in m_b, implying a total statistical plus theoretical error of order 16%. This would restrict 3σ sensitivity to h^0 vs. h_{SM} differences to $m_{A^0} \lesssim 300$ GeV.

(3) A third approach uses only the $\mu^+\mu^-$ collider measurements. We note that

$$W \equiv \Gamma(h \to \mu\mu)\Gamma(h \to b\overline{b}) = [\Gamma_h^{\mathrm{tot}}] \times [\Gamma(h \to \mu\mu)BF(h \to b\overline{b})]. \qquad (22)$$

In the MSSM (or any other type-II two-Higgs-doublet model) the $\mu\mu$ and $b\overline{b}$ squared couplings have exactly the same factor, call it f, multiplying the square of the SM coupling strength. Thus,

$$W = \Gamma(h \to \mu\mu)\Gamma(h \to b\overline{b}) \propto f^2 \left(\frac{g}{2m_W}\right)^4 m_\mu^2 m_b^2. \qquad (23)$$

Following our earlier discussion, in the MSSM f^2 would be $(1.3)^2 \sim 1.7$ along the 1.3 ratio contours for $\Gamma(h \to \mu\mu)$ in Figs. 16 and 17. For $m_h \gtrsim 100$ GeV, experimental errors in W of Eq. (22) would be dominated by the $\pm 10\%$ error on Γ_h^{tot}. The dominant systematic error would be that from not knowing the value of m_b: $\Delta W/W = 2\Delta m_b/m_b$. Thus, a combined statistical and theoretical 1σ error for W

41

below 20% is entirely possible for $m_h \gtrsim 100$ GeV, in which case deviations in f^2 from unity can be probed at the 3σ level for m_{A^0} values at least as large as $m_{A^0} \sim 400$ GeV. Since both $\Gamma(h^0 \to \mu\mu)$ and $\Gamma(h^0 \to b\overline{b})$ are relatively independent of the squark mixing scenario for fixed m_{h^0} and fixed m_{A^0}, a fairly reliable value of m_{A^0} would result from the determination of f^2.

By combining the strategies just discussed, one can do even better. Thus, a $\mu^+\mu^-$ collider has great promise for allowing us to measure the crucial $b\overline{b}$ and $\mu^+\mu^-$ couplings of a SM-like h, provided m_h is not within 10 GeV of m_Z (nor $\gtrsim 2m_W$) and that $m_A \lesssim 400$ GeV. In particular, for such masses we can distinguish the h^0 from the h_{SM} in a model-independent fashion out to larger m_{A^0} than at any other accelerator or combination of accelerators.

2.5.4 The $WW^\star$ and $ZZ^\star$ channels

Precision measurements of $\Gamma(h \to \mu^+\mu^-)BF(h \to X)$ are also possible for $X = WW^\star$ and, to a lesser extent, $ZZ^\star$, see Fig. 15. Once again, $\Gamma(h \to \mu^+\mu^-)$ can be determined in a model-independent fashion using $BF(h \to X)$ measured in the Zh mode, and $\Gamma(h \to X)$ can be computed in a model-independent fashion as the product $BF(h \to X)\Gamma_h^{\rm tot}$. We will not go through the error analysis in detail for these cases, but clearly determination of both the WW and ZZ couplings will be possible at a reasonable statistical level. Unfortunately, the h^0WW, h^0ZZ couplings are very close to the SM values for $m_{A^0} \gtrsim 2m_W$ and the expected statistical errors would not allow h^0 vs. h_{SM} discrimination.

3 Non-SM-like Higgs bosons in the MSSM

In what follows, we shall demonstrate that it is possible to observe the H^0 and A^0 in s-channel Higgs production for $m_{A^0} \sim m_{H^0} > \sqrt{s}/2$ over much of $(m_{A^0}, \tan\beta)$ parameter space. It is this fact that again sets the $\mu^+\mu^-$ collider apart from other machines.

1. The LHC can only detect the H^0 and A^0 for masses above 200–250 GeV if $\tan\beta$ is either large or $\lesssim 3$–5; a wedge of unobservability develops beginning at $m_{A^0} \gtrsim 200$ GeV, covering an increasingly wide range of $\tan\beta$ as m_{A^0} increases [29]. This is illustrated in Fig. 18 from Ref. [30].

2. At an e^+e^- collider, $Z^\star \to ZA^0, ZH^0$ production will be negligible when $m_{A^0} > 2m_Z$.

3. $e^+e^- \to Z^\star \to A^0 H^0$ could easily be kinematically disallowed, especially for e^+e^- machine energies in the $\sqrt{s} \sim 500$ GeV range — GUT scenarios often give $m_{A^0} \sim m_{H^0} \gtrsim 300$ GeV.

4. If an e^+e^- collider is run in the photon-photon collider mode, discovery of the H^0 and A^0 in the $m_{A^0}, m_{H^0} \gtrsim 200$ GeV region via $\gamma\gamma \to A^0, H^0$ requires extremely high luminosity ($\gtrsim 200$ fb^{-1}) [31].

5. s-channel production of the A^0 and H^0 will not be significant in e^+e^- collisions due to the small size of the electron mass.

A $\mu^+\mu^-$ collider can overcome the limitations 3 and 5 of an e^+e^- collider, though not simultaneously. If the $\mu^+\mu^-$ collider is run at energies of $\sqrt{s} = m_{A^0} \sim m_{H^0}$, then we shall find that s-channel production will allow discovery of the A^0 and H^0 if $\tan\beta \gtrsim 3 - 4$. Here, the kinematical Higgs mass reach is limited only by the maximum $\sqrt{s}$ of the machine. Alternatively, the $\mu^+\mu^-$ collider can be designed to have $\sqrt{s} \sim 4$ TeV in which case $m_{A^0} \sim m_{H^0}$ values up to nearly 2 TeV can be probed via the $Z^\star \to A^0 H^0$ process, a mass range that encompasses all natural GUT scenarios. We focus in this report on s-channel production and detection. In our analysis, we will assume that more or less full luminosity can be maintained for all $\sqrt{s}$ values over the mass range of interest (using multiple storage rings, as discussed in the introduction).

3.1   MSSM Higgs bosons in the s-channel: $\sqrt{s} = m_h$

Here we investigate the potential of a $\mu^+\mu^-$ collider for probing those Higgs bosons whose couplings to ZZ, WW are either suppressed or absent at tree-level — that is the A^0, the H^0 (at larger m_{A^0}), or the h^0 (at small m_{A^0}). The $WW^{(\star)}$ and $ZZ^{(\star)}$ final states in s-channel production are then not relevant. We consider first the $b\bar{b}$ and $t\bar{t}$ decay modes, although we shall later demonstrate that the relatively background free $H^0 \to h^0 h^0$ or $A^0 A^0 \to b\bar{b}b\bar{b}$, $H^0 \to ZA^0 \to Zb\bar{b}$ and $A^0 \to Zh^0 \to Zb\bar{b}$ modes might also be useful.

Figure 19 shows the dominant branching fractions to $b\bar{b}$ and $t\bar{t}$ of Higgs bosons of mass $m_{A^0} = 400$ GeV $\approx m_{H^0}$ versus $\tan\beta$, taking $m_t = 170$ GeV. The $b\bar{b}$ decay mode
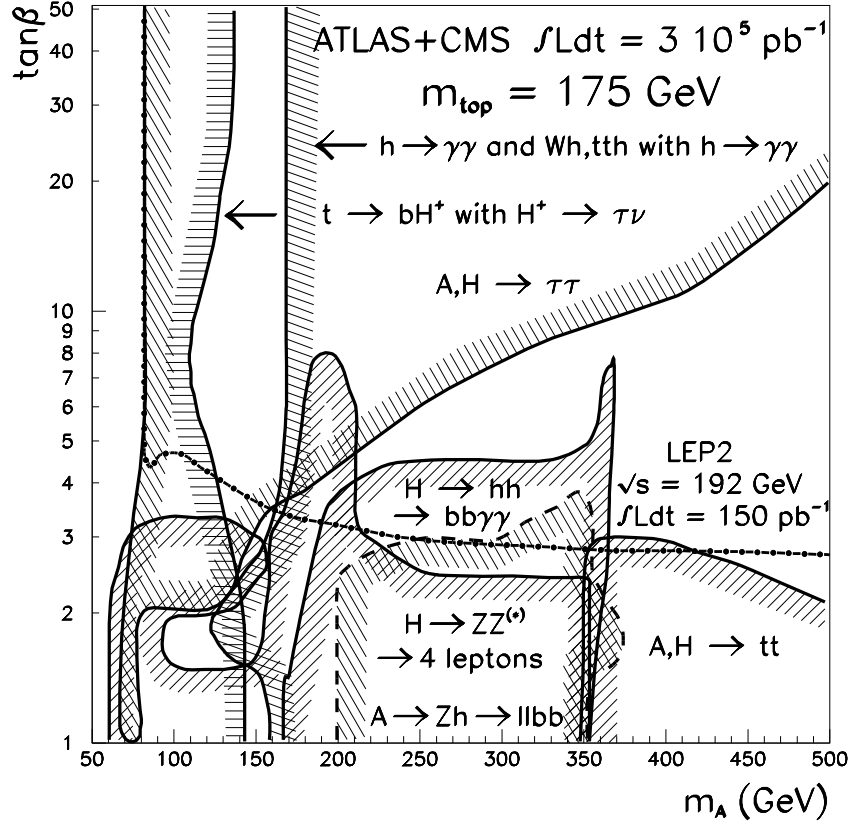
Figure 18: MSSM Higgs discovery contours (5σ) in the parameter space of the minimal supersymmetric model for ATLAS+CMS at the LHC: $L = 300$ fb^{-1} per detector. Figure from Ref. [30]. Two-loop/RGE-improved radiative corrections are included for m_{h^0} and m_{H^0} assuming $m_{\tilde{t}} = 1$ TeV and no squark mixing.

is dominant for $\tan\beta > 5$, which is the region where observable signal rates are most easily obtained. From the figure we see that $BF(H^0, A^0 \to b\bar{b})$ grows rapidly with increasing $\tan\beta$ for $\tan\beta \lesssim 5$, while $BF(H^0, A^0 \to t\bar{t})$ falls slowly.

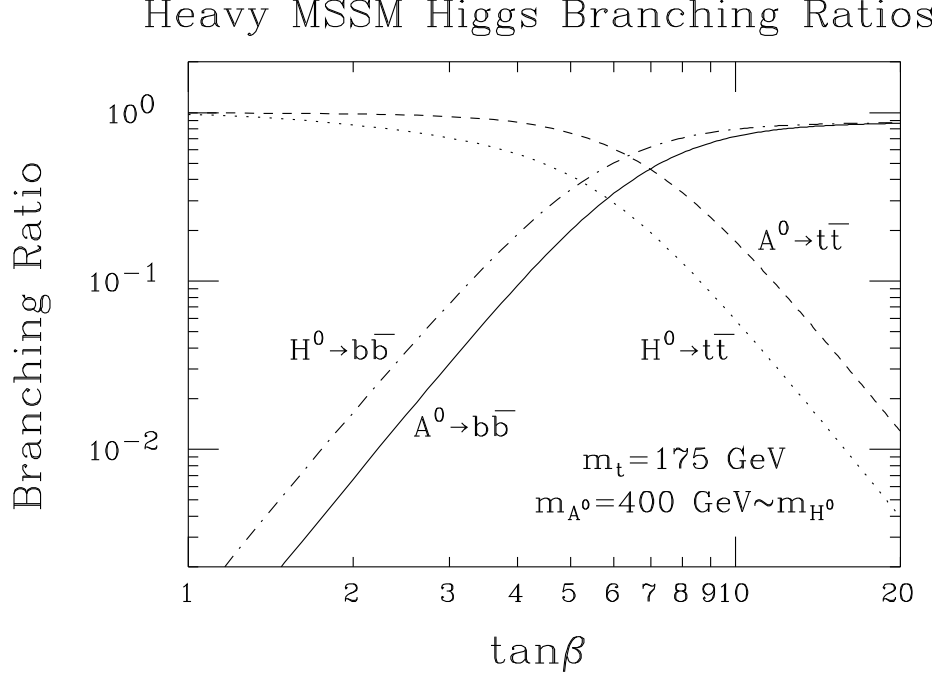## Heavy MSSM Higgs Branching Ratios

Figure 19: Dependence of the $b\bar{b}$ and $t\bar{t}$ branching fractions of the heavy supersymmetric Higgs bosons on $\tan\beta$. Results are for $m_t = 175$ GeV and include two-loop/RGE-improved radiative corrections to Higgs masses, mixing angles, and self-couplings, computed with $m_{\tilde{t}} = 1$ TeV neglecting squark mixing.

3.1.1 Resolution compared to Higgs widths

The first critical question is how the resolution in $\sqrt{s}$ compares to the H^0 and A^0 total widths. The calculated H^0 and A^0 widths are shown in Fig. 3 versus m_{H^0}, m_{A^0} for $\tan\beta = 2$ and 20. In Fig. 20 we give contours of constant total widths for the H^0 and A^0 in the $(m_{A^0}, \tan\beta)$ parameter space. For $m_{A^0}, m_{H^0} \lesssim 500$ GeV, the H^0 and A^0 are typically moderately narrow resonances ($\Gamma_{H^0, A^0} \sim 0.1$ to 6 GeV), unless $\tan\beta$ is larger than 20. For a machine energy resolution of $R = 0.06\%$, and Higgs masses in the 100 GeV to 1 TeV range, the resolution $\sigma_{\sqrt{s}}$ in $\sqrt{s}$ will range from roughly 0.04

GeV to to 0.4 GeV, see Eq. (6). Thus, Figs. 3 and 20 indicate that the H^0 and A^0 widths are likely to be somewhat larger than this resolution in $\sqrt{s}$. For $R = 0.01\%$, this is always the dominant situation.
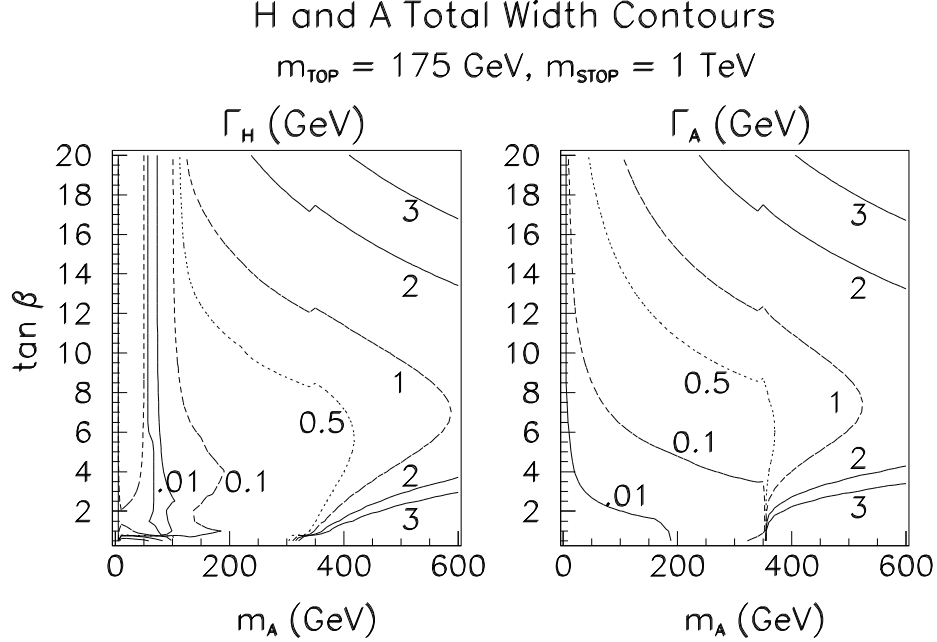

H and A Total Width Contours
$m_{TOP} = 175$ GeV, $m_{STOP} = 1$ TeV

Figure 20: Contours of H^0 and A^0 total widths (in GeV) in the $(m_{A^0}, \tan\beta)$ parameter space. We have taken $m_t = 175$ GeV and included two-loop/RGE-improved radiative corrections using $m_{\tilde{t}} = 1$ TeV and neglecting squark mixing. SUSY decay channels are assumed to be absent.

When the $\sqrt{s}$ resolution is smaller than the Higgs width, then Eq. (7), with $\sqrt{s} \sim m_h$ shows that the cross section will behave as the product of the $\mu\mu$ and final state branching fractions. For low to moderate $\tan\beta$ values, $BF(H^0, A^0 \to \mu\mu)$ and $BF(H^0, A^0 \to b\bar{b})$ grow with increasing $\tan\beta$, while $BF(H^0, A^0 \to t\bar{t})$ falls slowly. Thus, the number of H^0 and A^0 events in both the $b\bar{b}$ and $t\bar{t}$ channels increases with increasing $\tan\beta$. It is this growth with $\tan\beta$ that makes H^0, A^0 discovery possible for relatively modest values of $\tan\beta$ larger than 1. For higher $\tan\beta$ values, the $\mu\mu$ and $b\bar{b}$ branching fractions asymptote to constant values, while that for $t\bar{t}$ falls as $1/(\tan\beta)^4$. Thus, observability in the $t\bar{t}$ channel does not survive to large $\tan\beta$ values.
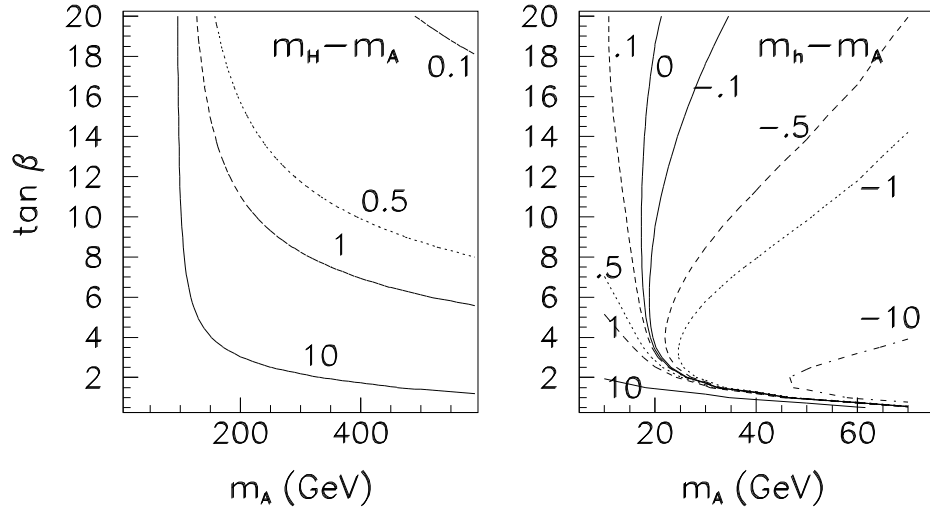
Figure 21: Contours of $m_{H^0} - m_{A^0}$ (in GeV) in the $(m_{A^0}, \tan\beta)$ parameter space. Two-loop/RGE-improved radiative corrections are included taking $m_t = 175$ GeV, $m_{\tilde{t}} = 1$ TeV, and neglecting squark mixing.

47

3.1.2 Overlapping Higgs resonances

The Higgs widths are a factor in the observability of a signal in that approximate Higgs mass degeneracies are not unlikely. For larger m_{A^0}, $m_{A^0} \sim m_{H^0}$, while at smaller m_{A^0} values, $m_{h^0} \sim m_{A^0}$ at larger $\tan\beta$, as illustrated in Fig. 21, where the plotted mass difference should be compared to the Higgs widths in Figs. 3 and 20. At large m_{A^0} and $\tan\beta$, there can be significant overlap of the A^0 and H^0 resonances. To illustrate the possibilities, we show in Fig. 22 the event rate in the $b\bar{b}$ channel as a function of $\sqrt{s}$ (assuming $L = 0.01$ fb^{-1} and event detection/isolation efficiency $\epsilon = 0.5$) taking $m_{A^0} = 350$ GeV in the cases $\tan\beta = 5$ and 10. Continuum $b\bar{b}$ background is included. Results are plotted for the two different resolutions, $R = 0.01\%$ and $R = 0.06\%$. For $R = 0.01\%$, at $\tan\beta = 5$ the resonances are clearly separated and quite narrow, whereas at $\tan\beta = 10$ the resonances have become much broader and much more degenerate, resulting in substantial overlap; but, distinct resonance peaks are still visible. For $R = 0.06\%$, at $\tan\beta = 5$ the resonances are still separated, but have been somewhat smeared out, while at $\tan\beta = 10$ the H^0 and A^0 peaks are no longer separately visible. The $R = 0.06\%$ smearing does not greatly affect the observation of a signal, but would clearly make separation of the H^0 and A^0 peaks and precise determination of their individual widths much more difficult.

In the following section, we perform our signal calculations by centering $\sqrt{s}$ on m_{A^0}, but including any H^0 signal tail, and vice versa. At small m_{A^0}, there is generally only small overlap between the A^0 and h^0 since their widths are small, but we follow a similar procedure there. We also mainly employ the optimistic $R = 0.01\%$ resolution that is highly preferred for a SM-like Higgs boson. Since the MSSM Higgs bosons do not have especially small widths, results for $R = 0.06\%$ are generally quite similar.

3.1.3 Observability for h^0, H^0 and A^0

We first consider fixed $\tan\beta$ values of 2, 5, and 20, and compute $\epsilon\bar{\sigma}_h BF(h \to b\bar{b}, t\bar{t})$ for $h = h^0, H^0, A^0$ as a function of m_{A^0}. (The corresponding h^0 and H^0 masses can be found in Fig. 2.) Our results for $R = 0.01\%$ appear in Figs. 23, 24, and 25. Also shown in these figures are the corresponding $S/\sqrt{B}$ values assuming an integrated luminosity of $L = 0.1$ fb^{-1}; results for other L possibilities are easily obtained by using $S/\sqrt{B} \propto 1/\sqrt{L}$. These figures also include (dot-dashed) curves for $R = 0.06\%$ in the $b\bar{b}$ channel at $\tan\beta = 2$.
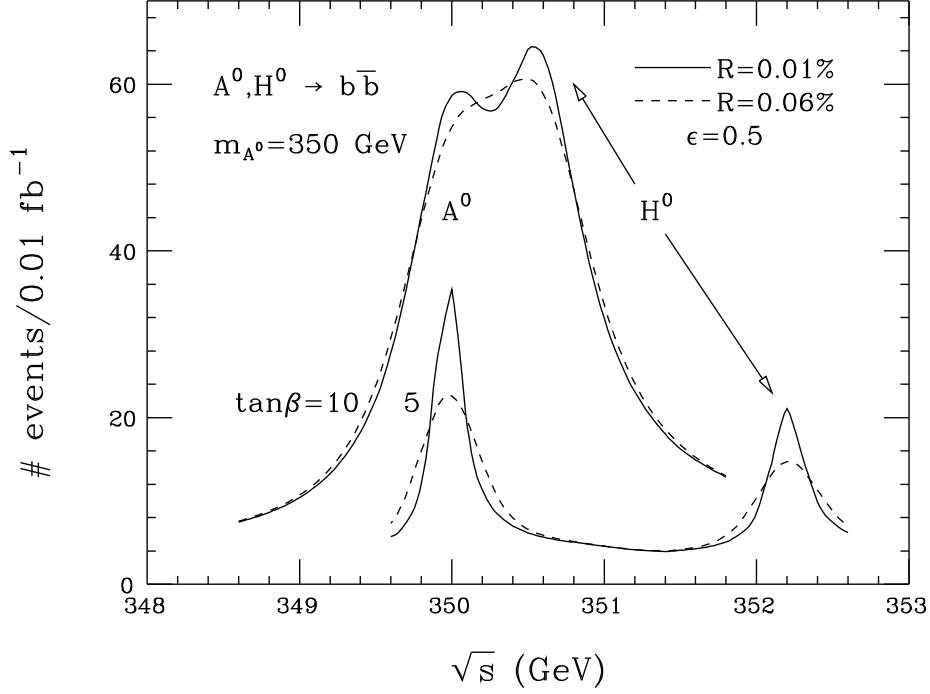
Figure 22: Plot of $b\overline{b}$ final state event rate as a function of $\sqrt{s}$ for $m_{A^0} = 350$ GeV, in the cases $\tan\beta = 5$ and 10, resulting from the H^0, A^0 resonances and the $b\overline{b}$ continuum background. We have taken $L = 0.01$ fb^{-1} (at any given $\sqrt{s}$), $\epsilon = 0.5$, $m_t = 175$ GeV, and included two-loop/RGE-improved radiative corrections to Higgs masses, mixing angles and self-couplings using $m_{\widetilde{t}} = 1$ TeV and neglecting squark mixing. SUSY decays are assumed to be absent. Curves are given for two resolution choices: $R = 0.01\%$ and $R = 0.06\%$

Figure 23 shows that the h^0 can be detected at the 5σ statistical level with just $L = 0.1$ fb^{-1} for essentially all of parameter space, if $R = 0.01\%$. Only for $\tan\beta \lesssim 2$ is m_{h^0} sufficiently near m_Z at large m_{A^0} (for which its $\mu^+\mu^-$ coupling is not enhanced) that more luminosity may be required. At low m_{A^0}, the h^0 is not SM-like and has highly enhanced $\mu^+\mu^-$ and $b\bar{b}$ couplings. It is also no longer extremely narrow, and is produced with a very high rate implying that high statistics studies of its properties would be possible. The $R = 0.06\%$ $\tan\beta = 2$ curve illustrates the large loss in observability that occurs for non-optimal resolution when the h^0 is SM-like at large m_{A^0} and has a very small width.
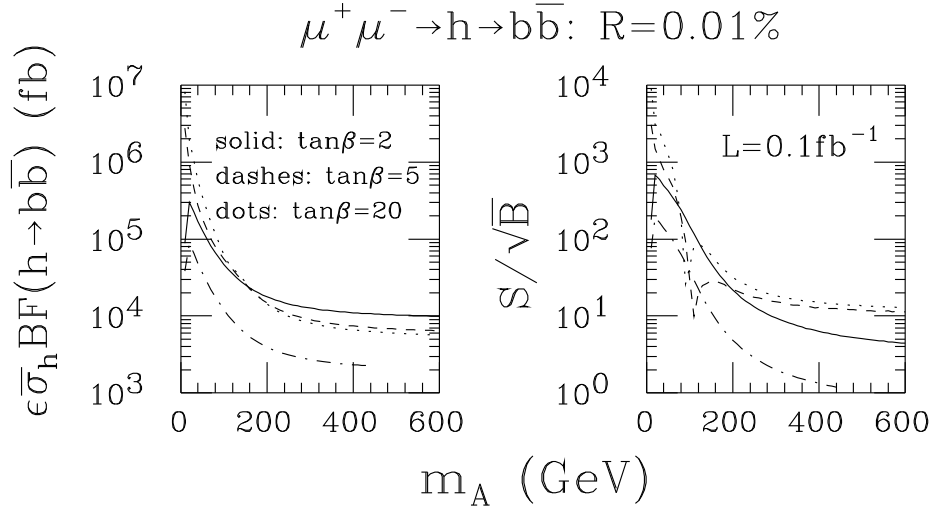

Figure 23: Plot of $\epsilon\bar{\sigma}_{h^0}BF(h^0 \to b\bar{b})$ versus m_{A^0} for $\tan\beta = 2$, 5 and 20. Also shown is the corresponding $S/\sqrt{B}$ for $L = 0.1$ fb^{-1}. We have taken $R = 0.01\%$, $\epsilon = 0.5$, $m_t = 175$ GeV, and included two-loop/RGE-improved radiative corrections to Higgs masses, mixing angles and self-couplings using $m_{\tilde{t}} = 1$ TeV and neglecting squark mixing. SUSY decays are assumed to be absent in computing BF. Also shown as the dot-dashed curve are the $R = 0.06\%$ results at $\tan\beta = 2$ in the $b\bar{b}$ channel.

Results for $\epsilon\bar{\sigma}_h BF(h \to b\bar{b}, t\bar{t})$ for $h = H^0$ and $h = A^0$ are displayed in Figs. 24 and 25, respectively, along with the corresponding $L = 0.1$ fb^{-1} $S/\sqrt{B}$ values. For a luminosity of $L = 0.01$ fb^{-1}, the $S/\sqrt{B}$ values of the figures should be reduced by a factor of 0.32. For $L = 0.3$, multiply by 1.7. This range of luminosities will be that which arises when we consider searching for the H^0 and A^0 by scanning in $\sqrt{s}$.

The dot-dashed curves illustrate the fact that $R = 0.06\%$ resolution does not cause a large loss in observability relative to $R = 0.01\%$ in the case of the A^0 and, especially, the H^0; the largest effect is for the $\tan\beta = 2$ case in the $b\bar{b}$ channel. For $\tan\beta = 5$ and 20, and for all $t\bar{t}$ curves, the results for $R = 0.06\%$ are virtually indistinguishable from those for $R = 0.01\%$.
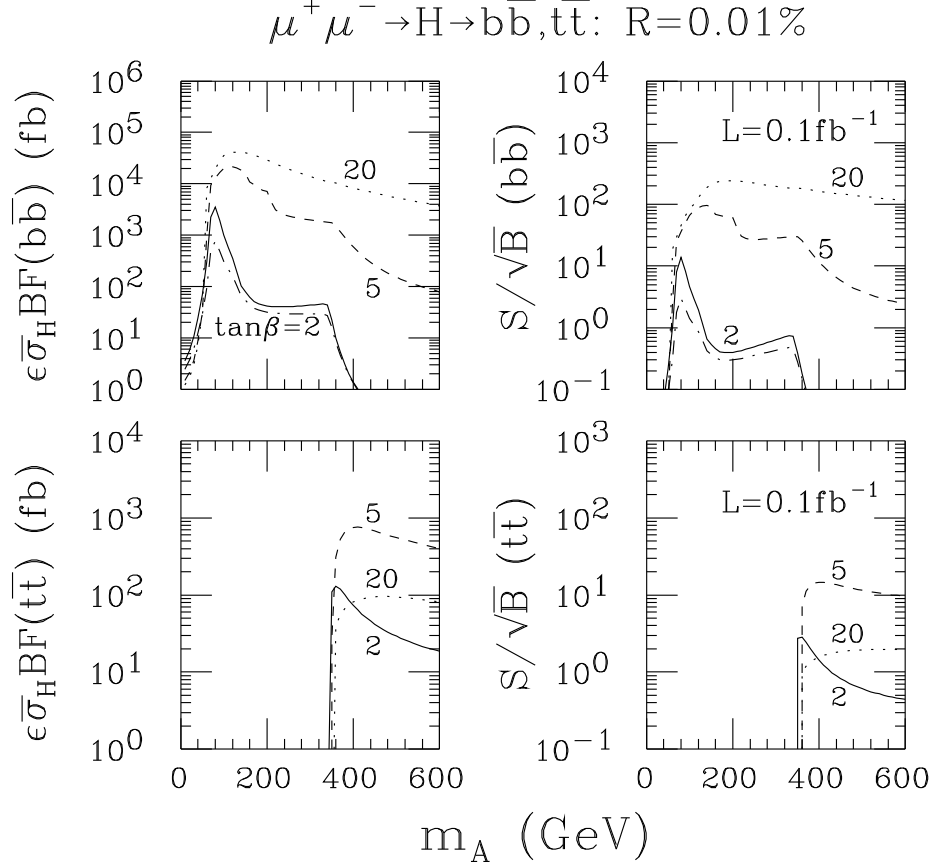

Figure 24: Plot of $\epsilon\bar{\sigma}_{H^0}BF(H^0 \to b\bar{b}, t\bar{t})$ versus m_{A^0} for $\tan\beta = 2$, 5 and 20. Also shown are the corresponding $S/\sqrt{B}$ values for $L = 0.1$ fb^{-1}. The inputs are specified in the caption of Fig. 23. Also shown as the dot-dashed curve are the $R = 0.06\%$ results at $\tan\beta = 2$ in the $b\bar{b}$ channel.

An alternative picture that is especially useful for assessing the parameter space region over which h^0, A^0 and/or H^0 discovery will be possible at the $\mu^+\mu^-$ collider is that given in Fig. 26, for which we have taken $R = 0.06\%$. The contours in $(m_{A^0}, \tan\beta)$ parameter space denote the luminosity required for a 5σ signal when $\sqrt{s}$
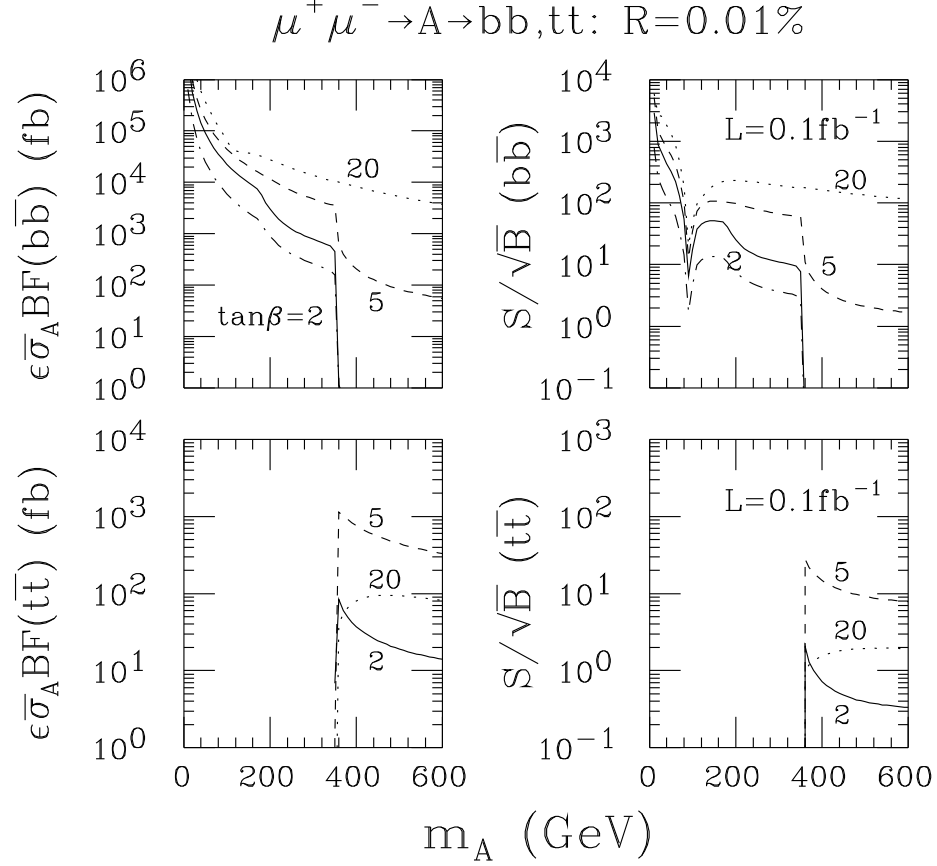
Figure 25: Plot of $\epsilon\overline{\sigma}_{A^0}BF(A^0 \to b\overline{b}, t\overline{t})$ versus m_{A^0} for $\tan\beta = 2$, 5 and 20. Also shown are the corresponding $S/\sqrt{B}$ values for $L = 0.1$ fb^{-1}. The inputs are specified in the caption of Fig. 23. Also shown as the dot-dashed curve are the $R = 0.06\%$ results at $\tan\beta = 2$ in the $b\overline{b}$ channel.

is taken equal to the Higgs mass in question. For the window labelled $H^0 \to b\bar{b}$ we take $\sqrt{s} = m_{H^0}$, for the $h^0 \to b\bar{b}$ window we take $\sqrt{s} = m_{h^0}$, while $\sqrt{s} = m_{A^0}$ for the $A^0 \to b\bar{b}$ and $A^0 \to t\bar{t}$ contours. The 5σ contours are for luminosities of $L = 0.001$, 0.01, 0.1, 1, and 10 fb^{-1}. The larger the L the larger the discovery region. In the case of $A^0 \to t\bar{t}$, 5σ is only achieved for the four luminosities $L = 0.01, 0.1, 1, 10$ fb^{-1}. In the case of the h^0, $L = 10$ fb^{-1} always yields a 5σ signal within the parameter space region shown.

Muon Collider bb and tt̄ 5σ Discovery Contours
For L=0.001, 0.01, 0.1, 1, and 10 fb⁻¹
$m_{TOP} = 175$ GeV, $m_{STOP} = 1$ TeV, R = 0.06%, $\varepsilon = 0.5$
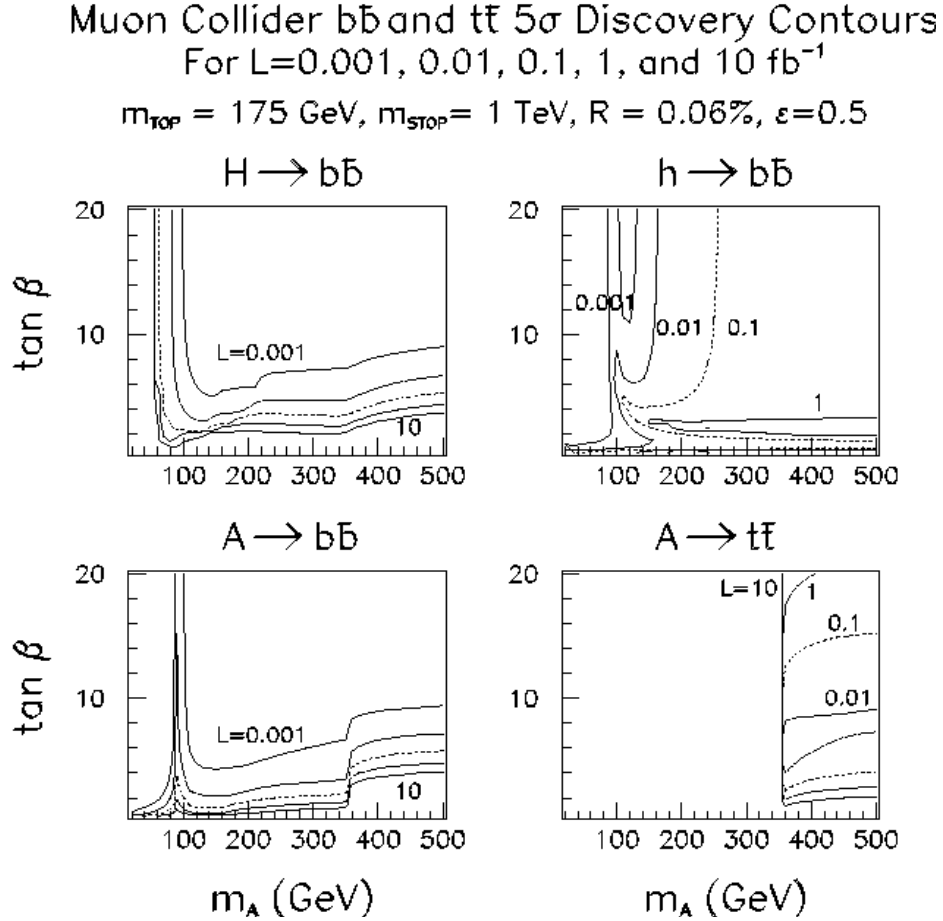
Figure 26: Contours in $(m_{A^0}, \tan\beta)$ parameter space of the luminosity required for 5σ Higgs signals. Contours for $L = 0.001$, 0.01, 0.1, 1, and 10 fb^{-1} are given. For $A^0 \to t\bar{t}$, $L = 0.001$ fb^{-1} does not yield a 5σ signal and no corresponding contour appears. For $h^0 \to b\bar{b}$, $L = 10$ fb^{-1} yields a 5σ signal for all of parameter space, and so only $L = 0.001 - 1$ fb^{-1} contours appear. The inputs are specified in the caption of Fig. 23.

With regard to the h^0, Fig. 26 shows that for $R = 0.06\%$ and luminosities some-what less than 1 fb^{-1}, h^0 could only be detected in the $b\bar{b}$ mode at large m_{A^0} if $\tan\beta$ is sufficiently far from 1 that m_{h^0} is not near m_Z. In contrast, when m_{A^0} is sufficiently small that m_{h^0} is small and the h^0 is no longer SM-like, and has enhanced $\mu\mu$ and $b\bar{b}$ couplings, rather modest luminosity is required for a 5σ signal at $\sqrt{s} = m_{h^0}$; for instance, $L \lesssim 0.001$ fb^{-1} will allow detection of a signal from the h^0 (and the possibly overlapping A^0) over most of the $m_{A^0} \lesssim 100$ GeV portion of parameter space even for $R = 0.06\%$. However, we have noted that it is theoretically quite likely that m_{A^0} is large and that the h^0 is SM-like. Detection of the H^0 and A^0 then becomes of paramount interest.

3.1.4 Detecting the H^0 and A^0 by scanning in $\sqrt{s}$

In order to discover the H^0 or A^0 in the $\gtrsim 250$ GeV region, we must scan over $\sqrt{s}$ values between 250 GeV and 500 GeV (the presumed upper limit for the FMC). The separation between scan points is determined by the larger of the expected widths and the $\sqrt{s}$ resolution, $\sigma_{\sqrt{s}}$. If $\tan\beta \gtrsim 2$, then for m_{H^0} and m_{A^0} near 250 GeV, the A^0 and H^0 widths are of order $0.05 - 0.1$ GeV. For masses near 500 GeV, their widths are at least 1 GeV (cf. Fig. 20). Meanwhile, for $R = 0.01\%$ ($R = 0.06\%$), $\sigma_{\sqrt{s}}$ ranges from ~ 0.018 GeV (~ 0.11 GeV) to ~ 0.035 GeV ($\sim .21$ GeV) as $\sqrt{s}$ ranges from 250 GeV to 500 GeV. Thus, it is reasonable to imagine using scan points separated by 0.1 GeV for $m_{A^0} \sim m_{H^0}$ near 250 GeV, rising to 1 GeV by $\sqrt{s} = 500$ GeV. It will also be important to note that the luminosity required per point for detection of the A^0 and H^0 is less for masses below $2m_t$ than above. In assessing the detectability of the H^0 and A^0 by scanning we devote

- $L = 0.01$ fb^{-1} to each of 1000 points separated by 0.1 GeV between 250 and 350 GeV,

- $L = 0.1$ fb^{-1} to each of 100 points separated by 0.5 GeV between 350 and 400 GeV,

- and $L = 0.3$ fb^{-1} to each of 100 points separated by 1 GeV between 400 and 500 GeV.

This selection of points more or less ensures that if the H^0 and A^0 are present then

one of the scan points would have $\sqrt{s} \sim m_{H^0}, m_{A^0}$ within either the $\sigma_{\sqrt{s}}$ resolution or the Higgs width. The total luminosity required for this scan would be 50 fb^{-1}.

We now employ the 5σ contours of Fig. 26 to assess the portion of $(m_{A^0}, \tan\beta)$ parameter space over which the above scan will allow us to detect the H^0 and A^0 in the $b\bar{b}$ and $t\bar{t}$ channels. The 5σ luminosity contours of interest will be the curves corresponding to $L = 0.01$ fb^{-1}, $L = 0.1$ fb^{-1} and $L = 1$ fb^{-1}. The 5σ contour for $L = 0.3$ fb^{-1} luminosity per point, as employed in our scan procedure from 400 to 500 GeV, is midway between these last two curves. Fig. 26 shows that, by performing the scan in the manner outlined earlier, one can detect the H^0, A^0 in the $b\bar{b}$ mode for all $\tan\beta$ values above about $2-4$ for $m_{H^0}, m_{A^0} \lesssim 2m_t$ and above about $3-5$ for $2m_t \lesssim m_{H^0}, m_{A^0} \lesssim 500$ GeV. Meanwhile, in the $t\bar{t}$ mode, the $A^0 \to t\bar{t}$ signal can be seen for $m_{A^0} \gtrsim 2m_t$ provided $\tan\beta \gtrsim 3$. Together, the $b\bar{b}$ and $t\bar{t}$ signals are viable for a remarkably large portion of parameter space, which includes, in particular, essentially all of the wedge region where the LHC lacks sensitivity (see Fig. 18). At worst, there would be a very small $\tan\beta$ window for $m_{A^0} \gtrsim 2m_t$ between $\tan\beta = 3$ and $\tan\beta = 4$, for which the signal might be missed during the above described scan and also no signal seen at the LHC. In practice, it might be desirable to simply devote several years of running to the scan in order to ensure that the A^0 and H^0 are detected if present.

The implementation of the above scan is very demanding upon the machine design because:

- several rings may be needed to have high luminosities over a broad range of $\sqrt{s}$;

- it must be possible *over this broad range of energies* to quickly (for example, once every hour or so in the 250–350 GeV range) reset $\sqrt{s}$ with an accuracy that is a small fraction of the proposed step sizes.

It is too early to say if these demands can both be met.

Finally, we note the obvious conflict between this scan and the desirable $\sqrt{s} = m_{h^0}$, $L = 50$ fb^{-1} study of the SM-like h^0. A multi-year program will be required to accomplish both tasks.

3.1.5 Non-$b\bar{b}$ final state modes for heavy Higgs detection

The reader may note that $\sqrt{s} = m_{H^0}$ does not yield an observable s-channel signal in the $b\bar{b}$ mode for $m_{A^0} \lesssim 100$ GeV. Although the H^0 is SM-like in this

parameter region in that it does not have enhanced coupling to $\mu\mu$ and $b\overline{b}$, its decays are dominated by h^0h^0 and, for $m_{A^0} \lesssim 60$ GeV, A^0A^0 pairs; ZA^0 decays also enter for small enough m_{A^0}. This means that the H^0 total width is quite large, in particular much larger than the $\sqrt{s}$ spread. The large total width also implies that $BF(H^0 \to \mu\mu)$ is small. Equation (11) then shows that the production rate for the H^0 will be small, and that the rate in the $b\overline{b}$ final state will be further suppressed by the small value of $BF(H^0 \to b\overline{b})$. The only possible channels for observation of the H^0 in the $m_{A^0} \lesssim 100$ GeV region are h^0h^0, A^0A^0, ZA^0. As we discuss below, these could prove to be viable.

The full set of channels to be considered are

$$H^0 \to h^0h^0, \qquad H^0 \to A^0A^0, \qquad H^0 \to ZA^0, \qquad A^0 \to Zh^0. \qquad (24)$$

The h^0h^0, A^0A^0 final states primarily ($\sim 80\%$ of the time) yield 4b's. The ZA^0, Zh^0 final states yield $2j2b$ about 60% of the time. In either case, we can demand that there be two pairs of jets, each pair falling within narrow mass intervals. In addition, two b-tags can be required. Thus, these channels will have small background. To illustrate the size of the signal in these channels, we present in Fig. 27 the $L = 10$ fb^{-1} signal rates for the above four modes, assuming a net 50% efficiency (including branching fractions and tagging efficiencies, as well as double mass-binning). In the $H^0 \to h^0h^0$ case, at least 50 events are obtained in essentially all but the $m_{A^0} = 60-230, \tan\beta \gtrsim 2.5$ region; the 5000 event contour is confined to a narrow region around $m_{A^0} = 65-70, \tan\beta \gtrsim 2$ and to the (disjoint) teardrop region labelled; the 50 and 500 event contours are as labelled. At least 500 events are predicted in the $m_{A^0} \lesssim 60$ region for all $\tan\beta$. In the $H^0 \to A^0A^0$ case, at least 500 events are obtained in the $m_{A^0} \lesssim 60$ and $\tan\beta \gtrsim 2$ region. In the $H^0 \to ZA^0$ case, only the 5 event level is achieved over even the small piece of parameter space shown. Finally, in the $A^0 \to Zh^0$ case all contours are easily identified by the labelling. No events are expected for m_{A^0} below about 200 GeV, where the $A^0 \to Zh^0$ decay mode is no longer kinematically allowed. It is kinematics that also dictates the rather restricted regions at low m_{A^0} for which $H^0 \to A^0A^0$ and $H^0 \to ZA^0$ events occur.

In order to discuss the observability of the above signals, we need to compute the background level, which we do not do in this report. After b-tagging and mass reconstruction we believe that backgrounds should be modest. In the absence of any explicit calculation we can only make the following guesstimates. Based on the event

56

Figure 27: Event rate contours for $H^0 \to h^0 h^0$, $H^0 \to A^0 A^0$, $H^0 \to Z A^0$ and $A^0 \to Z h^0$ in $(m_{A^0}, \tan\beta)$ parameter space for integrated luminosity $L = 10$ fb^{-1}. Contours for 5, 50, 500 and 5000 events are shown in the first and last cases. There are 500 or more $H^0 \to A^0 A^0$ events if $m_{A^0} \lesssim 60$ GeV and $\tan\beta \gtrsim 2$, but $H^0 \to Z A^0$ barely reaches the 5 event level. Two-loop/RGE-improved radiative corrections to Higgs masses, mixing angles and self-couplings are included, taking $m_t = 175$ GeV, $m_{\tilde{t}} = 1$ TeV and neglecting squark mixing.

rates of Fig. 27 it should be possible to study the $H^0 \to h^0 h^0$ channel over a significant fraction of parameter space with $L \sim 1$ fb^{-1}. In particular, luminosities at and above this level could open up the $m_{A^0} \lesssim 60$ GeV region for both this mode and the $H^0 \to A^0 A^0$ mode. In contrast, it will obviously require very substantial luminosity to detect $H^0 \to Z A^0$, even when not kinematically suppressed. A viable $A^0 \to Z h^0$ signal may be possible, when kinematically allowed, only so long as m_{A^0} and $\tan\beta$ are not large; when m_{A^0} is large the tree-level coupling is suppressed (which suppression occurs most rapidly at large $\tan\beta$) and there are too few events for a useful signal.

Although these modes provide somewhat more challenging signals than the $b\bar{b}$ channel signal, their observation would provide tests of important Higgs couplings. In particular, detection of the $H^0 \to h^0 h^0$ and $H^0 \to A^0 A^0$ modes would allow a direct probe of these very interesting Higgs boson self-couplings. The procedure will be outlined in a later section. In general, determination of the Higgs boson self-couplings is quite difficult at other machines. In particular, even when a relevant branching fraction can be measured, knowledge of the total width is required in order to extract the partial width and coupling. Without a $\mu^+\mu^-$ collider, measurement of the total width is only possible if the width is substantially larger than the resolution implied by final state mass reconstruction at the Higgs mass. This is not the case for the H^0 and A^0 unless $\tan\beta$ is very large.

3.2 MSSM Higgs boson detection using the bremsstrahlung tail spectrum

In this section, we discuss an alternative way of searching for the A^0 and H^0 by running the $\mu^+\mu^-$ collider at full energy but looking for excess events arising from the luminosity on the low-energy end of the bremsstrahlung tail (see Appendix C). This latter technique proves to be somewhat competitive with the scan technique just described, provided that excellent resolution in reconstructing the $b\bar{b}$ final state mass can be achieved and provided that large total integrated luminosity is devoted to such running. It would have two distinct advantages over the scanning approach.

- It would not require the construction of multiple rings in order to maintain high luminosity over a broad range of $\sqrt{s}$ collision energies.

- A large number of events in the Zh mode for the SM-like h^0 could be simulta-

neously accumulated.

As for the scan procedure, the bremsstrahlung tail technique is viable only if the $h \to \mu^+\mu^-$ coupling is significantly enhanced relative to the SM $h_{SM} \to \mu^+\mu^-$ coupling; only then is a Higgs boson with mass substantially below $\sqrt{s}$ produced at a large rate by virtue of the bremsstrahlung tail. Of course, once the H^0 and/or A^0 is found using the bremsstrahlung technique, it would then be highly desirable to run the machine with $\sqrt{s} \sim m_{H^0}, m_{A^0}$ in order to study in detail the widths and other properties of the H^0, A^0.

For our study of the bremsstrahlung tail possibility, we shall assume that the $b\bar{b}$ final state mass can be reconstructed to within ± 5 GeV. A full study of this mode of detection should generate events, smear the b jets using expected resolutions, allow for semi-leptonic b decays, and incorporate tagging efficiencies. The reconstructed mass of the $b\bar{b}$ final state for each event should then be binned and one would then look for a peak over the expected background level. We will not perform this detailed simulation here. Instead, we compute as a function of $m_{b\bar{b}}$ (the central value of the $b\bar{b}$ final state mass) the number of events in the interval $[m_{b\bar{b}} - 5 \text{ GeV}, m_{b\bar{b}} + 5 \text{ GeV}]$. In estimating the significance of any peak seen in the spectrum, we will choose $m_{b\bar{b}}$ at the center of the peak, and compare the excess of events in the above interval (the signal S) to the number of events expected if there is no Higgs boson present (the background B). The statistical significance will be computed as $S/\sqrt{B}$. In computing the number of events we assume an integrated luminosity of $L = 50$ fb^{-1} and assume an event reconstruction and tagging efficiency of $\epsilon = 0.5$. Correspondingly, only the continuum $b\bar{b}$ final states from $\gamma^\star, Z^\star$ processes will be included in B (using also $\epsilon = 0.5$). These latter assumptions are the same ones employed in our other analyses.

3.2.1 Mass peaks

It will be useful to first display some typical mass peaks. In Fig. 28, we plot the number of events in the interval $[m_{b\bar{b}} - 5 \text{ GeV}, m_{b\bar{b}} + 5 \text{ GeV}]$ as a function of $m_{b\bar{b}}$ for three m_{A^0} choices: $m_{A^0} = 120$, 300 and 480 GeV. In each case, results for $\tan\beta = 5$ and 20 are shown. The event enhancements derive from the presence of the H^0 and A^0 Higgs bosons. There would be no visible effect for the choice of $m_{A^0} = 100$ GeV for any $\tan\beta$ value below 20. This is because all the Higgs masses are sitting on the very large Z peak and, in addition, none of the $\mu^+\mu^-$ couplings are fully enhanced. For

the three m_{A^0} values considered in Fig. 28, we observe event excesses for $\tan\beta = 20$ in all cases. For $\tan\beta = 5$, the $m_{A^0} = 300$ GeV peak is clear, while $m_{A^0} = 480$ GeV yields a shoulder of excess events (that is statistically significant); nothing is visible for $m_{A^0} = 120$ GeV. For $\tan\beta \lesssim 2$, no peaks or excesses would be visible for any of the above m_{A^0} choices. Finally, we note that enhancements due to the h^0 resonance would not be visible, regardless of $\tan\beta$, for $m_{A^0} \gtrsim 100$ GeV.

3.2.2 Significance of signals

We will now proceed to survey the $S/\sqrt{B}$ expectations. We do this as a function of location in the $(m_{A^0}, \tan\beta)$ parameter space as follows. For each choice of $(m_{A^0}, \tan\beta)$ we determine m_{h^0} and m_{H^0}. We then compute $S/\sqrt{B}$ for the three locations $m_{b\bar{b}} = m_{h^0}$, $m_{b\bar{b}} = m_{H^0}$ and $m_{b\bar{b}} = m_{A^0}$, where S and B are computed by counting events in the $m_{b\bar{b}} \pm 5$ GeV window. Effects from overlapping Higgs resonances are included. The 5σ discovery contours for each of these three window locations are plotted in $(m_{A^0}, \tan\beta)$ parameter space for integrated luminosities of $L = 0.5, 5, 50$ and 200 fb^{-1} in Fig. 29, taking $\sqrt{s} = 500$ GeV and $R = 0.1\%$.

As expected from Fig. 28, the window centered at $m_{b\bar{b}} = m_{h^0}$ only yields a statistically significant excess if $\tan\beta$ is large and m_{h^0} is not near m_Z. (m_{h^0} near m_Z at high $\tan\beta$ corresponds to $m_{A^0} \sim 95$ GeV.) Since the Zh^0 mode will yield an observable signal regardless of the $(m_{A^0}, \tan\beta)$ values, the bremsstrahlung tail excess would mainly be of interest as a probe of the $\Gamma(h^0 \to \mu^+\mu^-)$ partial width prior to running at $\sqrt{s} = m_{h^0}$.

However, the ± 5 GeV intervals centered at $m_{b\bar{b}} = m_{H^0}$ and $m_{b\bar{b}} = m_{A^0}$ (which, include events from the overlapping A^0 and H^0 resonances, respectively) yield 5σ statistical signals for a substantial portion of parameter space if L is large. With $L = 50$ fb^{-1}, a 5 sigma discovery of the H^0 and A^0 using the $\sqrt{s} = 500$ GeV bremsstrahlung tail is viable down to $\tan\beta \gtrsim 6.5$ at $m_{A^0} = 250$ GeV improving to $\tan\beta \gtrsim 5$ at 480 GeV. This is not quite as far down in $\tan\beta$ as can be probed for $250 \lesssim m_{A^0} \lesssim 500$ GeV by the previously described scan over a series of $\sqrt{s}$ values using $0.01 - 0.3$ fb^{-1} of luminosity at each scan point. As m_{H^0}, m_{A^0} move closer to m_Z, the 5σ discovery contours move to much larger $\tan\beta$ values, whereas the scanning technique would yield 5σ signals for $\tan\beta$ values as low as $\tan\beta \sim 3 - 4$ all the way down to $m_{A^0} \gtrsim 60$ GeV.
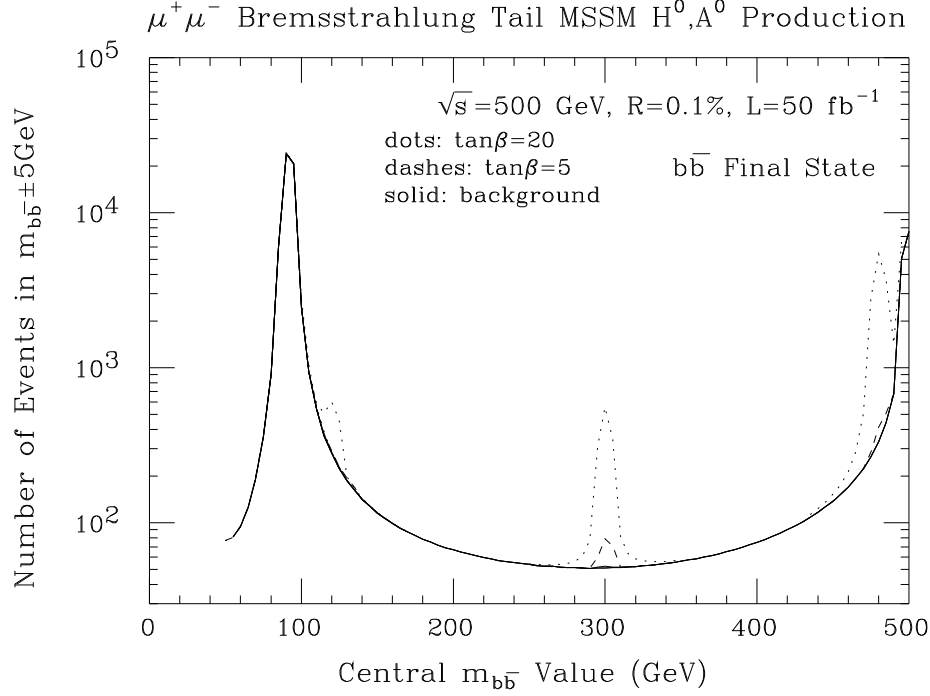
Figure 28: Taking $\sqrt{s} = 500$ GeV, integrated luminosity $L = 50$ fb^{-1}, and $R = 0.1\%$, we consider the $b\bar{b}$ final state and plot the number of events in the interval $[m_{b\bar{b}} - 5$ GeV$, m_{b\bar{b}} + 5$ GeV$]$, as a function of the location of the central $m_{b\bar{b}}$ value, resulting from the low $\sqrt{\hat{s}}$ bremsstrahlung tail of the luminosity distribution. MSSM Higgs boson H^0 and A^0 resonances are present for the parameter choices of $m_{A^0} = 120$, 300 and 480 GeV, with $\tan\beta = 5$ and 20 in each case. Enhancements for $m_{A^0} = 120$, 300 and 480 GeV are visible for $\tan\beta = 20$; $\tan\beta = 5$ yields visible enhancements only for $m_{A^0} = 300$ and 480 GeV. Two-loop/RGE-improved radiative corrections are included, taking $m_t = 175$ GeV, $m_{\tilde{t}} = 1$ TeV and neglecting squark mixing. SUSY decay channels are assumed to be absent.

61
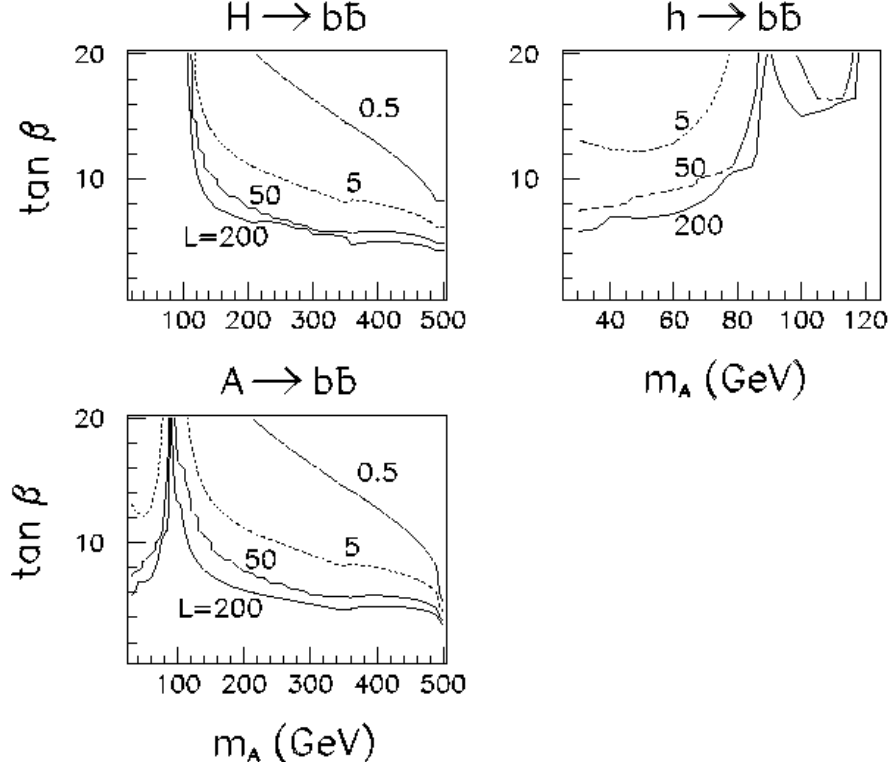
Figure 29: Taking $\sqrt{s} = 500$ GeV and $R = 0.1\%$, we consider the $b\bar{b}$ final state and compute the Higgs signal (S) and background (B) rates in the mass interval $[m_{b\bar{b}} - 5 \text{ GeV}, m_{b\bar{b}} + 5 \text{ GeV}]$, with $m_{b\bar{b}} = m_{H^0}$, $m_{b\bar{b}} = m_{h^0}$, and $m_{b\bar{b}} = m_{A^0}$, resulting from the low $\sqrt{\hat{s}}$ bremsstrahlung tail of the luminosity distribution. $S/\sqrt{B} = 5$ contours are shown for integrated luminosities of $L = 0.5$, 5, 50, and 200 fb^{-1}. Two-loop/RGE-improved radiative corrections are included, taking $m_t = 175$ GeV, $m_{\tilde{t}} = 1$ TeV and neglecting squark mixing. SUSY decay channels are assumed to be absent.

3.2.3   Strategy: scan vs. maximum energy

If $Z^\star \to H^0 A^0$ is not observed at a $\sqrt{s} = 500$ GeV e^+e^- machine and if discovery of the H^0 and A^0 in the $250 - 500$ GeV mass range is the primary goal, at the $\mu^+\mu^-$ collider it would be a close call as to whether it would be better to immediately embark on the $\sqrt{s}$ scan or accumulate luminosity at the maximum machine energy. The $\sqrt{s}$ scan probes $\tan\beta$ values that are lower by only 1 or 2 units than the bremsstrahlung tail search. This statement assumes that a final state mass resolution of order ± 5 GeV can be achieved (even after including all semi-leptonic decay effects and so forth) in the $b\bar{b}$ final state for the latter search. If not, the $\sqrt{s}$ scan is the preferred technique. Thus, resolution and missing energy could become critical issues for the detector(s) in deciding the best approach.

If an e^+e^- collider is not operational at the time a $\mu^+\mu^-$ collider begins running, then the decision as to which approach to choose for H^0 and A^0 discovery becomes even more delicate unless the LHC has clearly ruled out $m_{A^0}, m_{H^0} \lesssim 250$ GeV (which it probably can do — see Fig. 18). Without a lower bound on m_{A^0}, m_{H^0}, the $\sqrt{s}$ scan would have to be extended to lower $\sqrt{s}$, requiring more luminosity. In contrast, by accumulating $L = 50$ fb^{-1} at full energy, $\sqrt{s} = 500$ GeV, it would be possible to simultaneously either discover or rule out $m_{A^0}, m_{H^0} \lesssim \sqrt{s}/2$ for all $\tan\beta$ and $\sqrt{s}/2 \lesssim m_{H^0}, m_{A^0}, \lesssim \sqrt{s}$ for $\tan\beta \gtrsim 5-7$. Note that $m_{A^0}, m_{H^0} \lesssim \sqrt{s}/2 - 20$ GeV can be ruled out in the $Z^\star \to H^0 h$ mode with perhaps as little as $5 - 10$ fb^{-1}. For luminosities of order 10 fb^{-1} the bremsstrahlung tail technique would probe $\tan\beta \gtrsim 11$ for $m_{A^0} \sim 250$ GeV improving to $\tan\beta \gtrsim 6$ for $m_{A^0} \sim 500$ GeV. After accumulating the $L = 5 - 10$ fb^{-1}, the $\mu^+\mu^-$ collider could then be switched to the scan mode of operation if no signal has been found.

3.3   Detailed studies of the H^0 and A^0

However the H^0 and A^0 are first detected, one will wish to measure the total and partial widths of the H^0 and A^0. Once again, the $\mu^+\mu^-$ collider can play a crucial role. We will not give detailed estimates of what can be accomplished, but rather confine ourselves to outlining the procedures and strategies. The time scale and available luminosity for implementing these procedures depends dramatically upon whether or not one must first discover the H^0 and A^0 by scanning or in the bremsstrahlung tail (either of which would require a luminosity expenditure of $L \sim 50$ fb^{-1}), as opposed

63

to observing them at the LHC (typically possible for $\tan\beta \lesssim 3 - 4$ at high m_{A^0}) or at an e^+e^- collider (requiring $m_{A^0}, m_{H^0} \lesssim \sqrt{s}/2$).

One might presume that once a Higgs boson with $\Gamma_h^{\rm tot}$ larger than the rms $\sqrt{s}$ spread is discovered, direct measurement of the Higgs width would be quite straightforward with a simple scan over several $\sqrt{s}$ settings. This is indeed the case unless there is a second nearby Higgs boson. As it happens, the A^0 and H^0 are sufficiently degenerate in some regions of parameter space (large m_{A^0} and large $\tan\beta$), see Figs. 20 and 21, that a measurement of the widths of the A^0 and H^0 separately will require sorting out two overlapping resonance bumps, which, in turn, necessitates an appropriate scan. Two sample possibilities were illustrated earlier in Fig. 22, where the H^0 and A^0 resonance bumps that would appear as a function of $\sqrt{s}$ are illustrated for $m_{A^0} = 350$ GeV in the cases $\tan\beta = 5$ and 10. As noted earlier, separation of the peaks and precision width measurements are both much easier if we have excellent beam energy resolution; we assume $R = 0.01\%$. At $\tan\beta = 5$, we estimate that by accumulating roughly 0.01 fb^{-1} at each of 3 appropriately placed $\sqrt{s}$ choices near the center and on either side of each of the two separated peaks, the widths of the H^0 and A^0 could be measured to about 33%; 10% width determination would require about 0.1 fb^{-1} per point. At the higher $\tan\beta = 10$ value, one would clearly have to accumulate data in the dip between the overlapping peaks, near both peaks, below the double peak and above the double peak, and perform a fit to the two Higgs resonances simultaneously. A minimum of 5 data points would be required. Again, roughly 0.01 fb^{-1} per point would be needed to determine $\Gamma_{H^0}^{\rm tot}$ and $\Gamma_{A^0}^{\rm tot}$ to the 33% level, or 0.1 fb^{-1} per point for a 10% determination. Very large $\tan\beta$ values yield the worst scenarios since the H^0 and A^0 peaks are, then, simultaneously broad and very degenerate. Determination of the individual widths would become extremely difficult.

The production rate in a given channel is proportional to $BF(h \to \mu^+\mu^-)BF(h \to X)$ (for $\sigma_{\sqrt{s}} \ll \Gamma_h^{\rm tot}$), see Eq. (11). We then proceed as follows:

- $BF(h \to \mu^+\mu^-)$ and $BF(h \to b\bar{b})$ can be obtained individually if we use the type-II doublet prejudice that the $\mu^+\mu^-$ and $b\bar{b}$ couplings squared are modified relative to the SM coupling by the same factor, f. (A value of m_b must be specified.)

- Given the individual branching fractions, the partial widths can then be com-

puted:

$$\Gamma(h \to \mu^+\mu^-, b\bar{b}) = \Gamma_h^{\text{tot}} BF(h \to \mu^+\mu^-, b\bar{b}) \tag{25}$$

- One can use event rates in other observable channels, coupled with the $BF(h \to \mu^+\mu^-)$ determination, to obtain results for $BF(h \to X)$.

- $\Gamma_h^{\text{tot}} \times BF(h \to X)$ then yields the partial width and coupling for any observable channel X. For example, if the $H^0 \to h^0 h^0$ channel can be detected we could determine the very interesting associated partial width (and, thence, coupling) via $\Gamma(H^0 \to h^0 h^0) = \Gamma_{H^0}^{\text{tot}} BF(H^0 \to h^0 h^0)$ or, equivalently,

$$\Gamma(H^0 \to h^0 h^0) = \frac{[\Gamma_{H^0}^{\text{tot}}]^2 BF(H^0 \to \mu\mu) BF(H^0 \to h^0 h^0)}{\Gamma(H^0 \to \mu\mu)} . \tag{26}$$

Of course, if Γ_h^{tot} and $\sigma_{\sqrt{s}}$ are close in size, one must avoid the approximation of Eq. (11), but determination of f and the partial widths and branching fractions would nevertheless be straightforward.

3.4 Determining a Higgs boson's CP properties

A $\mu^+\mu^-$ collider might well prove to be the best machine for directly probing the CP properties of a Higgs boson that can be produced and detected in the s-channel mode. This issue has been explored in Refs. [32,33] in the case of a general two-Higgs-doublet model.

The first possibility is to measure correlations in the $\tau^+\tau^-$ or $t\bar{t}$ final states. Via such measurements, a $\mu^+\mu^-$ collider is likely to have greater sensitivity to the Higgs boson CP properties for $L = 20$ fb^{-1} than will the e^+e^- collider for $L = 85$ fb^{-1} (using correlation measurements in the Zh production mode) if $\tan\beta \gtrsim 10$ or $2m_W \lesssim m_h \lesssim 2m_t$. Indeed, there is a tendency for the $\mu^+\mu^-$ CP-sensitivity to be best precisely for parameter choices such that CP-sensitivity in the $e^+e^- \to Zh$ mode is worst. Somewhat higher total luminosity ($L \sim 50$ fb^{-1}) is generally needed in order to use these correlations to distinguish a pure CP-odd state from a pure CP-even state.

The second possibility arises if it is possible to transversely polarize the muon beams. Assume that we can have 100% transverse polarization and that the μ^+ transverse polarization is rotated with respect to the μ^- transverse polarization by an angle ϕ. The production cross section for a h with coupling $a + ib\gamma_5$ then behaves

as

$$\sigma(\phi) \propto 1 - \frac{a^2 - b^2}{a^2 + b^2} \cos \phi + \frac{2ab}{a^2 + b^2} \sin \phi \,. \tag{27}$$

To prove that the h is a CP admixture, use the asymmetry

$$A_1 \equiv \frac{\sigma(\pi/2) - \sigma(-\pi/2)}{\sigma(\pi/2) + \sigma(-\pi/2)} = \frac{2ab}{a^2 + b^2} \,. \tag{28}$$

For a pure CP eigenstate, either a or b is zero. For example, in the MSSM the Higgs sector is CP-conserving; $b = 0$ for the CP-even h^0 and H^0, while $a = 0$ for the CP-odd A^0. In such cases, it is necessary to employ a different asymmetry than that discussed in Ref. [33]. The quantity

$$A_2 \equiv \frac{\sigma(\pi) - \sigma(-\pi)}{\sigma(\pi) + \sigma(-\pi)} = \frac{a^2 - b^2}{a^2 + b^2} \tag{29}$$

is $+1$ or -1 for a CP-even or CP-odd h, respectively. Background processes in the final states where a Higgs boson can be most easily observed (*e.g.* $b\bar{b}$) can dilute these asymmetries substantially. Whether or not they will prove useful depends even more upon the very uncertain ability to transversely polarize the muon beams, especially while maintaining high luminosity.

Note that longitudinally polarized beams are not useful for studying the CP properties of a Higgs produced in the s-channel. Regardless of the values of a and b in the h coupling, the cross section is simply proportional to $1 - \lambda_{\mu^+}\lambda_{\mu^-}$ (the λ's being the helicities), and is only non-zero for LR or RL transitions, up to corrections of order m_μ^2/m_h^2.

4   Summary and Conclusion

A $\mu^+\mu^-$ collider would be a remarkably powerful machine for probing Higgs physics using direct s-channel production, and thus ultimately for finding the underlying theory of the scalar sector. In this report we have concentrated on the procedures and machine requirements for direct measurement of the properties of a Higgs boson.

4.1   SM-like Higgs boson

We expect that a SM-like h (which nominally includes the h^0 of the MSSM) will first be detected either at the LHC or in the Zh mode at an e^+e^- collider. If not, it

would be most advantageous to expend a small amount of luminosity at full machine energy to discover it in the Zh mode at the $\mu^+\mu^-$ collider. Once m_h is approximately known, a $\mu^+\mu^-$ collider can zero-in on $\sqrt{s} \simeq m_h$ for detailed studies of a SM-like Higgs boson provided $m_h \lesssim 2m_W$ (as is the case for the h^0 of the MSSM). The mass can be measured to a fraction of an MeV for $m_{h_{SM}} \lesssim 130$ GeV.

Crucial to a model-independent determination of all the properties of the Higgs boson at the $\mu^+\mu^-$ collider is the ability to make a direct precision measurement of its total width, which is very narrow for a SM-like h when $m_h < 2m_W$. The proposed method (described in Appendix C) relies on measuring the ratio of the central peak cross section to the cross section on the wings of the peak, a ratio that is determined by $\Gamma_h^{\rm tot}$ alone. Once $\Gamma_h^{\rm tot}$ is measured, determinations of the crucial $\mu^+\mu^-$ and $b\overline{b}$ couplings are possible. The precision for $\Gamma_h^{\rm tot}$ and the $\mu^+\mu^-$ and $b\overline{b}$ partial widths/couplings achieved for total integrated luminosity of $L = 50$ fb^{-1} and an excellent beam resolution of $R = 0.01\%$ would be sufficient to distinguish the MSSM h^0 from the SM h_{SM} at the 3σ statistical level for values of the parameter m_{A^0} as large as ~ 400 GeV provided that m_{h^0} is not in the range $80 \lesssim m_{h^0} \lesssim 100$ GeV (i.e. near m_Z). No other accelerator or combination of accelerators has the potential of seeing the h^0 vs. h_{SM} differences at this level of precision out to such large m_{A^0} values. For a SM-like Higgs with $m_h \gtrsim 200$ GeV, the event rate is too low for detection in the s-channel.

Machine requirements for the precision studies are:

- High luminosity $\mathcal{L} \gtrsim 2 \times 10^{33}$cm^{-2}s^{-1} at $\sqrt{s} \sim m_h$.

- Excellent beam energy resolution of $R = 0.01\%$.

- Ability to adjust the machine energy $\sqrt{s}$ accurately (to one part in a million) and quickly (once an hour in the intial scan to precisely determine m_h) over a $\sqrt{s}$ interval of several GeV.

4.2   Non-SM-like Higgs bosons

For other Higgs bosons with weak WW, ZZ couplings (such as the H^0 and A^0 of the MSSM), but enhanced $\mu^+\mu^-$ and $b\overline{b}$ couplings, discovery in s-channel collisions at the $\mu^+\mu^-$ collider is typically possible. There are three possible techniques. In order to compare these techniques it is reasonable to suppose that the H^0 and A^0 have been

excluded for $m_{H^0}, m_{A^0} \lesssim \sqrt{s}/2$ via the $Z^\star \to H^0 A^0$ mode at an e^+e^- collider running with $\sqrt{s} \sim 500$ GeV.

a) Scan method

In this approach, a scan for the H^0 and A^0 of the MSSM would be made over a sequence of $\sqrt{s}$ values all the way out to the maximal $\sqrt{s}$ value achievable at the $\mu^+\mu^-$ collider. Assuming that $L = 50$ fb^{-1} is devoted to the scan and that both the e^+e^- and the $\mu^+\mu^-$ colliders have maximal energies of order 500 GeV, discovery via the scan would be robust for $250 \lesssim m_{H^0,A^0} \lesssim 500$ GeV if $\tan\beta \gtrsim 3$ to 4. Fortuitously, the domain $250 \lesssim m_{H^0}, m_{A^0} \lesssim 500$ GeV, $\tan\beta \lesssim 3$, in which much more luminosity would clearly be required for discovery at the $\mu^+\mu^-$ collider, is a parameter region where the H^0 and A^0 are likely to be accessible at the LHC for accumulated luminosity of 300 fb^{-1} per detector (ATLAS+CMS), as illustrated in Fig. 18. There is, nonetheless, a small window, $3 \lesssim \tan\beta \lesssim 4$, at large m_{A^0} (between about 400 and 500 GeV) for which the LHC and the $\mu^+\mu^-$ collider might both miss seeing the H^0 and A^0 unless higher luminosities are accumulated.

In order that the required $L = 50$ fb^{-1} can be optimally distributed over the full $250 - 500$ GeV scan range in the course of a year or two of running, it would be necessary to design the storage ring or rings so that it would be possible to adjust $\sqrt{s}$ quickly and accurately (to within a small fraction of the step size, which must be $\lesssim 0.1$ GeV in some mass ranges) while maintaining the full luminosity.

b) Bremsstrahlung tail method

In this technique, the A^0 and H^0 search is made while running the $\mu^+\mu^-$ collider at full energy, looking for excess events arising from the luminosity at the low-energy end of the bremsstrahlung tail. This approach is competitive with the scan technique if the $b\bar{b}$ final state mass can be reconstructed with excellent resolution (roughly ± 5 GeV, including all detector effects and semi-leptonic b decays). The lower $\tan\beta$ limits for 5σ signals are about one to two units higher than for the scan technique in the $m_{A^0} = 250 - 480$ GeV range. Thus the bremsstrahlung search leaves a larger gap between the upper limit in $\tan\beta$ for which H^0, A^0 discovery would be possible at the LHC ($\tan\beta \lesssim 3 - 4$ at high

68

m_{A^0}) and the lower limit for which the H^0, A^0 would be detected at the $\mu^+\mu^-$ collider ($\tan\beta \gtrsim 5 - 7$) than would the scan technique.

The bremsstrahlung technique has the advantage of not requiring that high luminosity be maintained over a broad range of $\sqrt{s}$ collision energies while being able to step quickly and accurately in $\sqrt{s}$, but detector costs associated with the very demanding resolution in the $b\bar{b}$ invariant mass might be high.

c) Pair production

It may well be possible to build a $\mu^+\mu^-$ collider with $\sqrt{s}$ substantially above 500 GeV. If a $\sqrt{s} \geq 1$ TeV machine with high luminosity were built instead of a 500 GeV collider, it could discover the H^0, A^0 for $m_{H^0}, m_{A^0} \geq 500$ GeV in the pair production mode.

If the H^0, A^0 have already been discovered, either

- with $m_{H^0}, m_{A^0} \lesssim 250$ GeV in the $Z^\star \to H^0 A^0$ mode at an e^+e^- collider, or

- with $m_{H^0}, m_{A^0} \lesssim 2$ TeV in the $Z^\star \to H^0 A^0$ mode at a 4 TeV $\mu^+\mu^-$ collider, or

- with $m_{H^0}, m_{A^0} \lesssim 500$ GeV at the LHC (if $\tan\beta \lesssim 3 - 4$ or $\tan\beta \gtrsim 8 - 20$),

scanning over a broad energy range would not be necessary at the $\mu^+\mu^-$ collider. By constructing a single appropriate storage ring and devoting full luminosity to accumulating events at $\sqrt{s} \simeq m_{A^0}, m_{H^0}$, detailed studies of the total widths and partial widths of the A^0 and H^0 would then be possible at the $\mu^+\mu^-$ collider *for all* $\tan\beta$ *values above 1.*

4.3   Summary of machine and detector requirements

We re-emphasize the crucial machine and detector characteristics for detection and study of both SM-like Higgs bosons and non-SM-like Higgs bosons.

- High luminosity, $\mathcal{L} \gtrsim 2 \times 10^{33} \text{cm}^{-2}\text{s}^{-1}$, is required at any $\sqrt{s}$ where a Higgs boson is known to exist and throughout any range of energy over which we must scan to detect a Higgs boson.

- A machine design such that beamstrahlung is small compared to the effects of bremsstrahlung (included in our studies) is highly desirable for scan searches

69

and precision studies. However, significant beamstrahlung might improve the ability to discover Higgs bosons using the low-energy tail of the luminosity spectrum.

- An extremely precise beam energy, $R \sim 0.01\%$, will be needed for precision studies of a narrow-width SM-like Higgs boson. Such precise resolution is also extremely helpful in the zeroing-in scan for a very narrow SM-like and is not harmful for discovering a Higgs boson with broad width. Precision measurements of the non-SM-like H^0 and A^0 widths and separation of these two resonances when they overlap becomes difficult if R is substantially larger than 0.01%.

- To zero-in on $\sqrt{s} \simeq m_h$ for a narrow-width SM-like Higgs boson requires being able to rapidly set $\sqrt{s}$ with an accuracy that is small compared to the beam resolution R, for $\sqrt{s}$ values within about a few GeV of the (approximately known) value of m_h. To discover the H^0 and A^0 by scanning requires being able to rapidly set $\sqrt{s}$ with an accuracy that is small compared to their widths over a $\sqrt{s}$ interval of order several hundred GeV.

- To measure Γ_h^{tot} for a SM-like h to $\pm 10\%$, it must be possible to set $\sqrt{s}$ with an accuracy of order 1 part in 10^6 over $\sqrt{s}$ values in an interval several times $R m_h$, *i.e.* over an interval of tens of MeV. This (and the accuracy for the mass measurements) requires a machine design that allows quick spin rotation measurements of a polarized muon in the storage ring.

- If both muon beams can be polarized and the polarization (P) maintained through the cooling and acceleration process, the significance of the s-channel Higgs signal can be significantly enhanced provided the factor by which the luminosity is decreased is less than $(1 + P^2)/(1 - P^2)$.

- To detect non-SM-like Higgs bosons with enhanced $\mu^+\mu^-$ couplings in the bremsstrahlung luminosity tail when the machine is run at full energy, one needs excellent mass resolution ($\sim \pm 5$ GeV) in the $b\bar{b}$ final state mass as reconstructed in the detector.

In conclusion, if a Higgs bosons is discovered at the LHC and/or an e^+e^- collider, construction of a $\mu^+\mu^-$ collider with $\sqrt{s}$ covering the range of masses observed will

become almost mandatory purely on the basis of s-channel Higgs physics. There are many other motivations for building a $\mu^+\mu^-$ collider, especially one with $\sqrt{s} \gtrsim 2$ TeV, based on other types of new physics that could be probed. The physics motivations for a high-energy $\mu^+\mu^-$ collider will be treated elsewhere [34].

ACKNOWLEDGMENTS

A   Effects of bremsstrahlung

Soft photon radiation is an important effect that must be taken into account when considering the ultimate resolution in $\sqrt{\hat{s}}$ (where $\hat{s} = (p_{\mu^+} + p_{\mu^-})^2$ is the invariant energy squared of a given collision) and peak luminosity that can be achieved at an e^+e^- or $\mu^+\mu^-$ collider. In an often discussed approximation [35] the small Gaussian spread in $\sqrt{\hat{s}}$ about the nominal central machine energy, $\sqrt{s}$, resulting from purely machine effects is ignored, and the energy spread resulting from soft photon radiation is computed starting from $d\mathcal{L}/d\sqrt{\hat{s}} \propto \delta(\sqrt{\hat{s}} - \sqrt{s})$, where $\sqrt{s}$ is the nominal machine energy. For many types of physics, this is an entirely adequate approximation since the Gaussian spread is much smaller than the structure of the physical cross section. However, there are physical processes with $\sqrt{\hat{s}}$ structure that is much narrower than the expected Gaussian spread; production of a Higgs boson with very narrow width is a case in point. In this case, it is important to assess the distortion of the machine-level Gaussian shape due to soft photon radiation. Here we give the necessary formalism and derive an extremely accurate approximation to the exact result that is useful for numerical investigations.

We start from the basic machine-level Gaussian form:

$$\frac{d\mathcal{L}_0}{d\sqrt{\hat{s}}} = \frac{e^{-(\sqrt{\hat{s}}-\sqrt{s})^2/2\sigma^2_{\sqrt{s}}}}{\sqrt{2\pi}\sigma_{\sqrt{s}}} \equiv G(\sqrt{\hat{s}}, \sqrt{s}, \sigma_{\sqrt{s}}) \tag{30}$$

and $\sigma_{\sqrt{s}}$ where is the resolution in $\sqrt{\hat{s}}$. This form results from the convolution of two Gaussians for the individual beams. In general,

$$\frac{d\mathcal{L}}{d\sqrt{\hat{s}}} = \int dE_1 dE_2 f(E_1) f(E_2) \delta(\sqrt{\hat{s}} - \sqrt{4E_1 E_2}) \tag{31}$$

where the $f(E)$'s give the probability for finding an electron or muon of energy E; $\frac{d\mathcal{L}_0}{d\sqrt{\hat{s}}}$ of Eq. (30) results when the f's are standard Gaussian forms centered at $E_0 \equiv \sqrt{s}/2$ with resolutions σ_E, $G(E_i, E_0, \sigma_E)$; $\sigma_{\sqrt{s}}$ in Eq. (30) is then given by $\sigma_{\sqrt{s}} = \sqrt{2}\sigma_E$. However, E_1 and E_2 are degraded by soft photon radiation, so that the actual probability for finding energy E in any one beam is given by

$$f(E) = \int_0^1 \frac{dz}{z} D(z) G(E/z, E_0, \sigma_E) \tag{32}$$

where $D(z)$ is the probability distribution for finding an electron or muon with fraction z of its initial energy after the soft-photon radiation. Substituting into Eq. (31), we

obtain

$$\frac{d\mathcal{L}}{d\sqrt{\hat{s}}} = \int dE_1 dE_2 \int \frac{dz_1}{z_1} \frac{dz_2}{z_2} D(z_1) D(z_2) G(E_1/z_1, E_0, \sigma_E)$$

$$\times\, G(E_2/z_2, E_0, \sigma_E) \left[\frac{1}{\sqrt{z_1 z_2}} \delta\left(\sqrt{\frac{\hat{s}}{z_1 z_2}} - \sqrt{4 \frac{E_1}{z_1} \frac{E_2}{z_2}} \right) \right] \qquad (33)$$

where we have rewritten $\delta(\sqrt{\hat{s}} - \sqrt{4 E_1 E_2})$ in a useful form. Changing integration variables to E_1/z_1 and E_2/z_2, we see immediately that the E_i integrations including the δ function reproduce $d\mathcal{L}_0/d\sqrt{s'}$ evaluated at $s' = \hat{s}/(1-x)$, where $1 - x = z_1 z_2$. Introducing $\int dx \delta(1 - x - z_1 z_2) = 1$ under the integral in Eq. (33) we obtain

$$\frac{d\mathcal{L}}{d\sqrt{\hat{s}}} = \int \frac{dx}{\sqrt{1-x}} \frac{d\mathcal{L}_0}{d\sqrt{s'}} \bigg|_{s' = \frac{\hat{s}}{1-x}} \mathcal{D}(x) \qquad (34)$$

where

$$\mathcal{D}(x) = \int dz_1\, dz_2\, D(z_1) D(z_2) \delta(1 - x - z_1 z_2)\,. \qquad (35)$$

In the approximation of Ref. [35], $\mathcal{D}$ takes the form

$$\mathcal{D}(x) = C \left[\beta x^{\beta-1} \left(1 + \frac{3}{4}\beta \right) - \beta \left(1 - \frac{x}{2} \right) \right]\,, \qquad (36)$$

where $C \equiv 1 + \frac{2\alpha}{\pi}(\pi^2/6 - 1/4)$ and $\mathcal{D}$ has an implicit energy dependence coming from

$$\beta \equiv \frac{2\alpha}{\pi}(\log \frac{s'}{m^2} - 1) \qquad (37)$$

with $s' = \hat{s}/(1-x)$; in what follows we replace s' in this formula for β by $\hat{s}$, the error made in doing so being extremely small. Typical values of β for a $\mu^+\mu^-$ collider are $\beta \simeq 0.0632$ at $\sqrt{s} = 100$ GeV and 0.0792 at $\sqrt{s} = 500$ GeV.

To compute a given cross section, one must fold this result for the luminosity with the physical cross section:

$$\overline{\sigma} = \int d\sqrt{\hat{s}} \frac{d\mathcal{L}}{d\sqrt{\hat{s}}} \sigma(\sqrt{\hat{s}})\,, \qquad (38)$$

where the luminosity is that found from the convolution of Eq. (34). This is a numerically intensive operation in a number of cases of particular interest. Thus, it is useful to develop an analytic approximation to $d\mathcal{L}/d\sqrt{\hat{s}}$ in Eq. (34). This we have done by performing an expansion. Writing $x \equiv \epsilon/(1+\epsilon)$, defining

$$\sqrt{\hat{s}} \equiv \mu + \sqrt{s}, \quad a \equiv \frac{\sqrt{2}\mu}{\sigma_{\sqrt{s}}} \sqrt{1 + \frac{\mu}{\sqrt{s}}}, \quad \rho \equiv \frac{2\sqrt{2}\sigma_{\sqrt{s}}}{\sqrt{s}\sqrt{1 + \frac{\mu}{\sqrt{s}}}}\,, \qquad (39)$$

and changing variables to $y \equiv \epsilon/\rho$, the exponential in the Gaussian $d\mathcal{L}_0/d\sqrt{s'}$ in Eq. (34) takes the form

$$exp[-\mu^2/(2\sigma_{\sqrt{s}}^2)] \times exp[-y^2 - ay + \rho y^3/2 + \mathcal{O}(y^4)] \, . \tag{40}$$

The first term in Eq. (40) is the 'standard' Gaussian component. In the remaining part of the exponential, the strongly convergent quadratic component, $exp[-y^2]$, and the very small size of ρ guarantee that x takes on values of order ρ in $\mathcal{D}(x)$ and allows a convenient expansion, including $exp[\rho y^3/2] \simeq 1 + \rho y^3/2$. The most important component of the result derives from $\rho^\beta \beta(1 + \frac{3}{4}\beta) \int dy \, exp[-y^2 - ay] \, y^{\beta-1}$ which is easily expressed in terms of degenerate hypergeometric functions, $_1F_1$. Keeping some other smaller terms as well, we find the result:

$$\frac{\frac{d\mathcal{L}(\sqrt{\hat{s}})}{d\sqrt{\hat{s}}}}{\frac{d\mathcal{L}_0(\sqrt{\hat{s}})}{d\sqrt{\hat{s}}}} = \frac{C}{2} \left[-\beta \, e^{\frac{a^2}{4}} \sqrt{\pi} \, \rho \left(1 - \mathrm{Erf}(\frac{a}{2}) \right) + \frac{1}{2}\left(1 + \frac{3\beta}{4} \right) \beta \, \rho^{1+\beta} \right.$$

$$\times \left\{ \left(\Gamma(\frac{3+\beta}{2}) \, _1F_1(\frac{3+\beta}{2}, \frac{1}{2}, \frac{a^2}{4}) - a \, \Gamma(\frac{4+\beta}{2}) \, _1F_1(\frac{4+\beta}{2}, \frac{3}{2}, \frac{a^2}{4}) \right) \right.$$

$$\left. + \left(\Gamma(\frac{1+\beta}{2}) \, _1F_1(\frac{1+\beta}{2}, \frac{1}{2}, \frac{a^2}{4}) - a \, \Gamma(\frac{2+\beta}{2}) \, _1F_1(\frac{2+\beta}{2}, \frac{3}{2}, \frac{a^2}{4}) \right) \right\}$$

$$\left. + \left(1 + \frac{3\beta}{4} \right) \beta \, \rho^\beta \left(\Gamma(\frac{\beta}{2}) \, _1F_1(\frac{\beta}{2}, \frac{1}{2}, \frac{a^2}{4}) - a \, \Gamma(\frac{1+\beta}{2}) \, _1F_1(\frac{1+\beta}{2}, \frac{3}{2}, \frac{a^2}{4}) \right) \right] \, .$$

$$\tag{41}$$

The numerically most important term outlined above appears last, the others being quite small corrections thereto. From it we see the crucial dependence on ρ^β. This factor decreases (albeit very slowly because of the small size of β) with increasingly small $\sigma_{\sqrt{s}}$. This non-negligible loss of peak luminosity will be quantified below.

The result of Eq. (41) is extremely accurate for $|\mu/\sigma_{\sqrt{s}}| \leq 10$ and even for $\mu/\sigma_{\sqrt{s}} = -20$ deviates by only about 3% from a precise numerical evaluation of the integral. As will be illustrated, the effective luminosity remains approximately Gaussian in shape aside from a long low-energy tail. The effective width at half maximum of this approximately Gaussian peak is little altered, even for $R \equiv \sigma_E/(\sqrt{s}/2)$ values as small as 0.0001 (desirable to measure the precise mass and width of a very narrow Higgs

74

boson). As already noted, the most important effect of the soft-photon radiation is to reduce the effective peak luminosity height. The peak height ratio is that obtained by setting $\mu = 0$ (*i.e.* $a = 0$) in Eq. (41). The functional form simplifies significantly, and we obtain:

$$
\left. \frac{\frac{d\mathcal{L}(\sqrt{\hat{s}})}{d\sqrt{\hat{s}}}}{\frac{d\mathcal{L}_0(\sqrt{\hat{s}})}{d\sqrt{\hat{s}}}} \right|_{\sqrt{\hat{s}}=\sqrt{s}} = C \left\{ \rho_0{}^{\beta_0} \Gamma \left(1 + \frac{\beta_0}{2} \right) \left(1 + \frac{3}{4} \beta_0 \right) - \beta_0 \rho_0 \frac{\sqrt{\pi}}{2} \right.
$$

$$
\left. + \frac{\beta_0}{4} \left(1 + \frac{3}{4} \beta_0 \right) \rho_0{}^{\beta_0+1} \left[\Gamma \left(\frac{\beta_0 + 3}{2} \right) + \Gamma \left(\frac{\beta_0 + 1}{2} \right) \right] \right\}, \qquad (42)
$$

where ρ_0 and β_0 are the values of ρ and β at $\sqrt{\hat{s}} = \sqrt{s}$. In Eq. (42) the first term is the most important one.

$$
\text{R=0.01\%, } L^{\text{peak}}/L_0^{\text{peak}}=0.605, \ \sqrt{s}=100 \ \text{GeV}
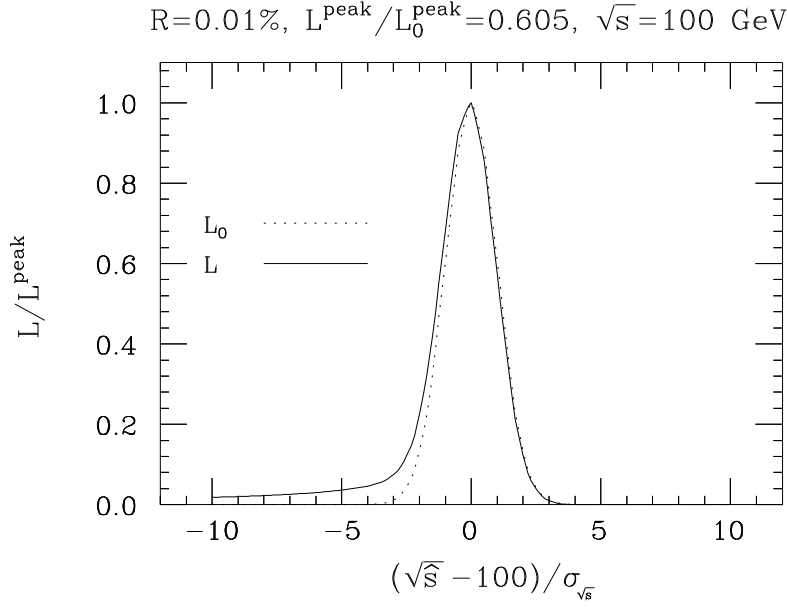$$

Figure 30: $d\mathcal{L}/d\sqrt{\hat{s}}$ relative to its peak value at $\sqrt{\hat{s}} = \sqrt{s}$ is plotted before and after soft-photon radiation. We have taken $\sqrt{s} = 100$ GeV and $R = 0.01\%$. The ratio of peak height after including soft-photon radiation to that before is 0.605.

We now illustrate the effects of the soft-photon radiation for a $\mu^+\mu^-$ collider. We first present in Fig. 30 a plot of $d\mathcal{L}/d\sqrt{\hat{s}}$ divided by its value at $\sqrt{\hat{s}} = \sqrt{s}$ as a

function of $(\sqrt{\hat{s}} - \sqrt{s})/\sigma_{\sqrt{s}}$ in the case where the beam resolution is 0.01% (that is $\sigma_E = 0.0001\sqrt{s}/2$), taking $\sqrt{s} = 100$ GeV. Results before $(\mathcal{L}_0)$ and after $(\mathcal{L})$ including soft-photon radiation are shown by the dotted and solid curves, respectively. The ratio of peak heights in this case is 0.605, *i.e.* roughly 40% of the peak luminosity is lost to soft-photon radiation. As promised, the peak remains close to the original Gaussian shape within $\pm 2\sigma_{\sqrt{s}}$ of the central peak, with a long tail extending to low $\sqrt{\hat{s}}$ values.

To further quantify the loss of peak luminosity that would be critical in searching for and studying a narrow Higgs boson resonance, we consider $\frac{d\mathcal{L}}{d\sqrt{\hat{s}}}/\frac{d\mathcal{L}_0}{d\sqrt{\hat{s}}}|_{\sqrt{\hat{s}}=\sqrt{s}}$ as a function of $\sqrt{s}$ and R in Fig. 31. From Fig. 31 one sees that the loss of peak luminosity decreases as the beam resolution becomes poorer, but increases as $\sqrt{s}$ increases (due to the increase of β with increasing $\sqrt{\hat{s}}$, see Eq. (37) and below).
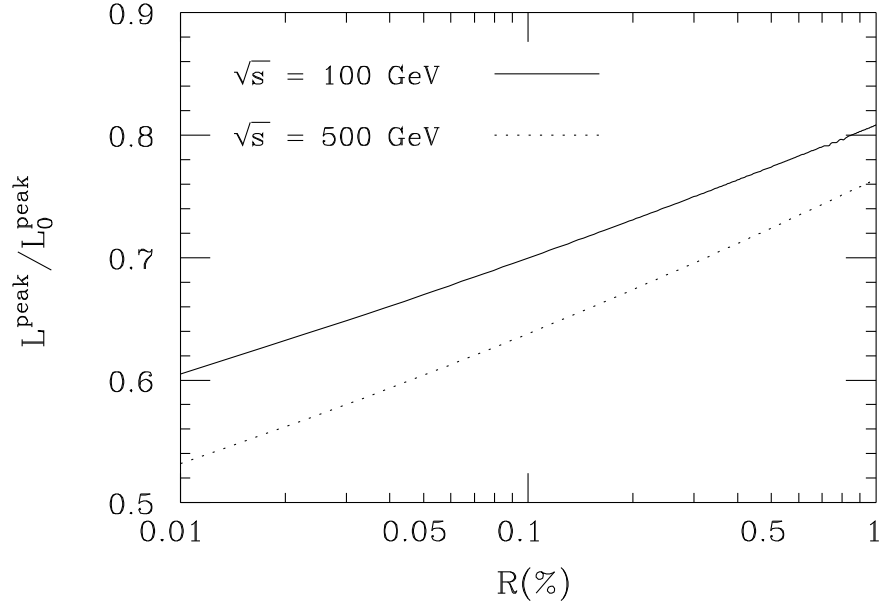

Figure 31: $\frac{d\mathcal{L}}{d\sqrt{\hat{s}}}/\frac{d\mathcal{L}_0}{d\sqrt{\hat{s}}}\Big|_{\sqrt{\hat{s}}=\sqrt{s}}$ as a function of R for $\sqrt{s} = 100$ and 500 GeV.

The results presented in the figures were obtained by direct numerical integration. However, the results from the approximate formulas, Eqs. (41) and (42), are essentially indistinguishable from those presented.

Finally, we present in Fig. 32 the full bremsstrahlung tail distribution $d\mathcal{L}/d\sqrt{\hat{s}}$ for the case of $R = 0.1\%$ and $\sqrt{s} = 500$ GeV. The integral $\int d\sqrt{\hat{s}}[d\mathcal{L}/d\sqrt{\hat{s}}]$ is normalized
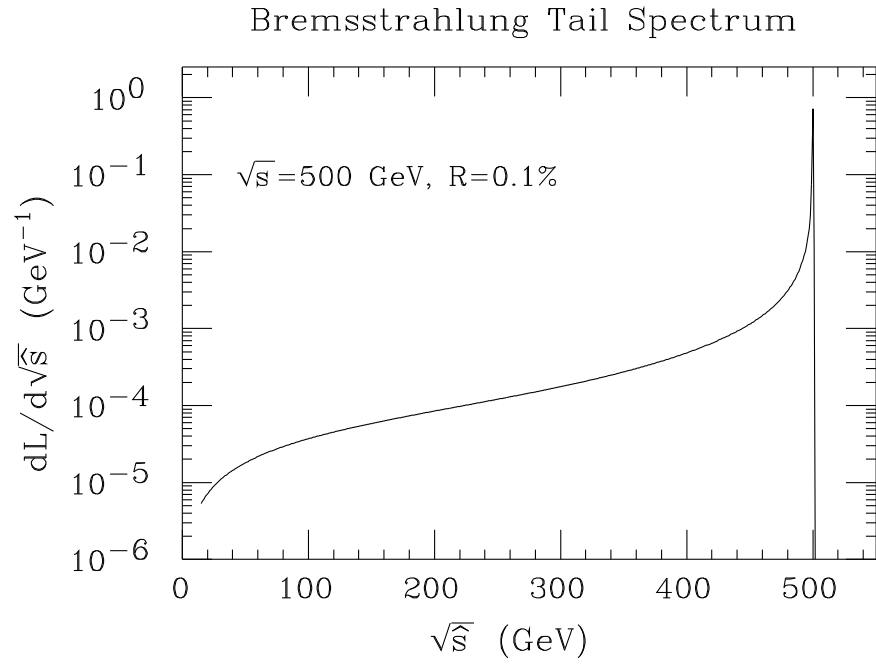
Bremsstrahlung Tail Spectrum

$\sqrt{s}$ =500 GeV, R=0.1%

Figure 32: $\frac{d\mathcal{L}}{d\sqrt{\hat{s}}}$ as a function of $\sqrt{\hat{s}}$ for $R = 0.1\%$ and $\sqrt{s} = 500$ GeV. The integral under the curve is normalized to 1.

to 1. The low-$\sqrt{\hat{s}}$ tail is quite independent of R. Only near the Gaussian peak region is there significant dependence of the spectrum on R. It is this spectrum that we have employed in discussing detection of Higgs bosons with enhanced $\mu^+\mu^-$ coupling using events from the bremsstrahlung tail when the $\mu^+\mu^-$ collider is run at full energy of $\sqrt{s} = 500$ GeV.

B   The $\boldsymbol{\mu^+\mu^- \to h \to WW^{(\star)}, ZZ^{(\star)}}$ modes

Whether we are above or below $2W$ or $2Z$ threshold, we include in our event rates an efficiency of 50% (after branching fractions) for isolating and reconstucting the final states of interest. Further, we search for the optimum choice of z_0 such that (in the center of mass) events with $|\cos\theta| > z_0$ are discarded. This is primarily useful for discarding the large number of forward/backward W's or Z's from the continuum backgrounds for m_h significantly larger than $2m_W$ or $2m_Z$.

(a). $\boldsymbol{m_h < 2m_W}$

We consider only those final states where the mass of the real W or Z can be reconstructed, thereby excluding $WW^\star \to 2\ell 2\nu$ and $ZZ^\star \to 4\nu$. For Higgs masses below $2m_W$ or $2m_Z$, we cannot use a mass constraint on the virtual boson to help isolate the $WW^\star$ or $ZZ^\star$ final state. Consequently, the pure QCD background to the $4j$ final state is very substantial, and a significant 4-jet Higgs signal is very difficult to obtain in this region. Thus, only the mixed hadronic/leptonic modes ($\ell\nu 2j$ for $WW^\star$ and $2\ell 2j$ and $2\nu 2j$ for $ZZ^\star$) and the visible purely leptonic $ZZ^\star$ modes (4ℓ and $2\ell 2\nu$) can be employed. The effective branching fractions (BF) for these final states are

$$BF_{WW}^{\text{eff}} \equiv BF(W^+W^- \to \ell\nu 2j) = 2(2/9)(2/3) \sim 0.3 \tag{43}$$

and

$$\begin{aligned} BF_{ZZ}^{\text{eff}} &\equiv BF(ZZ \to 4\ell + 2\ell 2j + 2\nu 2j + 2\ell 2\nu) \\ &= (0.067)^2 + 2[(0.067)(0.699) + (0.2)(0.699) + (0.067)(0.2)] \\ &\sim 0.42 \ . \end{aligned} \tag{44}$$

For virtual weak boson decays to leptons, the only backgrounds derive from the $W\ell\nu$, $Z2\ell$ and $Z2\nu$ processes. For virtual weak boson decays to jets, the background processes are $W2j$ and $Z2j$. In the $W^\star$ cases, the contribution to the cross section

from small $\ell\nu$ or $2j$ masses is well-behaved and small. Our procedure is to accept events from both the Higgs and background regardless of the virtual mass. For the $Z2\ell$ and $Z2j$ processes, the 2ℓ or $2j$ can arise from a $Z^\star$ *or* $\gamma^\star$. The virtual photon exchange causes a strong singularity and cross section growth for small 2ℓ and $2j$ virtual masses. In the $Z2\nu$ channel, especially for m_h near m_Z, there are likely to be significant backgrounds associated with limited detector acceptance (*e.g.* a three-jet event could produce two jets with mass near m_Z and the third jet could be soft or disappear down the beam pipe) and detector fluctuations and uncertainties. Hence, it is safer to require a minimum virtuality on the virtual 2ν. We have adopted the procedure of imposing a uniform cutoff, $M^{\star\,\mathrm{min}}$, on the invariant mass of the virtual $Z^\star$ in all channels — a search was performed to determine the optimal choice for $M^{\star\,\mathrm{min}}$ that maximizes the statistical significance of the Higgs signal. The resulting values for $M^{\star\,\mathrm{min}}$ as a function of Higgs mass are presented in Fig. 33. For the plotted $M^{\star\,\mathrm{min}}$ values one retains about 40% to 50% of the signal at the lower values of m_h, rising to 85% by $m_h = 175$ GeV.
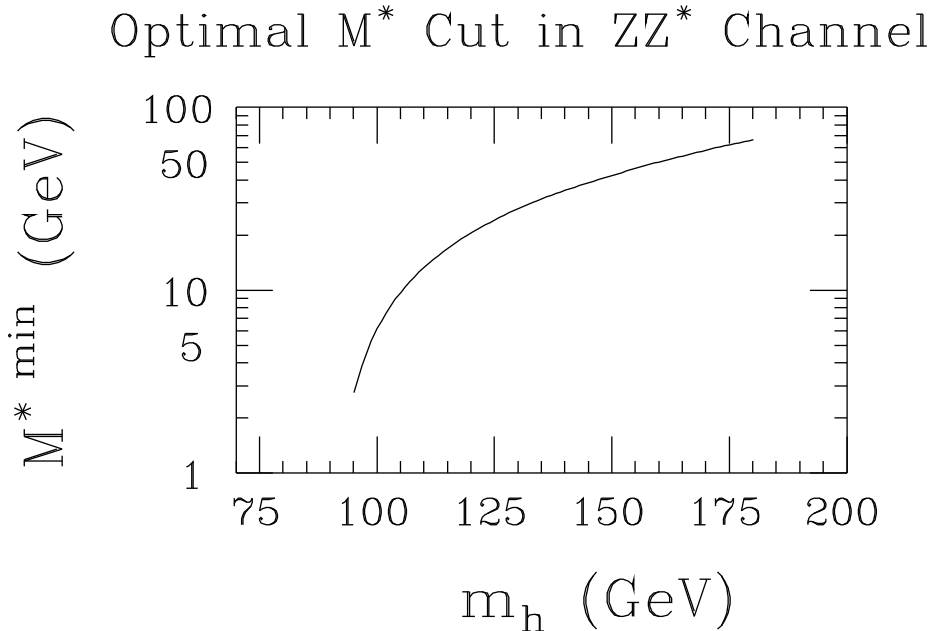
Optimal M* Cut in ZZ* Channel

Figure 33: The optimal choice for $M^{\star\,\mathrm{min}}$ in the $Z2j$, $Z2\ell$ and $Z2\nu$ final states is given as a function of m_h for a SM-like h.

(b). $m_h > 2m_Z$

Above $2W$ and $2Z$ thresholds, the only case for which mass reconstruction of both W's (Z's) is not possible is the $2\ell2\nu$ (4ν) final state. In all other final states Higgs mass reconstruction is possible from the final state particles (*e.g.* in the four-jet final states or the $2\ell2j$ and 4ℓ ZZ final states) or from the extremely precise determination of the incoming total momentum plus a reconstruction of one of the W's or Z's to determine the other W or Z (*e.g.* in the $\ell\nu2j$ WW final state and the $2\nu2j$ and $2\nu2\ell$ ZZ final states). Since both W's or Z's can be reconstructed above $2W$ or $2Z$ threshold, we can employ the $4j$ modes in addition to those listed in Eqs. (43) and (44); the pure QCD $4j$ background can be eliminated by requiring two equal mass pairs (within ±5 GeV of mass m_W or m_Z). The only significant background is then that from true continuum WW and ZZ production. Noting that we have already included a general 50% efficiency factor for cuts and reconstruction, a safe estimate in the above-threshold regions for the luminosity required for 5σ observation in the $4j$ channels can be obtained from the WW and ZZ curves of Fig. 10 by dividing by $[BF(W \to jj)^2/BF_{WW}^{\text{eff}}]^{1/2} \approx 1.2$ and $[BF(Z \to jj)^2/BF_{ZZ}^{\text{eff}}]^{1/2} \approx 1.1$, respectively.

C   Three-point determination of $m_{h_{SM}}$ and $\Gamma_{h_{SM}}^{\text{tot}}$

The procedure is as follows. We perform three measurements. At $\sqrt{s}_1 = m_{h_{SM}} + \sigma_{\sqrt{s}}d$ (where d is not known ahead of time, and will be determined by the procedure) we employ a luminosity L_1 and measure the total rate $N_1 = S_1 + B_1$. Next, we perform measurements at $\sqrt{s}_2 = \sqrt{s}_1 - n_{\sigma_{\sqrt{s}}}\sigma_{\sqrt{s}}$ and $\sqrt{s}_3 = \sqrt{s}_1 + n_{\sigma_{\sqrt{s}}}\sigma_{\sqrt{s}}$, yielding $N_2 = S_2 + B_2$ and $N_3 = S_3 + B_3$ events, respectively, employing luminosities of $L_2 = \rho_2 L_1$ and $L_3 = \rho_3 L_1$, with $\rho_{2,3} > 1 - n_{\sigma_{\sqrt{s}}} \sim 2$ and $\rho_2 = \rho_3 \sim 2.5$ are good choices for maximizing sensitivity and minimizing the error in determining d (*i.e.* $m_{h_{SM}}$) and $\Gamma_{h_{SM}}^{\text{tot}}$. We then define the ratios $r_2 \equiv (S_2/\rho_2)/S_1$ and $r_3 \equiv (S_3/\rho_3)/S_1$. Obviously, the ratios r_2 and r_3 are determined by d (*i.e.* by $m_{h_{SM}}$) and $\Gamma_{h_{SM}}^{\text{tot}}$: $r_i = r_i(d, \Gamma_{h_{SM}}^{\text{tot}})$. Conversely, we have implicitly $d = d(r_2, r_3)$ and $\Gamma_{h_{SM}}^{\text{tot}} = \Gamma_{h_{SM}}^{\text{tot}}(r_2, r_3)$. Determining the statistical errors $\Delta m_{h_{SM}}$ and $\Delta\Gamma_{h_{SM}}^{\text{tot}}$ is then simply a matter of computing the partial derivatives of d and $\Gamma_{h_{SM}}^{\text{tot}}$ with respect to the $r_{2,3}$ and the errors on the ratios $r_{2,3}$ implied by statistics.

Assuming precise knowledge of the background level $B \equiv B_1 = B_2/\rho_2 = B_3/\rho_3$,

the experimental error for either of the ratios is given by

$$\Delta r_i = \frac{\sqrt{r_i}}{\sqrt{\rho_i}\sqrt{S_1}} \times \sqrt{(1 + r_i\rho_i) + B/S_1(1/r_i + \rho_i r_i)}\,. \tag{45}$$

The errors in the experimental determination of d and $\Gamma^{\text{tot}}_{h_{SM}}$ are given by quadrature:

$$\Delta d = \left[(\frac{\partial d}{\partial r_2})^2(\Delta r_2)^2 + (\frac{\partial d}{\partial r_3})^2(\Delta r_3)^2\right]^{1/2} \tag{46}$$

$$\Delta\Gamma^{\text{tot}}_{h_{SM}} = \left[(\frac{\partial\Gamma^{\text{tot}}_{h_{SM}}}{\partial r_2})^2(\Delta r_2)^2 + (\frac{\partial\Gamma^{\text{tot}}_{h_{SM}}}{\partial r_3})^2(\Delta r_3)^2\right]^{1/2} \tag{47}$$

In practice, we compute the above partial derivatives by first computing

$$\mathcal{M} \equiv \begin{pmatrix} \frac{\partial r_2}{\partial d} & \frac{\partial r_2}{\partial \Gamma^{\text{tot}}_{h_{SM}}} \\ \frac{\partial r_3}{\partial d} & \frac{\partial r_3}{\partial \Gamma^{\text{tot}}_{h_{SM}}} \end{pmatrix} \tag{48}$$

and then inverting; *e.g.* $\frac{\partial d}{\partial r_2} = (\mathcal{M}^{-1})_{11}$. This is performed numerically, and the Δr_i's from Eq. (45) are then inserted in Eq. (47).

The above procedure is convenient in order to determine the luminosity required for $\Delta\Gamma^{\text{tot}}_{h_{SM}}/\Gamma^{\text{tot}}_{h_{SM}} = 1/3$ as a function of $m_{h_{SM}}$ for several possible choices of beam resolution. We have explicitly verified the accuracy and correctness of the procedure in several specific cases as follows. For a given $m_{h_{SM}}$ and $\Gamma^{\text{tot}}_{h_{SM}}$ we compute the event numbers $N_{1,2,3}$ and thence the ratios r_i ($i = 2, 3$) and their statistical errors. We then vary $m_{h_{SM}}$ and $\Gamma^{\text{tot}}_{h_{SM}}$ relative to their original values and determine $\Delta m_{h_{SM}}$ and $\Delta\Gamma^{\text{tot}}_{h_{SM}}$ as those shifts which result in $\Delta\chi^2 = 1$. Good agreement with the results from the above procedure is obtained.

REFERENCES

1. J.F. Gunion, A. Stange, and S. Willenbrock, Weakly Coupled Higgs Bosons, preprint UCD-95-28, to appear in *Electroweak Symmetry Breaking and New Physics at the TeV Scale*, to be published by World Scientific.

2. See J.F. Gunion, H.E. Haber, G.L. Kane and S. Dawson, *The Higgs Hunters Guide*, Addison-Wesley Publishing, and references therein.

3. M. Drees, Int. J. Mod. Phys. **A4**, 3635 (1989); J. Ellis *et al.*, Phys. Rev. **D39**, 844 (1989); L. Durand and J.L. Lopez, Phys. Lett. **B217**, 463 (1989); J.R. Espinosa and M. Quirós, Phys. Lett. **B279**, 92 (1992); P. Binétruy and C.A. Savoy, Phys. Lett. **B277**, 453 (1992); T. Morori and Y. Okada, Phys. Lett. **B295**, 73 (1992); G. Kane, *et al.*, Phys. Rev. Lett. **70**, 2686 (1993); J.R. Espinosa and M. Quirós, Phys. Lett. **B302**, 271 (1993); U. Ellwanger, Phys. Lett. **B303**, 271 (1993); J. Kamoshita, Y. Okada, M. Tanaka *et al.*, Phys. Lett. **B328**, 67 (1994).

4. V. Barger, *et al.*, Phys. Lett. **B314**, 351 (1993); P. Langacker and N. Polonsky, Phys. Rev. **D50**, 2199 (1994).

5. H. Haber, R. Hempfling and A. Hoang, CERN-TH/95-216.

6. M. Carena, J.R. Espinosa, M. Quiros and C.E.M. Wagner, Phys. Lett. **B355**, 209 (1995);
   J.A. Casas, J.R. Espinosa, M. Quiros and A. Riotto, Nucl. Phys. **B436**, 3 (1995).

7. For a review, see *e. g.*, J.F. Gunion and H.E. Haber, Nucl. Phys. **B272**, 1 (1986).

8. See, for example, R. Arnowitt and P. Nath, Phys. Rev. **69**, 725 (1992); Phys. Lett. **B289**, 368 (1992); G. G. Ross and R. G. Roberts, Nucl. Phys. **B377**, 571 (1992); S. Kelley, J. L. Lopez, D. V. Nanopoulos, H. Pois, and K. Yuan, Nucl. Phys. **B398**, 3 (1993); M. Drees and M. M. Nojiri, Phys. Rev. **D47**, 376 (1993); M. Olechowski and S. Pokorski, Nucl. Phys. **B404**, 590 (1993); D. J. Castaño, E. J. Piard, and P. Ramond, Phys. Rev. **D49**, 4882 (1994); V. Barger, M.S. Berger, and P. Ohmann, Phys. Rev. **D49**, 4908 (1994); M. Carena, M. Olechowski, S. Pokorski, and C.E.M. Wagner, Nucl. Phys. **B419**, 213 (1994); G. Kane, C. Kolda, and J. Wells, Phys. Rev. **D49**, 6173 (1994); W. de Boer, R. Ehret, and D.I. Kazakov, Z. Phys. **C67**, 647 (1995); M. Carena and C.E.M. Wagner, Nucl. Phys. **B452**, 45 (1995); S.F. King and P. White, Phys. Rev. **D52**, 4183 (1995).

9. V. Barger, M.S. Berger, R.J.N. Phillips, and A.L. Stange, Phys. Rev. **D45**, 4128 (1992); V. Barger, Kingman Cheung, R.J.N. Phillips, and A.L. Stange, Phys. Rev. **D46**, 4914 (1992).

10. J. Ellis, J.F. Gunion, H.E. Haber, L. Roszkowski and F. Zwirner, Phys. Rev. **D39**, 844 (1989); B.R. Kim, S.K. Oh and A. Stephan, *Proceedings of the 2nd International Workshop on "Physics and Experiments with Linear e^+e^- Colliders"*, eds. F. Harris, S. Olsen, S. Pakvasa and X. Tata, Waikoloa, HI (1993), World Scientific Publishing, p. 860: J. Kamoshita, Y. Okada and M. Tanaka, Phys. Lett. **B328**, 67 (1994); S.F. King and P.L. White, preprint SHEP-95-27 (1995), hep-ph 9508346; U. Ellwanger, M.R. de Traubenberg and C.A. Savoy, Z. Phys. **C67**, 665 (1995).

11. *Proceedings of the First Workshop on the Physics Potential and Development of $\mu^+\mu^-$ Colliders*, Napa, California (1992), Nucl. Instru. and Meth. **A350**, 24 (1994).

12. *Proceedings of the Second Workshop on the Physics Potential and Development of $\mu^+\mu^-$ Colliders*, Sausalito, California (1994), ed. by D. Cline, American Institute of Physics Conference Proceedings 352.

13. *Proceedings of the 9th Advanced ICFA Beam Dynamics Workshop: Beam Dynamics and Technology Issues for $\mu^+\mu^-$ Colliders*, Montauk, Long Island, (1995), to be published.

14. *Proceedings of the Third Workshop on the Physics Potential and Development of $\mu^+\mu^-$ Colliders*, San Francisco, California (1995), ed. by D. Cline, to be published.

15. V. Barger, M.S. Berger, K. Fujii, J.F. Gunion, T. Han, C. Heusch, W. Hong, S.K. Oh, Z. Parsa, S. Rajpoot, R. Thun and B. Willis, Physics Goals of a $\mu^+\mu^-$ Collider, appearing in Ref. [12], p. 55, hep-ph 9503258.

16. R.B. Palmer and A. Tollestrup, unpublished report.

17. D.V. Neuffer, Ref. [12], p. 22.

18. D.V. Neuffer and R.B. Palmer, Ref. [12], p. 70.

19. D.J. Miller, Ref. [12], p. 191.

20. V. Barger, M. Berger, J.F. Gunion, and T. Han, Phys. Rev. Lett. **75**, 1462 (1995).

21. R.B. Palmer, private communication.

22. G.P. Jackson and D. Neuffer, private communications.

23. See, for example, Z. Parsa, *$\mu^+\mu^-$ Collider and Physics Possibilities*, unpublished; K. Hagiwara and D. Zeppenfeld, Nucl. Phys. **B313**, 560 (1989), Appendix B.

24. For references to in-depth studies of physics at future e^+e^- colliders, see e.g. *Proceedings of the Workshop on Physics and Experiments with Linear Colliders*, ed. F.A. Harris, *et al.*, World Scientific (1993); *Proceedings of the Workshop on Physics and Experiments with Linear e^+e^- Colliders*, Waikoloa, Hawaii (April 1993), ed. F. Harris

et al. (World Scientific, 1993); JLC Group, KEK Report 92-16 (1992); *Proceedings of the Workshop on Physics and Experiments with Linear Colliders*, Saariselkä, Finland (Sept. 1991), ed. R. Orava *et al.*, World Scientific (1992).

25. P. Janot, *Proceedings of the 2nd International Workshop on "Physics and Experiments with Linear e^+e^- Colliders"*, eds. F. Harris, S. Olsen, S. Pakvasa and X. Tata, Waikoloa, HI (1993), World Scientific Publishing, p. 192, and references therein; T. Barklow and D. Burke, private communication.

26. See "JLC-I", KEK-92-16, December 1992.

27. K. Kawagoe, *Proceedings of the 2nd International Workshop on "Physics and Experiments with Linear e^+e^- Colliders"*, eds. F. Harris, S. Olsen, S. Pakvasa and X. Tata, Waikoloa, HI (1993), World Scientific Publishing, p. 660.

28. J.F. Gunion and H.E. Haber (unpublished).

29. Z. Kunszt and F. Zwirner, Nucl. Phys. **B385**, 3 (1992); H. Baer, M. Bisset, C. Kao, and X. Tata, Phys. Rev. **D46**, 1067 (1992); H. Baer, M. Bisset, D. Dicus, C. Kao, and X. Tata, Phys. Rev. **D47**, 1062 (1993); J.F. Gunion *et al.*, Phys. Rev. **D46**, 2040 (1992); J. Gunion and L. Orr, Phys. Rev. **D46**, 2052 (1992); J. Gunion, H. Haber, and C. Kao, Phys. Rev. **D46**, 2907 (1992); V. Barger, K. Cheung, R. Phillips, and A. Stange, Phys. Rev. **D46**, 4914 (1992); J. Dai, J. Gunion, and R. Vega, preprint UCD-95-25 (1995); ATLAS Technical Proposal, CERN/LHCC/94-43, LHCC/P2 (1994); CMS Technical Proposal, CERN/LHCC 94-38, LHCC/P1 (1994); D. Froidevaux, F. Gianotti, and E. Richter-Was, ATLAS Internal Note PHYS-No-64 (1995); F. Gianotti, to appear in the Proceedings of the European Physical Society International Europhysics Conference on High Energy Physics, Brussels, Belgium, July 27 - August 2, 1995.

30. D. Froidevaux, F. Gianotti, L. Poggioli, E. Richter-Was, D. Cavalli, and S. Resconi, ATLAS Internal Note, PHYS-No-74 (1995).

31. J.F. Gunion and H.E. Haber, *Proceedings of the 1990 DPF Summer Study on High Energy Physics: "Research Directions for the Decade"*, editor E. Berger, Snowmass (1990), p. 206; Phys. Rev. **D48**, 5109 (1993).

32. B. Grzadkowski and J.F. Gunion, Phys. Lett. **B350**, 218 (1995).

33. D. Atwood and A. Soni, Phys. Rev. **D52**, 6271 (1995).

34. V. Barger, M. Berger, J.F. Gunion, T. Han, and R. Phillips, in preparation.

35. E.A. Kuraev and V.S. Fadin, Sov. J. Nucl. Phys. **41**, 466 (1985); R.N. Cahn, Phys. Rev. **D36**, 266 (1987); M. Peskin, SLAC Summer Institute: 1989, p. 71.